

**Design and Analysis of a  
Rapid Kinetic Energy Transmission Mechanism**

By:

Brian Benson

A Thesis

Submitted to the Faculty

of

WORCESTER POLYTECHNIC INSTITUTE

In partial fulfillment of the requirements for the  
Degree of Master of Science

in

Mechanical Engineering

by:



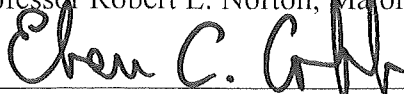
Brian C. Benson Jr

April 2011

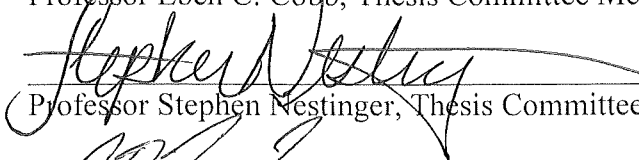
APPROVED:



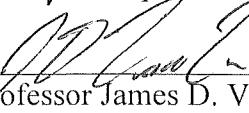
Professor Robert L. Norton, Major Advisor



Professor Eben C. Cobb, Thesis Committee Member



Professor Stephen Nestinger, Thesis Committee Member



Professor James D. Van de Ven, Graduate Committee Member

## **Abstract**

The rapid release of energy in mechanisms is often limited by conversion of potential energy to kinetic energy. The use of a flywheel to store energy over time eliminates this constraint. Using this principle, a lightweight and compact energy transmission mechanism has been developed for robotic combat applications. The purpose of the proposed design is to throw an opposing robot ten or more feet into the air. This design incorporates a flywheel, a self-resetting dog clutch with built in shock absorbing rubber for impact mitigation, and an optimized four-bar linkage to deliver the energy. A mathematical model of the dynamic system has been developed to analyze and aid in the design process. Testing of subsystems was performed to validate the design. A final design is proposed with the recommendation that it be built and tested. A validated design is applicable to many real-world problems that require rapid kinetic energy release including reconnaissance robots required to hop high fences.

## Acknowledgements

I would like to thank the following people for their contributions to this research.

Professor Robert L. Norton, for his wisdom and guidance throughout this project. Thank you for making this not only an extremely educational endeavor, but a fun one too. Your expertise in this subject area provided a seemingly endless source of answers to all of my questions and greatly enhanced both the quality of the project outcome and the experience I have come away with.

Professor Stephen Nestinger, for the many hours that he spent assisting me formulate the mathematical model, and for helping me debug when things weren't quite right. His guidance proved invaluable in making this project possible.

Professor Eben Cobb, for being an incredible resource for any modeling questions. If no one knew the answer, he knew of a book I could find it in.

Professor Taskin Padir, for his willingness to provide on the spot help with MATLAB and the mathematical modeling.

Brian and Cheryl Benson, for allowing me to perform the rather loud impact testing in their garage. More importantly for being a source of endless support and encouragement through my educational career and life. Without you I couldn't have made it this far.

Ciarán Murphy, for his unwavering help in proofreading my paper.

Michael Fagan for his assistance in manufacturing the impact mechanism.

## Table of Contents

Table of Figures .....	vii
Table of Tables .....	ix
Chapter 1: Introduction .....	1
1. Background.....	1
2. Literature Review .....	2
2.1 Flywheels .....	3
2.1.1 Introduction .....	3
2.1.2 Flywheels in the Literature.....	6
2.1.2.1 Hybrid-Driven Servo Press.....	6
2.1.2.2 Kinematic Optimization of Cam-Integrated Linkage .....	8
2.2 Clutches.....	10
2.2.1 Introduction .....	10
2.2.2 Means of Actuation .....	11
2.2.3 Means of Energy Transfer and Type of Engagement .....	12
2.2.4 Clutches in the Literature .....	16
2.2.4.1 Simulation of an Automotive Dry Clutch.....	16
2.2.4.2 Simulation of Frictional Surfaces and Clutch Mechanisms .....	19
2.2.4.3 Clutch Lock-up Model.....	21
2.2.4.4 Dual Belleville Washer Friction Clutch Design .....	24
2.3 Four-Bar Linkages .....	28
2.3.1 Introduction .....	28
2.3.2 Synthesis and Analysis.....	29
2.3.3 Four-Bar Linkages in the Literature.....	31
2.3.3.1 Lagrangian Dynamic Formulation of a Four-Bar Mechanism with Minimal Coordinates .....	31
2.4 Impact .....	33
2.4.1 Introduction .....	33
2.4.2 Impact Energy Method.....	33
2.5 Data Collection .....	35
2.6 Dynamic Modeling .....	37
2.7 Summary of Research .....	38
3. Overview .....	39

Chapter 2: Research Methodology.....	40
4. Introduction .....	40
4.1 Project Goal .....	40
4.2 Functional Requirements and Design Parameters .....	41
4.2.1 Energy Storage .....	42
4.2.2 Energy Release.....	44
4.2.3 Flywheel Engagement/Disengagement.....	45
4.2.4 System Design.....	48
4.3 Feasibility Analysis.....	57
4.3.1 Overview .....	57
4.3.2 Required Energy Transfer and Dynamics .....	57
4.4 Impact Mitigation.....	62
4.4.1 Introduction .....	62
4.4.2 Shock Absorption.....	62
4.4.3 Force versus Deflection at Low Strain Rate.....	64
4.4.4 Impact Testing.....	66
4.4.5 Reduced Impact Velocity and an Over-load Slip Clutch.....	73
4.5 Mathematical Model .....	74
4.5.1 Overview .....	74
4.5.2 Governing Equations.....	76
4.5.3 Model Implementation .....	80
4.5.4 Four-Bar Linkage Synthesis.....	85
4.5.4.1 Approach .....	85
4.5.4.2 Optimization Implementation.....	87
4.5.4.3 Optimization Process and Results .....	90
4.5.5 Model Results.....	97
4.5.6 Clutch Verification.....	100
4.5.6.1 Simple Clutch-Flywheel Prototype .....	100
4.5.6.2 Testing Results .....	103
4.6 Final Design.....	104
4.6.1 Cost-Benefit Analysis of the Design.....	104
4.6.2 Cost-Benefit Conclusion .....	107
4.6.3 Final Design Parameters.....	107
Chapter 3: Results and Conclusions .....	108

5. Results .....	108
6. Conclusion .....	111
7. Recommendations .....	112
Bibliography .....	114
Appendix A: Viability Analysis Calculations.....	116
Appendix B: Impact Testing.....	129
Appendix C: Four-Bar Synthesis and Optimization Programs.....	135
Appendix D: Mathematical Model of System Dynamics .....	143
Appendix E: Force and Stress Analysis of Dog Clutch Jaws .....	157

## Table of Figures

Figure 1: Seven Bar Linkage with 2 DOF (Tso & Li, 1998).....	6
Figure 2: Modified Two DOF Stephenson-type Linkage (Mundo, Danieli, & Yan, 2006).....	9
Figure 3: Motor-Clutch-Drive Train system to be Modeled (Mitchel & Gautheir Associates, 1990).....	19
Figure 4: The Clutch System (MathWorks, 2011).....	22
Figure 5: Clutch Model State Diagram (MathWorks, 2011).....	24
Figure 6: Key Components of the Friction Clutch (Shen & Weileun, 2007).....	27
Figure 7: A Simple Four-Bar Linkage.....	29
Figure 8: Planar Four-Bar Mechanism Under Consideration (Tang, 2006).....	32
Figure 9: Final Design CAD Model.....	51
Figure 10: Final Design CAD Model Exploded View.....	51
Figure 11: Female Side of Dog Clutch CAD model.....	52
Figure 12: Clutch Release and Catch Mechanism CAD Model.....	54
Figure 13: Sliding Push Collar CAD Model.....	55
Figure 14: Flywheel and Timing Pulley CAD Model.....	56
Figure 15: Assumed Speed and Acceleration of the Flywheel as a Function of Time.....	59
Figure 16: Clutch Torque Versus Time.....	59
Figure 17: Male Side Dog Clutch Initial Dimensions.....	61
Figure 18: Arbor Press Being Used to Determine Force vs Deflection.....	65
Figure 19: Force vs Deflection, Natural Gum Rubber.....	66
Figure 20: Projectile Motion Strobe Photograph.....	67
Figure 21: Rubber Impact Testing Mechanism.....	69
Figure 22: Rubber Holder and Steel Projectile.....	70
Figure 23: Rubber Impact Tester.....	71
Figure 24: New 60A Silicon Rubber Sample.....	72
Figure 25: 60A Silicon Rubber Sample After One Impact.....	72
Figure 26: Natural Gum Rubber Sample After One Impact.....	73
Figure 27: System Diagram of Final Design.....	74
Figure 28: Slip State Free Body Diagrams.....	76
Figure 29: Free Body Diagrams Stuck State.....	78
Figure 30: Program Flowchart.....	81
Figure 31: Optimization One: Total Moment of Inertia versus the Velocity Component Ratio.....	91
Figure 32: Optimization One: Total Moment of Inertia versus coupler Height (Vertical Displacement).....	92
Figure 33: Optimization One: Total Moment of Inertia versus the Velocity Component Ratio.....	93
Figure 34: Optimization Two: Total Moment of Inertia versus the Velocity Component Ratio.....	95
Figure 35: Optimization Two: total moment of inertia versus Coupler Height (Vertical Displacement).....	95
Figure 36: Optimized Linkage.....	97
Figure 37: Effective Moment of Inertia versus Angle of Four-bar Linkage.....	98

Figure 38: Example Result, Angular Position of Rotational Masses J1, J2 , and J3 versus Time .....	99
Figure 39: Example Result, Velocity of the Rotational Masses J1, J2, J3 versus Time	100
Figure 40: Example Result, Four-Bar and Projectile Trajectory .....	100
Figure 41: Clutch-Flywheel Prototype.....	101
Figure 42: Prototype Male Side Dog Clutch.....	102
Figure 43: Prototype Female Side Dog Clutch .....	102
Figure 44: Throw Height vs J1 J2 Initial Velocity .....	106
Figure 45: Final Design, Opposing Robot Trajectory .....	110
Figure 46: Final Design, Angular Position of the Flywheel (X2) and Four-bar Linkage Crank (X3) Versus Time.....	110
Figure 47: Final Design, Angular Velocity of the flywheel (V2) and Input Crank of the Four-Bar In linkage (v3) Versus Time.....	111
Figure 48, Final Mechanism CAD Design .....	111
Figure 49: Projectile Motion 40 PSI .....	129
Figure 50: Projectile Motion 60 PSI .....	129
Figure 51: Projectile Motion 80 PSI .....	130
Figure 52: Projectile Motion 100 PSI .....	130
Figure 53: Speed vs Pressure .....	131
Figure 54: 30A Silicon Rubber Sample After One Impact.....	132
Figure 55: 40A Silicon Rubber Sample After One Impact.....	133
Figure 56: 60A Silicon Rubber Sample After One Impact.....	133
Figure 57: Natural Rubber Sample After One Impact .....	133
Figure 58: EVA Foam Rubber Sample After One Impact.....	134
Figure 59: Natural Foam Gum Rubber Sample After One Impact.....	134
Figure 60: Polyurethane Foam Rubber Sample After One Impact.....	134

## Table of Tables

Table 1: Functional Requirments and Design Parameters .....	49
Table 2: Optimization One: Link length Ranges .....	90
Table 3: Optimization One: Linkage Options.....	93
Table 4: Optimization One: Linkage Dimensions .....	94
Table 5: Optimization Two: Link Length Ranges .....	94
Table 6: Optimization Two: Linkage Options .....	96
Table 7: Optimization One: Linkage Dimensions .....	96
Table 8: Prototype Testing Results .....	104
Table 9: Role of Torque Capacity on Safety Factor per Inch of Throw Height .....	107
Table 10: Projectile Motion Data Collected .....	130

# Chapter 1: Introduction

## 1. Background

Storage of energy and its conversion from potential to kinetic is an ongoing challenge in current and developing technology. This is proving to be especially true in the emerging robotics field, which is subject to size, weight, and longevity constraints. Current solutions typically entail potential energy being stored chemically in various types of batteries or fuels. It is then converted into mechanical kinetic energy by electric motors in the case of batteries or internal combustion engines in the case of chemical fuels. However, the efficiency and rate at which the energy can be converted is limited. This can be overcome through the use of a flywheel by gradually converting the potential electrical energy into kinetic energy and storing it in a flywheel over some period of time. That energy can then be quickly transferred by mechanical means.

Robotic combat is a sport in which competitors build custom "bots" and compete against one another with the goal of breaking or incapacitating the opponent. One method of accomplishing this is to throw or launch the other robot into the air. Traditionally pneumatics are used to power these throwing mechanisms. Typical pneumatic systems use an electric compressor to compress gas into accumulators. The accumulators are then put in the robot and are used to power pneumatic pistons, which convert the potential energy into kinetic energy. These systems are able to rapidly release energy but are bulky and heavy. An alternative solution is to use a flywheel. The energy source will be onboard batteries that power an electric motor that converts the electrical energy into rotational kinetic energy. This kinetic energy is then transferred into a flywheel that stores up the energy. Finally the energy is rapidly transferred to a four-bar linkage by way

of an intermittent clutch. The four-bar linkage acts as the throwing mechanism with a particular coupler curve designed to throw the opposing robot forward and upwards.

This thesis research seeks to design and investigate the dynamics of this flywheel, clutch, four-bar linkage system through both mathematical modeling and physical experimentation. The analysis of flywheels in which the loads are known is a common and well understood problem. The methodology for the analysis of four-bar linkages is also well defined and understood. Clutches are generally well understood. The unique aspect of this problem is the analysis and modeling of the coupling between the three systems, and how it affects the overall system performance.

The problem statement is then to concurrently design, model, and analyze this flywheel, clutch, and four-bar linkage system through CAD, mathematical modeling, and experimental testing. This mathematical model will be used to synthesize an optimum solution for a prescribed set of constraints. Sub-system prototypes will be built for experimental testing. The results of this testing will allow for a comparison and validation of the design and mathematical model. Items of interest are the dynamic properties of the system: position, velocity, and acceleration in addition to material selection and suitability. The modeling and testing of these items will aid in the design of the final system. This design can then be applied towards an actual combat robot or an alternative problem.

## **2. Literature Review**

The multitude of journal articles that have been identified focus on the analysis and/or modeling of the dynamics of flywheels, clutches, and linkages. In addition there

has been a particular focus on modeling techniques and approaches. The approaches and methodologies used by the authors will be discussed in this section.

## **2.1 Flywheels**

### **2.1.1 Introduction**

Energy storage and transfer is a paramount problem in our increasingly technological society. Our primary source of energy, fossil fuels, is starting to dwindle and society is looking towards both alternative energy sources and more efficient use of the energy available. Flywheels are becoming increasingly popular as an energy storage medium. They are analogous to an electrical inductor and are ideal in situations where the energy required by a system and its source fluctuate. Flywheels are able to filter out the power fluctuations by mechanically storing and releasing kinetic energy. This property makes them ideal for situations where large amounts of kinetic energy must be released rapidly, and a large device to convert potential to kinetic energy is not practical. A multitude of flywheel commercial applications exist. Automotive flywheels smooth out the intermittent power provided by the engine strokes(Ofria, 2007). Beacon Power Corporation builds flywheel energy storage systems capable of storing and delivering 25kWh of energy. This is done by spinning a flywheel at 16,000 rpm in a vacuum using magnetic bearings that allow the shaft to levitate (Beacon Power Corporation, 2010). Flywheels also have industrial applications such as in punch presses which again need to store energy up over time and release it rapidly.

The mathematics that govern flywheels are straightforward and use an energy based approach. The kinetic energy of a flywheel is described by:

$$K_e = \frac{1}{2}I_m\omega^2 \quad (1a)$$

where  $I_m$  is the mass moment of inertia of the flywheel and any other coupled rotating mass about the axis about which it is rotating, and  $\omega$  is the rotational velocity.

Flywheels are typically a circular disk rotating about its center. Therefore its mass moment of inertia can be described by the following equation:

$$I_m = \frac{m}{2}(r_o^2 + r_i^2) \quad (1b)$$

where  $r_i$  is the inner radius,  $r_o$  is the outer radius, and  $m$  is the mass.

The mass of such a disk is described by:

$$m = \pi \frac{\gamma}{g}(r_o^2 - r_i^2)t \quad (1c)$$

where  $\gamma$  is the material weight density,  $g$  is the acceleration due to gravity, and  $t$  is the disk thickness. Combining equations 1b and 1c gives the mass moment of inertia in terms of disk geometry:

$$I_m = \frac{\pi \gamma}{2g}(r_o^4 - r_i^4) \quad (1d)$$

Mass moment of inertia is additive, meaning that if a more complicated geometry is chosen then that geometry can be broken down into its basic shapes, the mass moment of inertia calculated for each, and then summed to provide the total moment of inertia.

Stresses in flywheels are dominated primarily by the centrifugal forces trying to pull the flywheel apart. These forces are analogous to the forces in a thick-walled pressurized cylinder and can therefore be calculated similarly.

The tangential stress can be described by:

$$\sigma_t = \frac{\gamma}{g}\omega^2\left(\frac{3+\nu}{8}\right)\left(r_i^2 + r_o^2 + \frac{r_i^2 r_o^2}{r^2} - \frac{1+3\nu}{3+\nu}r^2\right) \quad (1e)$$

The radial stress can be described by:

$$\sigma_r = \frac{\gamma}{g}\omega^2\left(\frac{3+\nu}{8}\right)\left(r_i^2 + r_o^2 - \frac{r_i^2 r_o^2}{r^2} - r^2\right) \quad (1f)$$

where  $\gamma$  is the material weight density,  $\omega$  is the angular velocity in rad/sec,  $\nu$  is Poisson's ratio,  $r$  is the radius at the point of interest, and  $r_i$ ,  $r_o$  are the inside and outside radii of the solid disk flywheel(Norton R. L., 2006).

## 2.1.2 Flywheels in the Literature

### 2.1.2.1 Hybrid-Driven Servo Press

The press in the stamping manufacturing process can be greatly improved with increased control of the press's movement and force. Normal presses are not easily adjustable for different uses. To remedy this, servo presses were created where the movement is controlled completely by a servo motor. However, for larger applications this is cost prohibitive. The solution to this is to combine the two types of presses into a hybrid-driven servo press, with both a servo and a flywheel powering the stamping motion. To accomplish this Tso and Li of Tsing-Hua University investigated the use of a seven-bar linkage with two degrees of freedom. This can be seen in Figure 1.

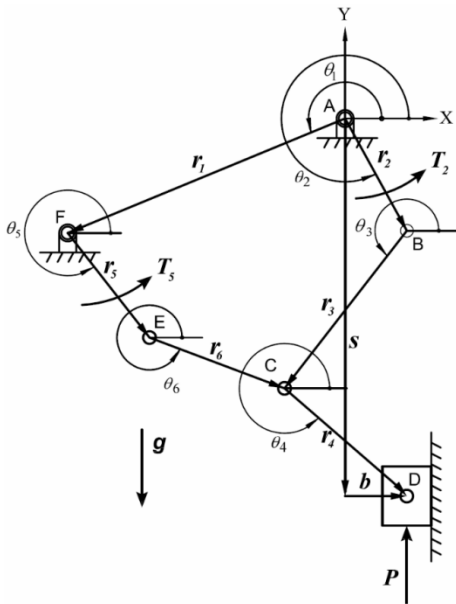


FIGURE 1: SEVEN BAR LINKAGE WITH 2 DOF (TSO & LI, 1998)

A flywheel provides an input to link 2 for one DOF and the servomotor for link 5.

This solution increases the press capacity and allows for a smaller, less expensive

servomotor. To analyze the seven-bar linkage the researchers used the vector loop method to solve for the positions all of the links. Using the principle of energy conservation they were able to determine how much force the servo press exerted and what percentages came from the flywheel and servomotor. This was accomplished by first integrating the punch force over displacement to determine the energy exerted. The energy of the two rotational inputs was estimated by integrating the torque output over angular displacement. A key assumption to be noted for this example is they considered the mass of the linkages and ram to be negligible compared to the output load, and therefore did not account for their mass. The researchers determined that for each motion created there is a different maximum stamping capacity. This is related to that motion's mechanical advantage and transmission angle, and is dependent on the input-link angle values. This differs from a standard servo press in which the capacity remains the same even with varying motions. This is because the capacity available is limited directly by the power of the motor.

The researchers also performed an experimental study in which they measured the input torques of the servomotor and flywheel and output force of the press. To instrument the servo press they used two angular encoders with a resolution of  $10^4$  pulse/revolution at the input links. They placed a linear scale at the ram to measure the punch displacement. This sensor was capable of a resolution of  $1\ \mu\text{m}$  and accuracy of  $5\ \mu\text{m}$ . In addition a dynamometer was installed to sense the stamping load. Tso and Li concluded that the capacity of the hybrid-driven servo press is not unique but depends on the press motion. It does however allow for a smaller servomotor to be used and still achieve a large stamping capacity(Tso & Li, 1998).

Li, Zhang, and Zheng of the Shijazhuang Mechanical Engineering College have also researched this type of solution. For their solution they used a hybrid-driven nine-bar press. To analyze and model the dynamics they applied numerical simulation to the whole system and used Lagrangian mechanics to derive equations of motion. In short, Lagrangian mechanics is an approach that combines conservation of energy and conservation of momentum(Haron). After deriving the positions of the linkage throughout time, they were able to determine velocity and acceleration by simply taking the time derivatives. This model takes into account the mass of the links and gravity, but assumes ideal operating conditions and ignores motor loss effects. Using this methodology the author was able to derive a system of first order differential equations and solve them using a fourth order Runge-Kutta method for integration. This research did not go so far as to actually do physical experimentation but went in depth in terms of the mathematical model. From the model and simulation the author concluded that a hybrid-driven press is indeed feasible for precision drawing(Li, Zhang, & Zheng, 2008). The approaches used in creating the dynamic models are an excellent example of a successful approach in modeling the dynamics of a flywheel powered linkage. Therefore this paper is highly applicable to creating dynamic models of dynamic systems involving a flywheel and linkage.

#### **2.1.2.2 Kinematic Optimization of Cam-Integrated Linkage**

A second approach to the problem of optimizing the kinematics of a deep draw press is through a cam-integrated linkage. Mundo, Danieli, and Yan of the University of Calabria and National Cheng Kung University presented a methodology for kinematic optimal synthesis of cam-integrated linkages. The methodology entailed two portions, the

first of which is creating a modified Stephenson-type linkage. A ground pivot is turned into a slider, increasing the degrees of freedom by one, so the designer can choose the necessary precision positions. This is shown in Figure 2.

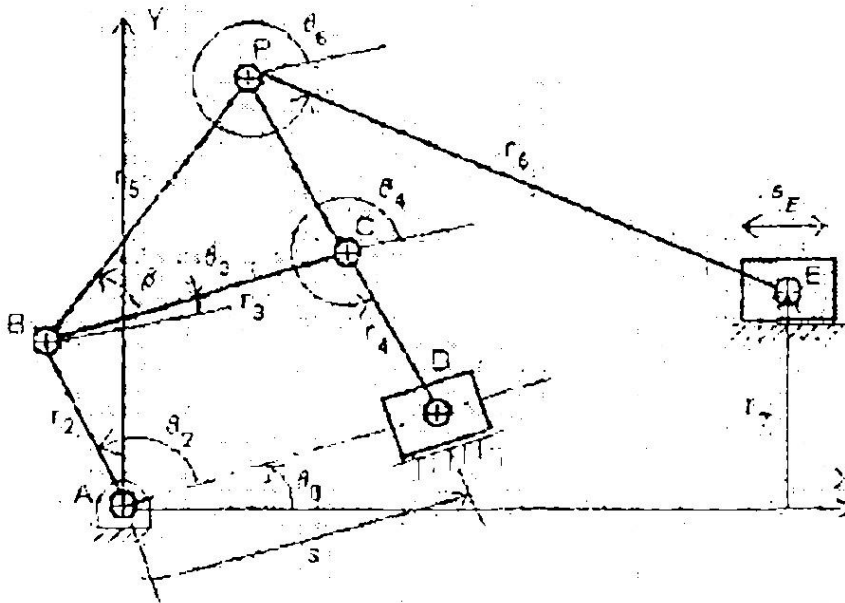


FIGURE 2: MODIFIED TWO DOF STEPHENSON-TYPE LINKAGE (MUNDO, DANIELI, & YAN, 2006)

By performing an inverse kinematic analysis for each of the 200 precision positions a cam pair can be synthesized to act as an input that removes one DOF. A constant input velocity on the input crank will remove the other DOF. This will result in a cam-integrated linkage capable of producing any desired motion. This direct solution methodology did not yield an optimum solution as the design of the cam followed no real design rules. The authors proposed a methodology to find a global optimum solution by taking into account dimensional and kinematic constraints for both the linkage and cam-follower. They then set up an optimization formulation by defining a number of parameters to minimize and a set of constraints. This constrained problem was then transformed into an unconstrained problem by penalty formulation to allow for

optimization by evolutionary theory. This means that when a constraint is violated, a large value is added to the objective function. This approach allows for the optimization algorithm to converge towards the desired global optimum. Using this methodology the authors were able to provide two optimized examples that could exactly reproduce the desired function. The authors conclude that this methodology is indeed sound and improvement could include the consideration of the dynamic characteristics of the mechanism in the optimization(Mundo, Danieli, & Yan, 2006). This methodology is of high interest to the problem at hand. It covers both the kinematic analysis of a flywheel and linkage based system in addition to offering a sound methodology for optimizing a mathematical model. These are both very useful to this research.

## **2.2 Clutches**

### **2.2.1 Introduction**

Norton describes a clutch as an interruptible connection between two rotating shafts (Norton R. L., 2006). In this application a clutch will allow the spinning flywheel to engage and disengage the input link of a four-bar linkage. The clutch must satisfy a number of requirements to serve its purpose. It must engage quickly to maximize the power transfer and be able to handle that power transfer without failure. However the clutch should also not engage so quickly as to cause a large enough acceleration to cause damage. Norton classifies clutches and brakes in three ways: the means of actuation, the means of energy transfer, and the type of the engagement. These will be examined in detail in the context of this application.

### **2.2.2 Means of Actuation**

The means of actuation can be mechanical, pneumatic and hydraulic, electrical, or automatic. Each actuation method has its own inherent advantages and disadvantages for different applications. These are related to size, weight, power source, and actuation control.

Mechanical actuation involves a physical means for actuation. In this application, an example would be a lever on the front of the robot that is pushed/moved when driven into another robot. This would ensure the four-bar linkage would only actuate when the opposing robot is in the correct position. This actuation technique has been done before for a similar application with success (Heatherington, 2008). However, it does not allow for easy manual input without added complexity. It also adds the additional challenge of having it automatically disengage.

Pneumatic and hydraulic actuation involves fluid pressure driving a piston, thereby actuating the clutch. In many applications this type of actuation is ideal. For example, vehicle brakes work with hydraulics. The hydraulic actuation allows the mechanism that compresses the fluid and the piston to be far removed from the brake system due to the ease of routing fluid lines. However, this is not a requirement for this application and hydraulics and pneumatics can be heavy, bulky, and relatively expensive to achieve the desired performance in this application. For this reason, these will not be explored further.

Electrical actuation is most often used in electromagnetic clutches. The electricity excites a magnetic coil thereby creating a magnetic field. This magnetic field can be used in a variety of ways to create the interruptible connection. This method has the potential

to work well for this application. The robot is powered by electricity so the power source is already present. It allows for manual engagement and disengagement of the clutch with ease using common electronics.

Automatic actuation is when a clutch engages without an external input. An example is an overload clutch that allows relative motion between two shafts when the torque exceeds a specific value. This type of clutch is not appropriate as the primary interruptible connection for this application for a number of reasons. First, the clutch needs to engage based on an input. This input can be from the operator or a sensor on the robot. Second, this type of actuation method is not typical for instances where the clutch is disengaged, and then must engage at the appropriate time. This type of clutch may be appropriate if used in addition to a second clutch. In such a case it would serve as an overload clutch to prevent damage to the system.

The most promising means of actuation for this application is either a combination of electrical and mechanical techniques or a strictly electrical solution. Both approaches allow for easy control of the clutch remotely through off-the-shelf electrical circuits. In addition they allow the clutch to be powered by the same electrical power source as the rest of the robot.

### **2.2.3 Means of Energy Transfer and Type of Engagement**

The means of energy transfer and type of engagement are often coupled. Therefore, it is more suitable to review them in their respective combinations. The basic types of energy transfer are positive contact, friction, overrunning, magnetic, and fluid coupling. These will be discussed with their appropriate types of engagement.

Positive contact clutches engage by means of a positive mechanical contact. The type of engagement is by mechanical interference. This can be through a variety of contact surfaces called jaws with shapes including square, spiral and toothed. The positive contact allows for transmission of high torque with no slip once the clutch is engaged. However, it is typically limited to a maximum engagement speed of 300 rpm (Norton R. L., 2008). Due to the relatively low lifespan required by this application it is possible to design a clutch that will work at much higher speeds. An additional option is the combination of a friction-type clutch and positive contact, otherwise known as a synchromesh clutch. In this mechanism, the friction type clutch allows the two shafts to reach a lower relative velocity before engaging the positive contact clutch. The positive contact clutch is very promising as a solution to intermittently engage the flywheel to the four-bar linkage. Both high torque load and quick engagement are necessary, and a positive contact clutch offers both attributes. The key challenge is to overcome the speed restraint and ensure that the clutch does not destroy itself from the high acceleration.

A friction clutch is the most common type of clutch. Its engagement is through the frictional force created between two or more surfaces to create a frictional torque. The three most common types of engagement are axial, radial, and cone. An axial clutch has the frictional surfaces flat and perpendicular to the axis of rotation. This allows for a linear actuation parallel to the axis of rotation. A radial clutch has cylindrical frictional surfaces and is engaged through a force in the radial direction. A common example would be a centrifugal clutch or drum brake. One feature of using such a clutch is it would allow it to be designed as self-energizing. With the correct geometry the friction pad can be designed such that when engaged, the forces acting on it cause it to engage

even further, thereby energizing itself. A conical clutch has the frictional surfaces as two cones. However, they are subject to grabbing during engagement and to unreliable disengagement. Typically, one surface is metal and the other a high friction material. To increase the capacity of axial clutches multiple disks can be used to better transfer the energy. These clutches can be dry or wet in the latter case being in an oil bath. The oil bath greatly reduces the coefficient of friction but assists in cooling. This type of clutch is worth considering for this application. Challenges include engaging the clutch quickly enough, and then dealing with the heat developed from the initial slippage.

An overrunning clutch is an automatic, one way clutch that engages in one direction and spins freely in the other. The means of energy transfer is again positive mechanical contact. The type of engagement comes in three forms: roller, sprag, and spring wound. All of these rely on friction or interference. A roller clutch has inner and outer races comparable to a ball bearing. However, wedge shaped cavities between the races cause the balls or rollers to jam in one direction, but spin freely in the other. A sprag clutch is similar. However, there is no wedge shaped cavity and instead of balls or rollers, there are odd-shaped "sprags" which jam in one direction but allow movement in the other. Finally, a spring clutch incorporates a tightly wound spring around a shaft. When the shaft is spun in one direction the spring tightens thereby increasing the torque capacity, when it spins in the opposite direction the spring loosens and is allowed to slip. This type of clutch in its automatic form is of no use for this application. However, if a method was developed to manually engage and disengage the mechanisms used to transfer the torque, then it could be of use.

The use of magnetic fields is another form of energy transfer. One example is the magnetic-particle clutch. The type of engagement involves a gap between two surfaces with a fine ferrous powder. When an electromagnet is energized it creates a magnetic field with flux lines that the powder forms chains along. This couples the two surfaces with varying torque capacity based on the strength of the magnetic field, which can be adjusted by varying the current flow. A second type of engagement is seen in the magnetic hysteresis clutch. There is no mechanical contact between the two rotating elements, which results in zero friction when disengaged. Instead a magnetic field causes a holding force that dictates the maximum torque capacity. These are often used to control torque because the maximum torque load is independent of the speed. The eddy-current clutch is similar to the hysteresis clutch in its construction. However, in this case there are coils in the clutch that set up eddy currents, which couple the clutch together. Relative motion is necessary to generate the eddy currents that make the coupling. For this reason, a hysteresis clutch is far from ideal. Magnetic particle and hysteresis clutches are promising for the application presented in this thesis because there is no mechanical engagement, meaning fewer parts to break. However, a challenge will be finding an electromagnetic clutch capable of the required torques within the size and weight restrictions. Additionally they are subject to drag and friction when disengaged.

Fluid coupling clutch's means of energy transfer and type of engagement is through the transmission of torque through a fluid. Typically, two impellers are placed in a fluid bath, one for the input and one for the output. The rotation of the input impeller imparts angular momentum to the surrounding fluid. This is then transferred through the fluid to the second impeller causing it to spin. This type of clutch is always subject to

some slip, as the two impellers will never reach the same speed. It also provides extremely smooth starts and is capable of absorbing shocks. This type of clutch is ideal for limiting torque and shock loads through a system. However, there is no good way to engage or disengage the clutch, so it is not very useful for the purpose of this thesis. Positive contact, friction, and magnetic clutches offer the most promising characteristics for this application.

#### **2.2.4 Clutches in the Literature**

The analysis of clutches in the literature has been done a number of times for numerous applications. Each of the instances examined took a different approach in their methodology of analyzing the engagement of the clutch, often looking at different aspects. These approaches are outlined in respect to how they relate to this thesis.

##### **2.2.4.1 Simulation of an Automotive Dry Clutch**

Serrarens, Dassen, & Steinbuch looked at both the simulation and the control of dry clutches in passenger cars (2004). The author's objectives included creating a dynamic model that described the engagement of the clutch, the design of a controller to smoothly engage the clutch, then simulate and analyze the engagement of the clutch based on the model, and finally use the model to optimize and analyze the clutch engagement within a set of parameters. Many of these objectives are comparable to those in this project, primarily simulation, analysis, and optimization of a clutch design. The clutch examined in this scenario consists of two plates, that can be moved together by the actuator that exerts a force on one of plates (the pressure plate). The other plate is connected to the crankshaft and is called the friction plate. As the plates push together the

frictional force transfers torque from the engine to the drive train. Initially the two plates will move relative to one another while transferring torque, but after a limited amount of time they will "stick" and move as one. The author's approach included breaking the powertrain system down into its basic subsystems. Each subsystem was described with a differential equation in terms of the torque, and then various techniques were used to combine these into a total powertrain model.

The torque of the engine was restricted by an upper and lower bound in addition to assuming it had infinitely fast dynamics. The motion of the engine is governed by the following differential equation:

$$J_e * \dot{\omega}_e = T_e - T_c \quad (2a)$$

Where  $J_e$  is the engine inertia,  $\dot{\omega}_e$  is the first derivative of the engine speed,  $T_e$  is the engine torque, and  $T_c$  is the clutch torque. The clutch must be described in two scenarios, when it is slipping and when it is sticking. The dynamics of the clutch when slipping can be described by the following differential equations:

$$J_c * \dot{\omega}_c = T_c - T_d - b_c * (\omega_c - \omega_t) \quad (2b)$$

$$\dot{T}_d = k(\varphi_d) * (\omega_c - \omega_t) \quad (2c)$$

Where  $J_c$  is the clutch inertia,  $\dot{\omega}_c$  is the first derivative of the clutch speed,  $T_c$  is the clutch torque,  $b_c$  is the clutch damping,  $\omega_c$  is the clutch speed,  $\omega_t$  is the transmission torque, and  $k(\varphi_d)$  is the nonlinear stiffness of the coil springs in-line with the clutch. The torque through the clutch can then be described as:

$$T_c = F_n * \mu * R_a * \text{Sin}(\omega_c - \omega_t) \quad (2d)$$

Where  $\mu$  is the coefficient of friction of the clutch surface,  $R_a$  is the active radius of the clutch plates, and  $F_n$  is the normal force acting on the clutch plate. When the clutch is at

the point of sticking it loses one degree of freedom and the engine is rigidly coupled to the clutch disk. The dynamics of the clutch can then be described by combining the equations for the engine and clutch:

$$(J_e + J_c) * \dot{\omega}_e = T_e - T_d - b_c * (\omega_c - \omega_t) \quad (2e)$$

The clutch remains stuck so long as the torque transmitted through the clutch ( $T_c$ ) remains below the maximum transmittable torque or until it is disengaged.

The transmission, shafts, wheels, tires, and vehicle were all described in a similar fashion by developing differential equations in terms of the torque for each subsystem. Next, different approaches to combining all of these governing equations into one system were attempted. The first of these was a Lagrangian approach using reduced matrices. Effectively, the equations are written in matrix form and set up such that through a matrix multiplication the degrees of freedom of the model are reduced by one, from slipping to sticking. The authors state one disadvantage of this method is that it "makes implementation overhead in a simulation model less compact" (Serrarens, Dassen, & Steinbuch, 2004). The second methodology used was a state space formulation. A disadvantage of this approach was that it required twice as many computations because for each time step both the sticking and slipping scenario is calculated. The final methodology avoided the disadvantages of the first two models by using the Karnopp approach. By using equations 2a and 2b for the slipping and sticking phase, no switching in the system description is necessary. By simply changing the clutch torque ( $T_c$ ) from an external input variable controlled by  $F_n$  to a constrained value dictated by the maximum transmittable torque, the authors were able to successfully use this Karnopp model to

describe the clutch engagement. Such an approach would be a viable methodology in describing the system presented in this paper.

#### 2.2.4.2 Simulation of Frictional Surfaces and Clutch Mechanisms

Mitchell & Gauthier Associates attacked a comparable problem to that of the aforementioned automotive dry clutch (Mitchel & Gauthier Associates, 1990). The authors describe the problem in a similar way. The engagement of a clutch causes two separate masses to start to behave as one having equal speeds. The best way to model this is not as two separate systems with different degrees of freedom, but as two separate masses with different accelerations when slipping and equal when stuck. This is the same conclusion that Serrarean, Dassen & Seinbuch came to in their Karnopp model. A block diagram graphically describing the system to be modeled can be seen in Figure 3.

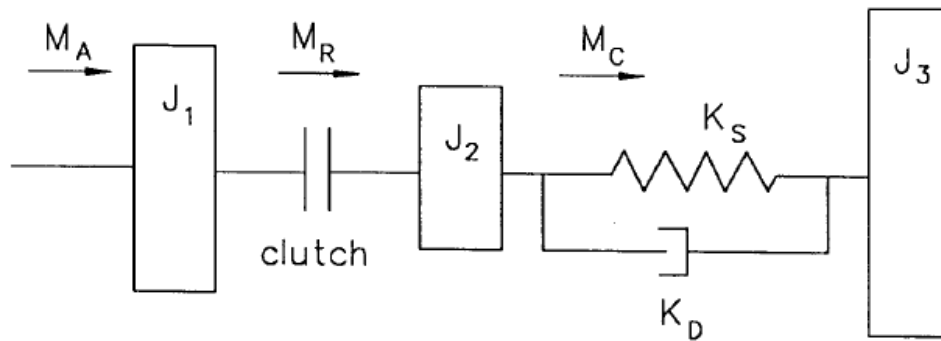


FIGURE 3: MOTOR-CLUTCH-DRIVE TRAIN SYSTEM TO BE MODELED (MITCHEL & GAUTHEIR ASSOCIATES, 1990)

This system is comparable to that of the flywheel-powered four-bar linkage. They model the system to have three coupled masses.  $J_1$  is the inertia of the engine and flywheel and it is subjected to an input torque of  $M_A$ .  $J_2$  is the inertia of the driven clutch plate and any associated gears, and it can transmit a torque equal to  $M_R$  through it before slipping occurs. Finally the inertia of the remainder of the drive train is equal to  $J_3$  and is coupled

to  $J_2$  by a torsion spring and damper. With this system the equations of motion can be described as follows:

$$\dot{\omega}_1 = \frac{(M_A - M_R)}{J_1} \quad (3a)$$

$$\dot{\omega}_2 = \frac{(M_R - M_C)}{J_2} \quad (3b)$$

$$\dot{\omega}_3 = \frac{M_C}{J_3} \quad (3c)$$

The torque  $M_C$  is a result of the windup of the torsion spring with a stiffness of  $K_S$  and damping rate of  $K_D$  and can be described as follows:

$$M_C = K_S \int (\omega_2 - \omega_3) dt + K_D (\omega_2 - \omega_3) \quad (3c)$$

Two methods were used to model the friction torque through the clutch. The first is called the simple limited large linear slope equations. The clutch can be considered to be the equivalent of a large viscosity with a torque proportional to the slip speed but limited to a maximum value when the clutch begins to slip. The equations are then:

$$\dot{\omega}_1 = \frac{-M_R}{J_1} \quad (3d)$$

$$\dot{\omega}_2 = \frac{M_R}{J_2} \quad (3e)$$

Consider  $M_R$  to be proportional to the slip speed:

$$M_R = M_{RW}(\omega_1 - \omega_2) \quad (3f)$$

It can be concluded that:

$$\dot{\omega}_1 = \frac{-M_{RW}(\omega_1 - \omega_2)}{J_1} \quad (3g)$$

$$\dot{\omega}_2 = \frac{M_{RW}(\omega_1 - \omega_2)}{J_2} \quad (3h)$$

A reasonable value for  $M_{RW}$ (the slip rate) that matches the physical world can then be chosen and the accelerations calculated.

A second method is also examined that uses an event finder to determine when the clutch is sticking or slipping and then uses the appropriate equations based on those findings. During slipping the motion of the two masses can be modeled by:

$$\dot{\omega}_1 = \frac{(M_A - M_R)}{J_1} \quad (3i)$$

$$\dot{\omega}_2 = \frac{(M_R - M_C)}{J_2} \quad (3j)$$

When the masses become stuck their accelerations become equal, and the equations become:

$$\dot{\omega}_1 = \frac{(M_A - M_C)}{J_1 + J_2} \quad (3k)$$

$$\dot{\omega}_2 = \dot{\omega}_1 \quad (3l)$$

When in the stuck mode, the torque across the clutch must be monitored to determine if slipping is about to occur. This can be calculated with the following equation:

$$M_R = J_2 * \dot{\omega}_2 + M_C \quad (3m)$$

Using this equation the torque can be monitored to determine when slipping starts. Using this approach to model the clutch in the flywheel powered four-bar linkage should work well.

### 2.2.4.3 Clutch Lock-up Model

MathWorks demonstrated a method of modeling the lock up of a clutch using Simulink(MathWorks, 2011). While this thesis does not use Simulink, the approach can still be utilized. The problem is analyzed with the existence of two modes of operation, slipping and lockup, also known as disengaged and engaged. The transition between these two states is difficult to model. It is the transition of the system when it loses a degree of freedom. The approach taken in this example uses a lumped-parameter model,

with two dynamic models that it switches between at the appropriate times. The overall system being modeled can be seen in Figure 4.

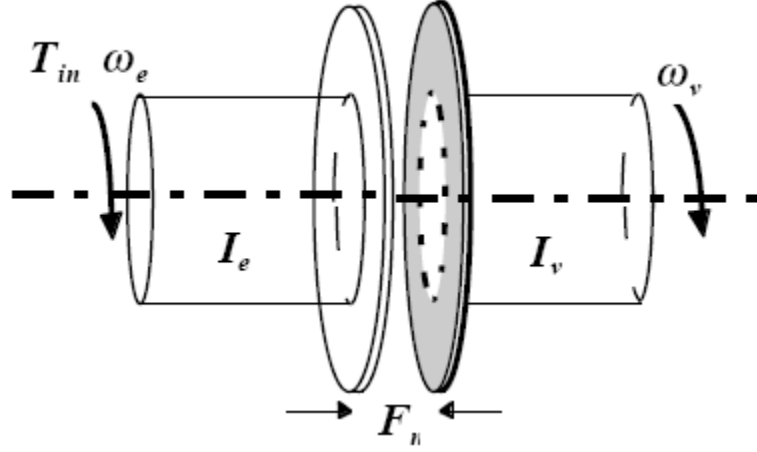


FIGURE 4: THE CLUTCH SYSTEM (MATHWORKS, 2011)

It considers the following variables:

$T_{in}$  = input (engine) torque;

$F_n$  = normal force between friction plates;

$I_e, I_v$  = moments of inertia for the engine and for the transmission / vehicle;

$T_{in}$  = input (engine) torque;

$b_e, b_v$  = damping rate at the engine and transmission / vehiclesides of the clutch;

$u_k, u_s$  = kinetic and static coefficients of friction;

$\omega_e, \omega_v$  = angular speeds of the engine and transmission input shafts;

$r_1, r_2$  = inner and outer radii of the clutch plate friction surfaces;

$R$  = equivalent net radius;

$T_{cl}$  = torque transmitted through the clutch;

$T_l$  = friction torque required fo the clutch to maintain lockup;

The state equations for the coupled system are then derived:

$$I_e \dot{\omega} = T_{in} - b_e \omega_e - T_d \quad (4a)$$

$$I_v \dot{\omega}_v = T_d - b_v \omega_v \quad (4b)$$

Next the torque capacity of the clutch is derived:

$$(T_f)_{max} = \iint_A \frac{r \times F_f}{A} da = \frac{F_n \mu}{\pi(r_2^2 - r_1^2)} \int_{r_2}^{r_1} \int_0^{2\pi} r^2 dr d\theta = \frac{2}{3} R F_n \mu \quad (4c)$$

$$R = \frac{r_2^3 - r_1^3}{r_2^2 - r_1^2} \quad (4d)$$

The kinetic coefficient of friction is used when the clutch is slipping, allowing for full capacity in the direction that opposes slip.

$$T_{fmaxk} = \frac{2}{3} R F_n \mu_k \quad (4e)$$

$$T_d = \text{sgn}(\omega_e - \omega_v) T_{fmaxk} \quad (4f)$$

The locked state can be modeled knowing that the angular velocities of engine and transmission are identical. So the system torque must be applied to the entire systems inertia. This allows equations 4a and 4b to be combined.

$$\omega_e = \omega_v = \omega \quad (4g)$$

$$(I_e + I_v) \dot{\omega} = T_{in} - (b_e + b_v) \dot{\omega} \quad (4h)$$

Thus by combining equations 4a and 4b the torque transmitted by the clutch when fully engaged can be described by:

$$T_c = T_f = \frac{I_v T_{in} - (I_v b_e - I_e b_v) \omega}{I_v + I_e} \quad (4i)$$

The clutch is then locked or engaged until the magnitude of the input torque exceeds the static friction capacity,  $T_{fmaxs}$ , defined as:

$$T_{fmaxs} = \frac{2}{3} R F_n \mu_s \quad (4j)$$

Finally a state diagram was created to describe the behavior of the clutch. This is seen in Figure 5.

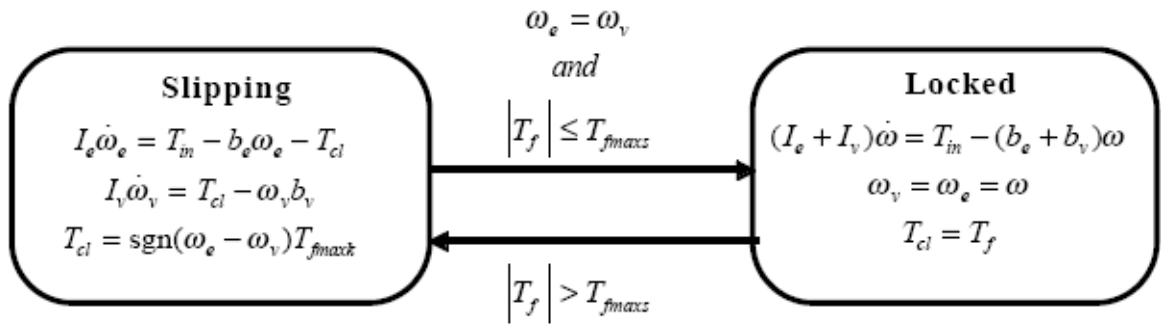


FIGURE 5: CLUTCH MODEL STATE DIAGRAM (MATHWORKS, 2011)

To develop the model from these governing equations two options were available. The first of which was to compute the clutch torque transmitted for each time instance and compare it against the maximum torque. The second was to use two different dynamic models, using each one when appropriate. The example uses the latter option.

The use of Simulink to develop this mathematical model of the dynamic system may prove to be the best option. It proved to work very well for this application, which was similar in its general goals.

#### 2.2.4.4 Dual Belleville Washer Friction Clutch Design

A successful design for this application may require a torque limiting clutch to assist in ensuring that its operation will not prematurely break the mechanism by overloading the gear train. One such design is outlined by Shen and Fang of the National Tsing Hua University (Shen & Weileun, 2007). An adjustable friction clutch using slotted Belleville washers (or conical disk springs) was designed that uses fewer parts and is easy to assemble. This is ideal for the presented application because in most cases fewer parts results in lighter and more reliable system. This friction clutch transmits the torque through the frictional forces between two surfaces (disks). The torque is a function

of the effective radius of the mating frictional surfaces, the normal force, and the coefficient of friction. When the torque being transmitted through the clutch exceeds the clutches limit it will slip, thus acting as a an overload protection device. The relationship between the torque capacity and the clamping force exerted by the Belleville washer is described by:

$$T = p * \mu * R_f \quad (5a)$$

$R_f$  for a brand new clutch is described by:

$$R_f = \frac{2}{3} \left( \frac{r_b^3 - r_a^3}{r_b^2 - r_a^2} \right) \quad (5b)$$

After uniform wear the friction radius becomes:

$$R_f = \left( \frac{r_b + r_a}{2} \right) \quad (5c)$$

Where  $r_b$  is the outer radii and  $r_a$  is the outer radii

The Belleville washer, which acts as both the spring and the friction plate for this design, must also be described in terms of both the exerted force and the effective frictional area for a given compression. For large deformations the load-deflection relationship is highly nonlinear. Therefore, only a small deflection is required to predict the characteristics of the Belleville spring.

The study presented the following formulation for predicting the relation of spring features and stiffness for slit Belleville washers.

$$P = \frac{r_2 - r_1}{r_2 - r_0} * \frac{C_1 C_2 E * t^4}{r_2^2} \quad (5d)$$

where  $r_0$  is the inner radii,  $r_1$  is the radii of the outer portion of the slit,  $r_2$  is the radii of the outer edge of the spring,  $E$  is the Young's modulus, and  $t$  is the thickness.  $C_1$  and  $C_2$  can be described by:

$$C_1 = \left( \frac{\alpha+1}{\alpha-2} - \frac{2}{\log \alpha} \right) \pi \left( \frac{\alpha}{\alpha-1} \right)^2 \quad (5e)$$

$$C_2 = \frac{\delta_3}{(1-\nu^2)t} \left[ \left( \frac{H}{t} - \frac{\delta_3}{t} \right) \left( \frac{H}{t} - \frac{\delta_3}{2t} \right) + 1 \right] \quad (5f)$$

where  $H$  is the free height minus the thickness,  $\nu$  is the Poisson's ratio,  $\alpha$  is the radius ratio ( $\frac{r_2}{r_1}$ ),  $\delta_1 - \delta_3$  are deflections of the Belleville spring described by:

$$\delta_1 = \delta_3 \frac{r_2 - r_0}{r_2 - r_1} \quad (5g)$$

$$\delta_2 = K \frac{4P(r_1 - r_0)^3}{Eb_0 t^3 m} (1 - \nu^2) \quad (5h)$$

where  $b_0$  is the width of the slit datum,  $m$  the number of slits, and  $K$  the constant described by:

$$K = \frac{3}{\left(1 - \frac{b}{b_0}\right)^3} \left[ \frac{1}{2} - 2 \left( \frac{b}{b_0} \right) + \left( \frac{b}{b_0} \right)^2 \left( \frac{3}{2} - \log_{10} \frac{b}{b_0} \right) \right] \quad (5i)$$

Using these formulations a Belleville washer clutch was designed and tested. The constructed clutch can be seen in Figure 6. The key components of the friction clutch are: driven gear #1, nut #2, setscrew #3, washer #4, Belleville springs #5, friction plate lining #6, intermediate plates #7, stud #8, and drive gear #9.

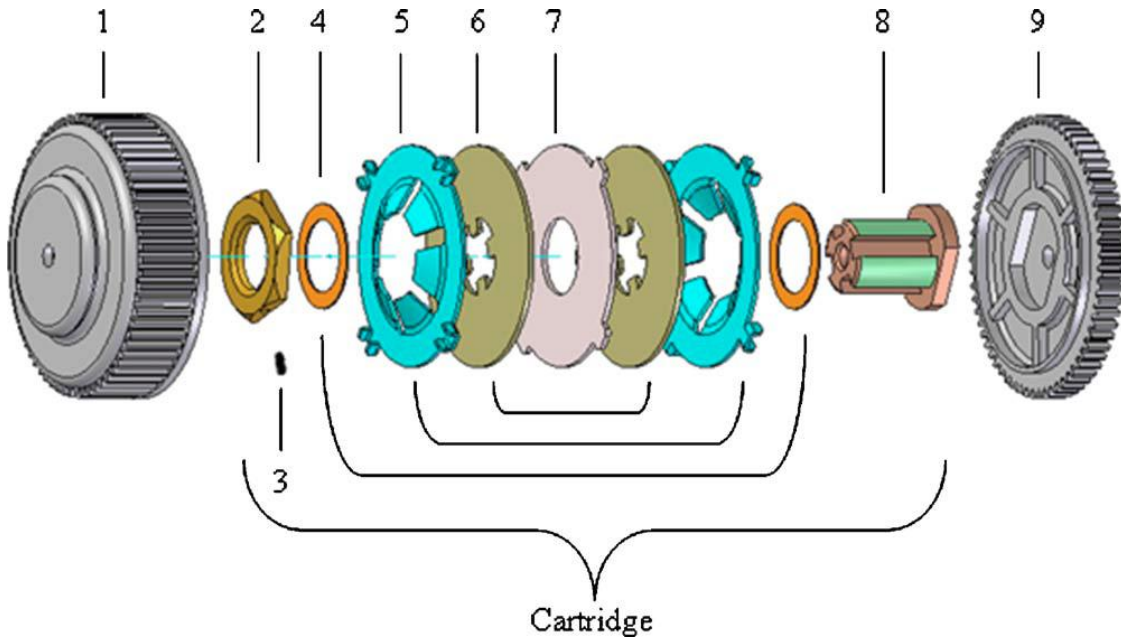


Figure 6: Key Components of the Friction Clutch (Shen & Weileun, 2007)

The study found that this design was indeed successful and the clutch capacity proved to be as expected and consistent for a variety of speeds (20, 40, and 60 rpm). It is expected a comparable design can be used to serve as an overload clutch for the flywheel powered four bar linkage.

Norton discusses the characteristics of Belleville washers without slots(Norton R. L., 2006). Comparable to the aforementioned washers they are defined by their outer diameter ( $D_o$ ), inner diameter ( $D_i$ ), height ( $h$ ), and thickness ( $t$ ). They are best suited to applications requiring high forces with minimal deflection. The ratio of the diameters  $D_o$  to  $D_i$  is called  $R_d$ , and the spring has maximum energy storage capacity at  $R_d$  equal to 2. The ratio of the height to thickness determines if the effective spring rate is linear with a positive or negative slope with increasing deflection, or constant for a given deflection range. An  $\frac{h}{t}$  ratio equal to .4 results in a linear relationship, at  $\frac{h}{t}$  equal to 1.414 the relationship has a portion from 80% to 120% deflection over which force deviates less

than 1%. In addition a deflection from 55% to 145% results in a deviation in force less than 10%. For ratios of  $\frac{h}{t}$  greater than 1.141 the relationship becomes bimodal. Norton recommends operating Belleville washers between 15% and 85% deflection when placed against a flat surface. The effective spring rate of Belleville washers is nonlinear, so it must be defined using a more complicated model than used for standard helical springs. This relationship is defined as follows:

$$F = \frac{4*E_y}{K_1*D_o^2(1-\nu^2)} \left[ (h - y) \left( h - \frac{y}{2} \right) t + t^3 \right] \quad (6a)$$

where:

$$K_1 = \frac{6}{\pi*\ln(R_d)} \left[ \frac{(R_d-1)^2}{R_d^2} \right] \quad (6b)$$

$$R_d = \frac{D_o}{D_i} \quad (6c)$$

$y$  is the deflection,  $E_y$  is young's modulus, and  $\nu$  is Poisson's ratio.

This type of spring is ideal for the purpose of a friction based disk slip clutch. By choosing a spring with an  $\frac{h}{t}$  ratio close to 1.414 it will approximate a constant force spring such that the clutches' slip torque will be fairly independent of the compression of the spring and therefore more reliable if assembled imprecisely.

## 2.3 Four-Bar Linkages

### 2.3.1 Introduction

A four-bar linkage is the simplest pin-jointed mechanism that has one degree of freedom and allows for controlled motion. It is the most common linkage found in machinery and can be found in many forms including slider-cranks and cam-followers. The simplest solution that meets the design criteria is usually the best and therefore the

four-bar is often the most desirable option for many motion problems. A four-bar linkage consists of four binary links connected with revolute (pin) joints. Figure 7 illustrates a four-bar linkage with link 1 being fixed to ground, link 2 and 4 being cranks or rockers and link 3 being the coupler link. By varying the link lengths the movement of the coupler link, and therefore any point fixed to the coupler can be altered to create a variety of coupler curves.

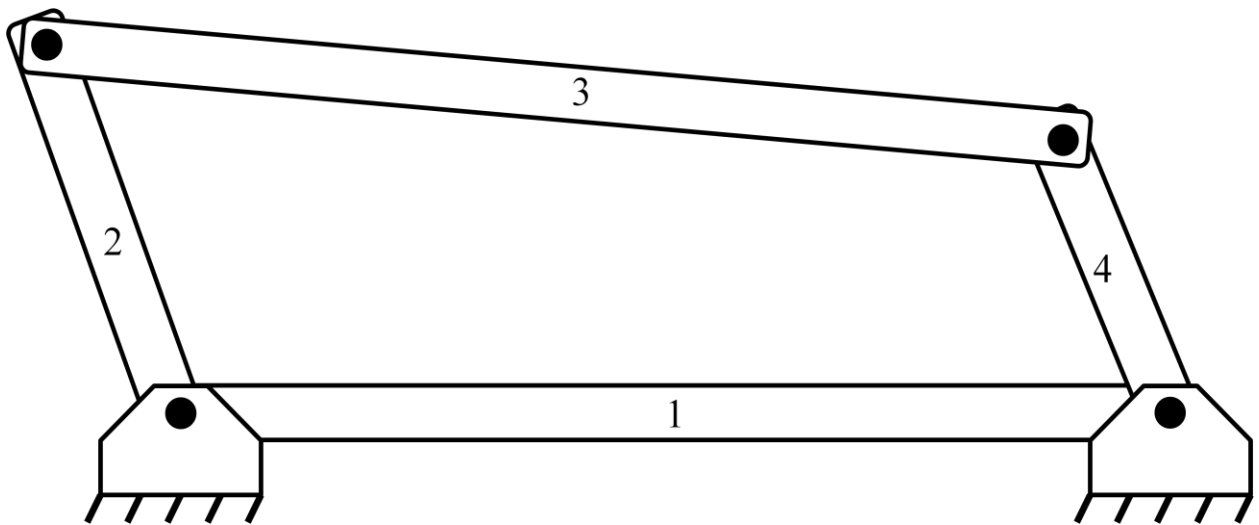


FIGURE 7: A SIMPLE FOUR-BAR LINKAGE

### 2.3.2 Synthesis and Analysis

Linkages can be synthesized and analyzed through graphical or analytical techniques. A variety of methodologies and tools are available for doing so. These techniques allow for the engineer to make design decisions about the desired motion in order to achieve satisfactory linkages. The engineer can prescribe or determine the position, velocity, and acceleration through its range of motion. For more information refer to Norton's *Design of Machinery: An Introduction to the Synthesis and Analysis of Mechanisms and Machines* (Norton R. L., 2008).

Prior to synthesis a number of design decisions must be made about the desired linkage. One of these decisions is what the linkage is intended to control with its movement. The engineer has three options. These are function generation, path generation, and motion generation. Function generation is defined as *the correlation of an input motion with an output motion in a mechanism*. Path generation is defined as *the control of a point in the plane such that it follows some prescribed path*. Motion generation is defined as *the control of a line in the plane such that it assumes some prescribed set of sequential positions*. Each of these types of generations require different consideration during linkage synthesis including techniques and the number of free choices for those respective techniques.

Design quality can be measured by a few standard metrics. The first of these is the existence of toggle positions that prevent the linkage from reaching all of the desired positions. A toggle position consists of the co-linearity of two moving links. From this toggle position the linkage has the ability to move in up to two distinct directions. Depending on the driving link its direction of movement may be unpredictable, or limited. Carefully choosing which link to drive can avoid such problems. A linkage can also have stationary positions from which certain input links cannot be back driven. These positions are also dependent on the co-linearity of links. The transmission angle of a set of links is a measure of the quality of the force and velocity transmission through a joint. It can be defined as *the angle between the output link and the coupler*. It is the acute angle between two links and varies continuously as the linkage goes through its entire motion. The optimum angle is 90 degrees such that all of the force resulting from the torque produced by the input link is transmitted tangentially into the second link. For

transmission angles less than 90 degrees some percentage of the force is being transmitted into the second link radially and acting only to put the second link in tension or compression and increase joint forces(Norton R. L., 2008).

### **2.3.3 Four-Bar Linkages in the Literature**

#### **2.3.3.1 Lagrangian Dynamic Formulation of a Four-Bar Mechanism with Minimal Coordinates**

This thesis required that a four-bar linkage's effective mass moment of inertia be calculated for a range of input crank angles. The Lagrangian approach provides a concise method for performing this calculation. Chin Pei Tang of The University of Texas at Dallas detailed the steps in formulating a dynamic equation of motion for a four-bar linkage in the minimal coordinate form using the Lagrangian formulation. Tang's results were very applicable to this research and therefore utilized. The Lagrangian formulation allowed Tang to model the mechanism in one equation using only one coordinate system. This is a simpler form than typical approaches that require multiple, generalized coordinate systems to simplify the modeling process. In brief, Tang began by writing loop-closure equations,

$$-l_1 \cos(\theta) - l_2 \cos(\alpha) + l_0 + l_3 \cos(\phi)=0 \quad (7a)$$

$$-l_1 \sin(\theta) - l_2 \sin(\alpha) - l_3 \sin(\phi)=0 \quad (7b)$$

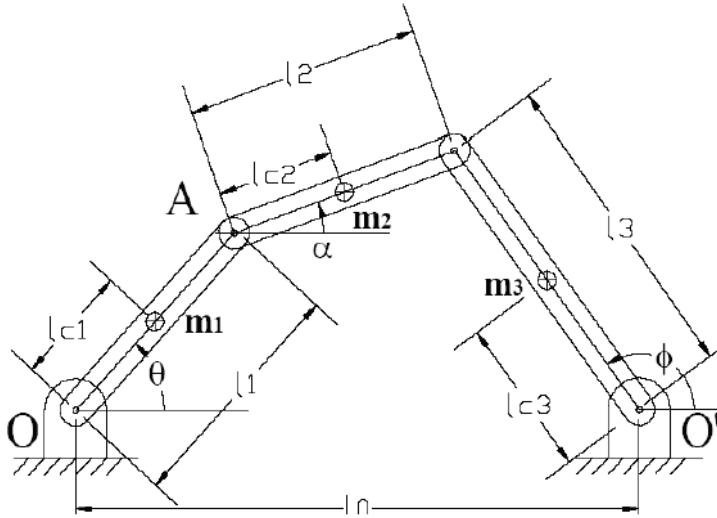


FIGURE 8: PLANAR FOUR-BAR MECHANISM UNDER CONSIDERATION (TANG, 2006)

then rearranged equations 7a and 7b and through a series of techniques, and solved  $\alpha$  and  $\phi$  in terms of  $\theta$ . Differentiating equations 7a and 7b yielded the angular velocities of each link which are described in terms of  $\dot{\theta}$ . The Lagrangian approach describes systems in terms of energy. As such this system is defined by its total kinetic energy minus the total potential energy. The author concludes with a final full dynamic equation, which in its compact form is seen in equation 7c.

$$M(\theta)\ddot{\theta} + V(\theta, \dot{\theta}) = \tau_{\theta} \quad (7c)$$

For a more detailed version of the equation please refer to the original document (Tang, 2006).

This formulation allows for a very short closed-form equation of the system. This comes at the expense of providing less information, than other methods. Other methods such as the vector-loop equation method calculate the position of each link by vector analysis. The velocity and acceleration can then be found by taking the derivative of the closed form equation. Using this, joint forces and all other relevant information can be

calculated. This alternate methodology provides more information than the Lagrangian formulation but with the addition of more calculations.

## **2.4 Impact**

### **2.4.1 Introduction**

The final design may incorporate a dog clutch capable of transferring a large amount of torque very quickly, but at the expense of a various harsh engagement. The male side of the dog clutch is moving very quickly and upon engagement impacts the female side of the dog-clutch which starts with a velocity of zero. Therefore to ensure the expected continual functionality of the dog-clutch the forces due to impact must be examined. To do this an energy approach can be used.

### **2.4.2 Impact Energy Method**

Impact is different from static loading due to the difference in time that the force is applied over. There are two types of impact: striking impact and force impact. A striking impact occurs when the two colliding bodies have some distance between them which is taken up by the moving body until they meet and impact occurs. A force impact occurs when both bodies are in contact but a force is suddenly applied from one to the other. An example of this is a weight suddenly being placed on a beam. For the case of the dog-clutch a striking impact occurs. The impact force can be estimated using an energy method. This energy method can underestimate the force by roughly 30%, so this must be taken into account. There are a number of assumptions that must be made when estimating a striking impact using this energy method. The first is that no permanent deformation occurs, or the stresses remain in the elastic region of the materials involved.

Additionally, the striking object is considered rigid and its mass is considered small relative to the struck object. These assumptions enable a key assumption to be made. That the energy possessed by the striking object is absorbed elastically by the struck object at its maximum deflection. Treating the struck object as a spring the energy stored within it upon impact can be described by equation 8a.

$$E_{PE} = \frac{F_i^2}{2k} \quad (8a)$$

Where  $E_{PE}$  is the energy capable of being stored,  $F_i$  is the impact force, and  $k$  is the spring constant of the material being struck. The energy stored in the striking object before impact can be described by equation 8b.

$$E_{KE} = \frac{mv_i^2}{2} \quad (8b)$$

Where  $E_{KE}$  is the energy stored in the striking object,  $m$  is the mass of the striking object, and  $v_i$  is the velocity of the striking object. Equations 8a and 8b can be set equal to one another, and  $F_i$  solved for. This results in equation 8c. Depending on the impact some energy may be dissipated as heat or noise. This is accounted for by a dissipation factor  $\eta$ . When dissipation is negligible  $\eta$  is equal to 1.

$$F_i = v_i \sqrt{\eta * m * k} \quad (8b)$$

For instances where the energy available in the striking object is not related strictly to its mass and velocity, the formulas can be adjusted accordingly based on the derivations.

A second approach is available that involves analyzing elastic stress waves caused by an impact, in the material of interest. This approach utilizes the mass and velocity of the striking object, and the dimensions, density, and Young's modulus of the struck object. It examines the movement of waves through the struck object and from this determines the stresses. The technique is limited, however, in that it is only applicable to

relatively simple shapes. For a complicated design such as the dog clutch that has been designed this approach is less useful(Johnson, 1972). An alternative approach is to use a software package to analyze the impact such as LS-DYNA, a general purpose transient dynamic finite element program (Livermore Software Technology Group, 2007).

## **2.5 Data Collection**

The goal of this thesis is to design, model, and experimentally test sub-systems of the flywheel powered four-bar linkage. Therefore an appropriate approach for collecting data during the testing is required. The mathematical model will be capable of calculating the position, speed, and acceleration of the flywheel and four-bar linkage. The difference between the two will be a result of any slippage in the clutch and the deflection of the shock absorber. The flywheel and input link of the four-bar linkage both have rotary motion. Therefore in order to measure either, the prototype must be instrumented with rotational sensors at the input link of the four-bar linkage and the flywheel shaft. The primary focus of the desired mechanism is the transfer of energy from the flywheel to the opposing robot. Energy is primarily a function of velocity, implying that it is logical to monitor velocity for the validation. This is also ideal because position and acceleration are only one step away through a integration and differentiation, respectively. If, for example, position were measured, then a differentiation would be required for velocity. This often leads to computational noise, even if the sensor's resolution is at least 10 times greater than what is mechanically required. If acceleration is desired then another differentiation is required, leading to further complications (Slocum, 1992).

Angular velocity is measured with rotary velocity transducers known as tachometers. There are a variety of tachometers types including mechanical ones based on the Coriolis force, digital tachometers, permanent magnet stator dc tachometers, drag-torque tachometers, dc brushless tachometers, and digital shaft encoders. One mechanical tachometer relies on vibration and the precession of a rotating body. It detects the angular velocity electronically with a piezoelectric element by measuring the displacement of a vibratory member being influenced by the Coriolis force, which is proportional to the angular velocity. This type of tachometer, however, is not that popular(Electronic Manufacturers, 2007). Digital tachometers differentiate the output of an optical or hall-effect encoder. This is essentially a position sensor and is again subject to noise spikes, although it is not affected by electrical noise. A permanent magnet stator dc tachometer is analog and is the opposite of a dc motor. The rotation of the armature past the magnets induces a voltage proportional to the rotational speed of the armature. One downside to this type of tachometer is that it has a small number of armature coils. As the brushes pass from one set of windings to the next it results in a pulsating output known as a ripple. Increasing the number of coils and filtering techniques can alleviate this issue. Drag-torque tachometers are made up of a magnet that rotates inside of a cup. The rotating magnet induces eddy currents which produce a torque on the cup proportional to the velocity. This type of tachometer is subject to thermally induced errors. DC brushless tachometers are similar to permanent magnet stator dc tachometers but are essentially turned inside out. As the name describes, there are no brushes, so some electrical means of switching between the windings is necessary. This eliminates the ripple effect and brush maintenance but increases cost and complexity(Slocum, 1992).

Another option is digital shaft encoders. They are a relatively inexpensive possibility, the primary challenge being packaging and data collection.

The problem with almost all testing is that the very act of measuring the test changes the results. Therefore measuring techniques that have minimal effect are preferred. High speed video cameras allow for data collection with a lot more context and minimal interference. Speeds of 1000 frames per second can be expected and give a better overall picture of what is happening. For example, a tachometer typically will give a speed, but unless its resolution is considerably high it won't show vibrations. On the other hand high speed video can require considerable more time to analyze than measured data.

Given the options reviewed, a high speed video camera was chosen as the best data collection method for multiple reasons. It is readily available for use, it has minimal interference on the actual test, it does not require any additional equipment beyond the camera, and it is much easier to determine how the collected data is associated with mechanical behavior.

## **2.6 Dynamic Modeling**

Dynamic modeling uses a mathematical model to represent a dynamic system so as to describe the dynamic behavior of the actual system. The purpose of this is to better understand a mechanical system when dynamics are introduced. The mechanical system can often be simplified by making key assumptions in the model. For example by considering the different components in a mechanical system as point masses connected by massless rods, the required calculations decrease considerably and the model is easier

to conceptualize. In order to make these simplifying assumptions a few key rules must be followed:

1. The mass of the model must equal that of the original body
2. The center of gravity must be in the same location as that of the original body
3. The mass moment of inertia must equal that of the original body.

There are numerous methods for developing a mathematical model to describe a dynamic mechanical system(Belliveau, 2002). The most popular of which in the reviewed literature is the Lagrangian approach. The Lagrangian approach effectively uses Newton's laws and looks at the conservation of energy and momentum. This approach makes sense when the item of interest is the energy transfer and the finer details such as internal forces are not required to be known. A second approach that is popular is a lumped parameter model in which the system is simplified and then described using kinematic and dynamic equations of motion. These can include modeling the mechanical system as a series of differential equations in state space that can then be solved numerically.

## **2.7 Summary of Research**

The literature that has been reviewed shows that there has been no previous work that exactly addresses the topic of an intermittently flywheel-powered four-bar linkage. Similar mechanisms have been created, analyzed, and modeled for punch presses, but for much different purposes that look at different parameters. None of the presented punch press papers examined the clutch aspect and how it affects the system. Much literature was found in relation to clutches, but again for different purposes, and they only addressed the clutch aspect, not how the engagement of the clutch affects the system as a whole. Finally the topic of four-bar linkages is very well known with much literature

available for their synthesis and analysis. All of the information that has been found and presented is critical in better understanding the problem and provides a number of potential approaches in addressing it.

### **3. Overview**

The research methodology followed the natural progression of starting very broadly and transitioning to more specific research as the key problems were identified. First the project goals, and functional requirements with associated design parameters were identified. This resulted in a proposed mechanism that required key design values to be chosen. Next an analysis was performed in order to verify the feasibility of the proposed design and identify its limitations. This analysis showed that the primary limiting factor in the design was the ability to mitigate the impact force in the dog clutch. An impact force mitigation strategy was chosen and experimental testing performed to verify the solution. Testing subsequently showed that the proposed solution did not solve the problem effectively. A secondary solution was implemented consisting of a torque limiting overload slip clutch in-between the flywheel and male side of the dog-clutch. To prove this solution and better understand the system, a mathematical model of the dynamic system was created using MATLAB. The model was used as a tool to perform a cost-benefit analysis for each design parameter value capable of being changed. This showed that a torque limiting overload slip-clutch did not provide any benefit. This resulted in the conclusion that the primary limiting factor in launching an opposing robot upwards into the air using the proposed mechanism is the rubber shock absorber material limitations when subjected to high-velocity impact. With this limitation known, a final

design is proposed that represents the maximum capabilities of the mechanism in its current state.

## **Chapter 2: Research Methodology**

### **4. Introduction**

This section outlines the research methodology. The design process is very iterative and as such, the methodology outlined in this section cannot be organized to perfectly match the actual design. Therefore this section is organized according to the overall methodology used during the research process and incorporates the final results of each step. It must be kept in mind that each step was influenced by prior and subsequent steps due to its iterative nature. Therefore do not consider any step described here to be independent of the rest, but rather a part of the overall process outlined.

#### **4.1 Project Goal**

The research methodology began with a goal to quantify the desired results of the project. This goal was used to analyze and compare different options when making necessary design decisions. As these design decisions were made and the problem better analyzed, the project's specifications grew more detailed. The following goal and design specifications are the result of these iterations.

##### **Goal**

Analyze and design a lightweight and compact energy transmission mechanism for the purpose of throwing an opposing thirty pound robot ten or more feet into the air in the sport of robotic combat.

## Design Specifications

- General
  - Capable of being implemented on a 30 pound combat robot
  - Capable of actuating at least 20 times in a 3 minute period with no external interaction beyond activation
  - Electromechanical assembly must weigh less than 15lbs (not including batteries)
  - Must be powered by less than 60 volts dc
  - Must be able to be controlled remotely
  - Must be able to be mechanically locked when not in use
  - Must fit into a box 18x12x8 inches when in the smallest configuration.
- Flywheel
  - Disk with maximized moment of inertia
  - Less than 3 inches wide
  - Maximum of 8 inch diameter
  - Spins on an axis parallel with the ground
  - Capable of handling forces/stresses caused by centripetal forces
- Clutch
  - Clutch must be able to fully engage, disengage, and transfer the required energy in under 50 milliseconds
  - Must be functional for at least 100 cycles with minimal repair/replacement ( for example replacing consumables)
  - Able to be engaged/disengaged remotely
- Four-Bar Linkage
  - Must be theoretically able to launch a 30 pound robot at least 10 feet vertically (406 joules of energy)
  - Can have a maximum coupler point thrower vertical displacement of 12 inches
  - Throws the robot forward and upwards
  - In reference to the opposing robot when the four-bar is at the end of its throw, the vertical component of the velocity must be larger than its horizontal component.
  - The vertical component of acceleration must always be positive.

## 4.2 Functional Requirements and Design Parameters

The design process was heavily influenced by the use of functional requirements and design parameters. This methodology consists of determining what the problem to be

solved is and then asking what functional requirements the solution requires. Once the functional requirements are known, then design parameters can be brainstormed. Design parameters are the physical embodiment of the solution that meets the functional requirements. Three high-level design parameters were created and the best solution then chosen using the design specifications as a base of measure. The following sections outline the decision process for the high-level subsystems.

#### **4.2.1 Energy Storage**

##### **Functional Requirement**

Method of storing energy to be released very rapidly as kinetic energy.

##### **Design Parameter**

Energy takes two forms: kinetic and potential. These two forms can be stored using a variety of methods including chemical, biological, thermal, mechanical, electrical, and electrochemical. Each of these methods has its own advantages and disadvantages for this application. Chemical storage methods include fossil fuels and bio-fuels. However the North East Robot Club prohibits the use of internal combustion engines in competition. This effectively eliminates chemical methods as a viable option. Biological and thermal storage methods are simply not a practical method for this application due to the inherent energy conversion challenges. Electrochemical methods include batteries and fuel cells and are a common solution for mobile energy storage needs. The most popular battery technology currently used combat robots are lithium ion A123 batteries. Lithium-ion batteries have the highest power density of readily available battery technologies(All About Batteries, 2011). Electrical storage methods include capacitors and super-capacitors. These are capable of storing up electrical energy over

time and rapidly releasing it but are far from ideal for long term energy storage. Finally mechanical energy storage methods include compressed air, hydraulics, springs, and flywheels. Each of these are effectively mechanical capacitors or inductors with their own set of properties. Considering these restrictions the following energy storage methods are available:

- Chemical Battery
- Electrical Capacitor
- Compressed Air (Pneumatics)
- Hydraulics
- Spring
- Flywheel

The Robot Fighting League requires that all flywheels, hydraulics, and springs store zero energy at the start of the match. This means that the energy must be stored in a battery or pneumatics before the match. Pneumatics are the most common solution for launching robots into the air, however pneumatics can often be bulky and have a relatively low energy density when taking the entire system into account. Therefore, batteries are the best option for storing the energy before the match. This leaves the remainder of the methods as a way to have an energy storage buffer. A bank of capacitors can be used to store up battery energy for quick release but electric motors are limited by heat buildup in how quickly they can convert electric energy to kinetic energy. This can be mitigated through various cooling techniques and motor size. However, for these options to have any appreciable effect, the size and weight of the system must be greatly increased. Hydraulics are very heavy in comparison to all of the other options and are

less than ideal in for quick-response systems. Springs as a form of energy storage are an excellent choice and require that the spring be deflected. Typically this will be done relatively slowly with high torque through an electric motor and gearbox. In order to achieve the desired gear reduction a large and heavy gearbox will be necessary, at the expense of both weight and efficiency. Additionally a method of engagement and disengagement will be required. In order to increase the energy stored, the size of the spring would have to be increased, and the rest of the system scaled proportionally. This system is viable but would become quite complicated. The final option to buffer the energy is a flywheel. An electric motor can be used to convert the electric energy of the battery to kinetic energy in the flywheel where it is stored up over time. The energy can then be transferred to the other robot through a mechanism to be chosen. The unique aspect of a flywheel is that the energy stored is proportional to the square of the velocity. Therefore it is quite easy to increase the energy stored with minimal effect to the rest of the system, within practical limitations. Therefore, of all of the options available a flywheel is the best solution taking into account complexity, size, weight, and energy density.

#### **4.2.2 Energy Release**

##### **Functional Requirement**

Release the kinetic energy stored in the flywheel into the opposing robot.

##### **Design Parameter**

A variety of methods exist to release or transfer energy from a flywheel to an external mass. The best method is a linkage. Three practical options exist in terms of linkages to do this. These are a two-bar linkage, or lever, a four-bar linkage, or a six-bar

(or greater) linkage. A two-bar is the simplest solution, however it is restricted in that the point of force application is forced to move through a circular arc. The disadvantage to this is that as the point of force application moves upwards it also moves backwards, while the opposing robot is either moving forward or not moving horizontally. This means that at some point during the arc the opposing robot may fall off the linkage. It is advantageous in its simplicity. The second option is a four-bar linkage. This type of linkage is extremely common and versatile. A four-bar allows a variety of motions including having the coupler point move upward as well as forward. It is more complicated than a two-bar but avoids the disadvantages of a two-bar. The final solution option is six or more bars. This options allows much more flexibility in terms of the coupler point motion, but at the expense of greater complexity and weight. For most applications six or more bars are considered over-kill as you can get the same result with four-bars. That is the case for this application. Weighing the advantages and disadvantages between the two-bar and the four-bar, the latter offers much better coupler motion control in comparison to the two-bar, with minimal additional complexity.

### **4.2.3 Flywheel Engagement/Disengagement**

#### **Functional Requirement**

Engage and disengage the flywheel with the energy release linkage.

#### **Design Parameter**

A variety of methods exists to engage and disengage the flywheel with the energy release linkage. The first incorporates a specialized linkage, while the second two use a clutch and/or cam capable of interfacing with any linkage. These options are discussed as follows:

- Linkage Method

The first method is inspired by the punch press mechanisms discussed in the literature review and involves the design of a linkage with two degrees of freedom. One input would be the flywheel, and the second would be a simple actuator. The linkage would be synthesized such that when in a particular orientation a link rigidly connected to the flywheel would spin with the flywheel, but would be in an effective dwell position relative to the coupler point of the linkage. In other words part of the linkage would spin continuously but allow the other part (the coupler) to remain stationary. Then by changing the orientation of the appropriate link, the linkage would come out of the dwell and the flywheel would power the coupler link. This effectively creates a linkage based clutch that avoids many of the problems experienced by traditional clutches. It does add complexity and weight to the system, but the overall benefits may outweigh the disadvantages.

- Cam Method

The second method is to transmit the force from the flywheel to the coupler link through a cam, instead of directly powering an input link. This design would still require a clutch, but would allow much more control. With a more traditional design, when the clutch is engaged the flywheel instantly sees the load of both the four-bar linkage and the thirty pound weight at the coupler point, limited only by the maximum torque capacity of the clutch. However if a cam were placed between the coupler or input link and the flywheel, the system could be designed to engage at any practical rate desired. This would reduce the shock to the system on activation and allow more control in the design.

Downsides, however, are that a clutch is still necessary in addition to a cam, so the benefits are at the expense of more space and weight.

- Clutch Method

A clutch is the most straightforward solution method for this problem. To decide what type of a clutch to use a variety of requirements must be met. It must be compact and lightweight. The clutch must fit in the space the size of a 4 inch cube and weigh no more than 3 pounds. A brief examination (seen in Appendix A: Viability Analysis Calculations) of the required energy transfer with respect to time indicates that the torque required at the four bar linkage starts at a very high level. This is good when considering the flywheel because it has its greatest energy in the beginning, but raises a problem for the clutch. Clutches have a torque build up time that dictates how long it takes to go from disengaged to fully engaged. The implication of this is that the clutch is weakest when the required linkage torque is greatest. A positive contact clutch has the smallest torque build up time of all of the clutch types. However, it is the harshest engagement method. Electromagnetic clutches with suitable torque specifications on the order of 600 in\*lb are far too heavy for this application, weighing between 15 and 100lbs(Ogura Industrial Corp). A frictional clutch may be possible, but developing a system to handle both the torque, and engage and disengage quickly enough would be difficult within the size and weight constraints. A friction clutch feasibility study can be found in Appendix A: Viability Analysis Calculations, which indicates that it is practical. The most practical solution is a positive contact clutch. However the system must be designed such that the stresses do not exceed what the materials can handle. To account for this a hybrid solution may be necessary. There is a design trade-off between speed of engagement and

maximum allowable stresses. This may be approached using a positive contact approach (dog clutch) in addition to a torque limiting clutch, such as a frictional slip clutch. The dog clutch allows for a short torque build up time and can handle high torque loads. The slip clutch limits the torque to the maximum required and makes a gear reduction system feasible. The introduction of compliance into the dog clutch can assist in controlling the acceleration and jerk. Jerk being the rate of change of acceleration with respect to time. This compliance can be in the form of a replaceable rubber insert designed to deform on each cycle. These solutions allow for a number of adjustable design parameters to produce the desired system response.

- Conclusion

All three of the options presented are viable. Trial linkages were synthesized to determine the feasibility of the linkage method. It was decided that such a linkage is possible, but synthesizing one with the appropriate characteristics would be quite difficult within the packaging limitations. A cam approach does allow for complete control of the acceleration of the input link of the four-bar linkage but still requires the use of a clutch. Additionally, such a cam would have to be quite large and therefore heavy in order to have the desired effect. Finally a clutch mechanism is the most straight forward in terms of implementation and has the added benefit of a number of design parameters to control the system response. Of the various types of clutches available a dog clutch is the only one to meet all of the requirements.

#### **4.2.4 System Design**

In sections 3.3.1 through 3.3.3 different options were explored for each portion of the high-level system design. The conclusion was to use a chemical battery to power an

electric motor that spins up a flywheel. The flywheel acts as a "mechanical inductor" in that it can store up energy slowly and then release it rapidly. The kinetic energy of the flywheel is transferred into a four-bar linkage which is used to release the energy into the opposing robot in a controlled manner. The flywheel will be continuously spinning so a dog clutch will be used to engage and disengage the four-bar linkage with the flywheel. The flywheel and four-bar linkage design is relatively straightforward in terms of critical decisions that have to be made about the various aspects. However, the dog clutch design introduces a number of possibilities. In order to make these decisions, the same process was used; a functional requirement was determined with associated design parameters brainstormed. Comparing these ideas the best solution was chosen. Table 1 shows these functional requirements and design parameters for the entire system. The design parameter in bold indicates the one(s) chosen.

TABLE 1: FUNCTIONAL REQUIRMENTS AND DESIGN PARAMETERS

#	Functional Requirements	#	Design Parameters	
<b>FR 1</b>	Method of storing energy to be released very rapidly as kinetic energy.	<b>DP 1</b>	Compressed Air (Pneumatics)	
			Hydraulics	
			Spring	
			<b>Flywheel</b>	
<b>FR 1.1</b>	Method of supplying energy to be stored	<b>DP 1.1</b>	<b>DC Motor</b>	
			<b>Chemical Battery</b>	
			Electrical Capacitor	
<b>FR 1.2</b>	Method of transmitting energy to be stored	<b>DP 1.2</b>	<b>Timing Belt Pulley System</b>	
<b>FR 2</b>	Release kinetic energy into the opposing robot to throw it	<b>DP 2</b>	Two-Bar Linkage	
			<b>Four-Bar Linkage</b>	
			Six-Bar Linkage (or greater)	
<b>FR 3</b>	Intermittently couple the flywheel with the four-bar linkage	<b>DP 3</b>	2 DOF Linkage	
			Clutch and Cam	
			<b>Clutch</b>	Friction
				Overrunning
				Magnetic
				Fluid Coupling
	<b>Positive Contact (Dog-Clutch)</b>			
<b>FR 3.1</b>	Engage	<b>DP 3.1</b>	<b>Mechanism to engage the dog clutch</b>	
<b>FR</b>	Hold male and female sides of the dog	<b>FR</b>	<b>Tri-Lever Hooked Catch</b>	

<b>3.1.1</b>	clutch apart	<b>3.1.1</b>	Electromagnet
<b>FR 3.1.2</b>	Release the male and female sides of the dog clutch so they can engage	<b>FR 3.1.2</b>	<b>Force-closed cam powered by a servo motor to open the tri-lever hooked catch</b> Cable system to open tri-lever, springs to close
<b>FR 3.1.3</b>	Force the male and female side of the dog clutch together	<b>FR 3.1.3</b>	<b>Belleville Washer Stack</b> Coil spring Face cam Solenoid Pneumatics DC linear actuator
<b>FR 3.2</b>	Transmit Torque	<b>DP 3.2</b>	<b>Three bosses on the male side of the dog clutch, three mating slots on the female side</b>
<b>FR 3.3</b>	Disengage	<b>DP 3.3</b>	<b>Mechanism to disengage the dog clutch</b>
<b>FR 3.3.1</b>	Separate the male and female side of the dog clutch	<b>DP 3.3.1</b>	<b>Face cam to push the male side of the dog clutch away from the female. Powered by the motion of the mechanism</b>
<b>FR 3.3.2</b>	Reengage the method of holding the male and female side of the dog clutch apart	<b>DP 3.3.2</b>	<b>Force-closed cam powered by a servo motor to close the tri-lever hooked catch</b> Tension or Compression spring to open the tri-lever hooked catch

The brainstorming and design decisions made resulted in a mechanism design.

This design was implemented in the CAD software package Solidworks. Special care was taken to ensure that the mechanism design took into account availability of parts, weight, manufacturability, maintainability, and functionality. The final design is shown in Figure 9. As stated the methodology, the design process was highly iterative and so the presented final design is the product of many refinements. The forthcoming section discuss the detailed design of each subsystem.

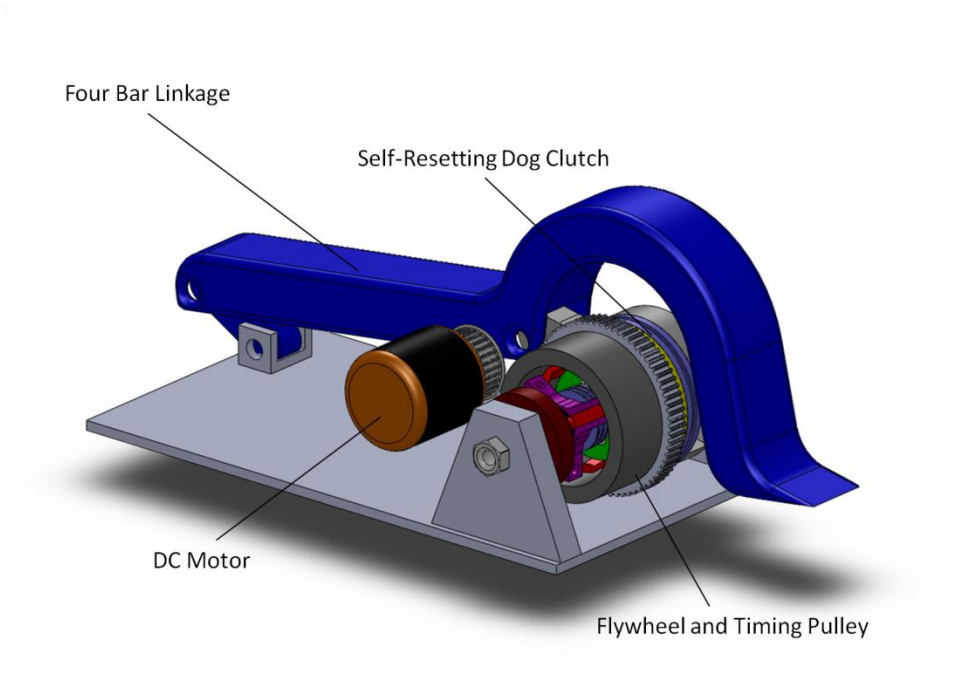


FIGURE 9: FINAL DESIGN CAD MODEL

An exploded view of the flywheel and dog clutch mechanism with the input link of the four-bar linkage can be found in Figure 10.

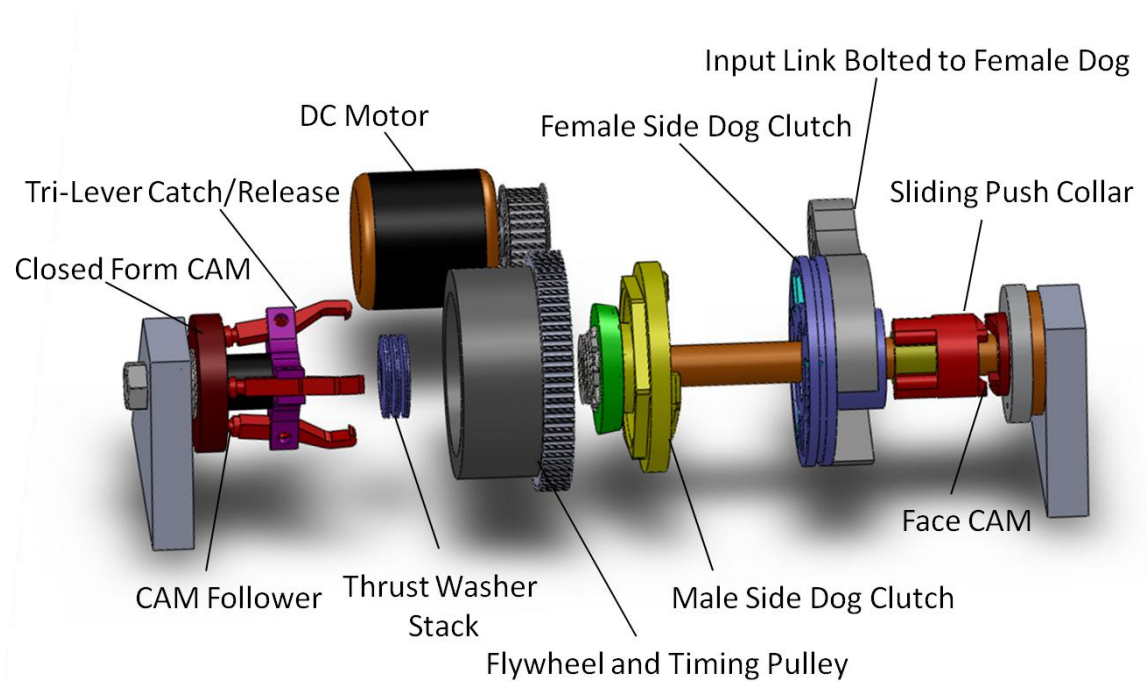


FIGURE 10: FINAL DESIGN CAD MODEL EXPLODED VIEW

The mechanism operates in the following fashion. The primary function is to engage the male and female sides of the dog clutch. The female side of the dog clutch is fixed to the input link through a series of bolts. Three slots are equally spaced around the female side and gradually slope inwards as shown in Figure 11. At the end of each slot is a pocket for the rubber shock absorber. The pocket is sized such that the rubber cannot fall out and is inserted from the back of the clutch, which is the side that the input link of the four-bar linkage attaches to. The input link of the four-bar linkage has a U shape so that it can be easily removed without disassembling the entire mechanism. The male side of the clutch is essentially the negative of the female side, aside from adjustments made for tolerance purposes.

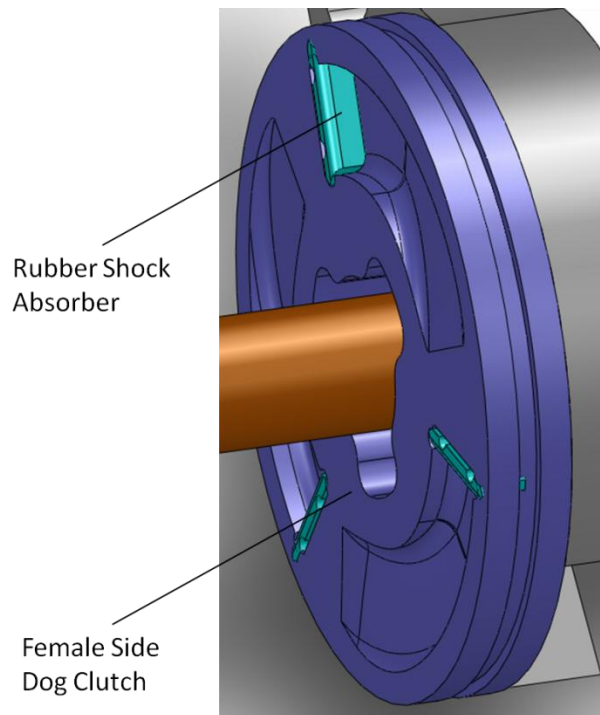


FIGURE 11: FEMALE SIDE OF DOG CLUTCH CAD MODEL

The system is designed so that the female side of the dog clutch can only rotate 90 degrees, and does not move axially. The 90 degrees was a design decision based on the re-engagement method. The male side is able to rotate continuously and also has limited

axial movement. This allows it to engage and disengage with the female side. To engage the dog clutch a Belleville (thrust) washer stack is preloaded during assembly causing the female and male side to always be forced together. To hold the male side away from the female side a tri-lever catch release mechanism is used. These three levers are able to open and close, and have a hook at the end of each that can hook on the catch plate as shown in Figure 12. The catch plate comprises of a circular plate that bolts to the male side of the dog clutch, and a needle thrust bearing. The needle thrust bearing is what the hooks actually rest on in the disengaged clutch position and allows for the male side of the dog clutch to spin free of the tri-lever catch and release. To actuate the three levers a force-closed cam was chosen in conjunction with springs that force the tri-lever to want to remain in the open position. Three cam followers are screwed into the end of each lever and have a spherical ball end. The closed force cam has three equally spaced profiles that match each other at their intersection. This profile is a dwell-rise-fall-dwell. Rotating it 120 degrees causes the tri-lever catch and release to open with a smooth and controlled motion and results in the engagement of the clutch. After the cam opens the tri-lever and the clutch is engaged, the tri-lever closes due to the spring force. The catch plate is then forced back into the grasp of the tri-lever and re-hooked. To release the clutch again the servo motor powering the force-closed cam only has to spin another 120 degrees in the same direction.

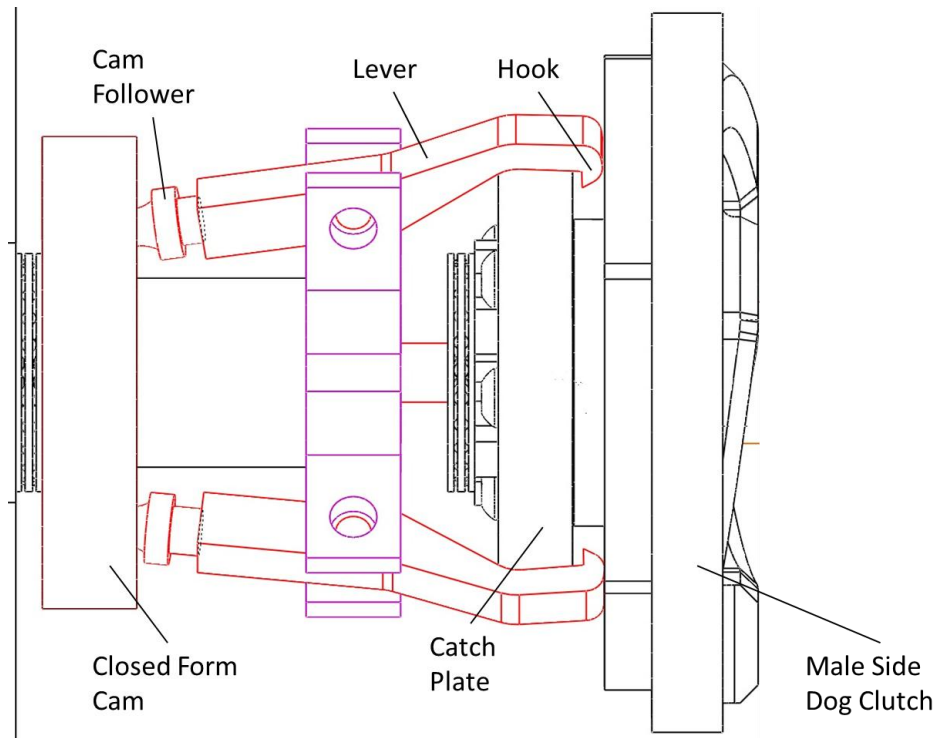


FIGURE 12: CLUTCH RELEASE AND CATCH MECHANISM CAD MODEL

After the male side of the dog clutch is engaged, it then has to be disengaged after 90 degrees of rotation. An automatic mechanical solution was chosen consisting of a face cam fixed to ground on the opposite side of the female side of the dog clutch, as shown in Figure 10 and Figure 13. This face cam has three cam profiles that are dwell-rise, equally spaced around its axis. A sliding push collar is on the inside of the female side of the dog clutch. The two are designed such that the push collar is free to move axially but is locked in rotation with the female side of the dog clutch. When the clutch engages the output side is forced to rotate. As it rotates the face cam on the sliding push collar slides along the dwell on the opposing face cam. After 60 degrees of rotation the push collar is forced to move axially away from the face cam due to the profile. This is able to slide axially, independent of the female side of the dog clutch, and push against the male side. This forces the male side of the dog clutch over, compressing the springs, and allowing

the tri-lever catch and release to again hook the catch plate. To reset the female side of the dog clutch a spring is attached to the four-bar linkage to pull it back into place.

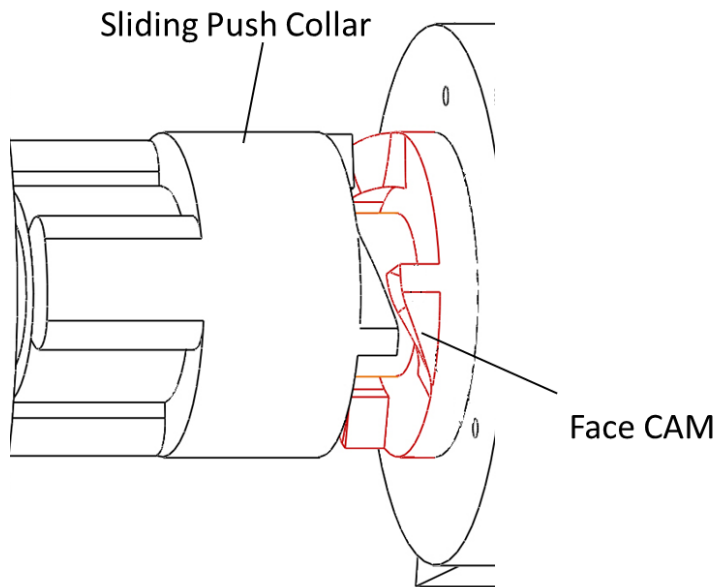


FIGURE 13: SLIDING PUSH COLLAR CAD MODEL

Finally a flywheel consisting of a steel hollow cylinder is attached to the male side of the dog clutch via screws and a mating hex boss and pocket. This is shown in Figure 14. The placement of the flywheel minimizes the additional size of the mechanism. Furthermore, the hollow design of the flywheel maximizes its specific mass moment of inertia. A timing pulley is attached to the flywheel and can be powered by a dc brushless motor. A hex interface is designed into the flywheel for torque transmission and packaging constraints.

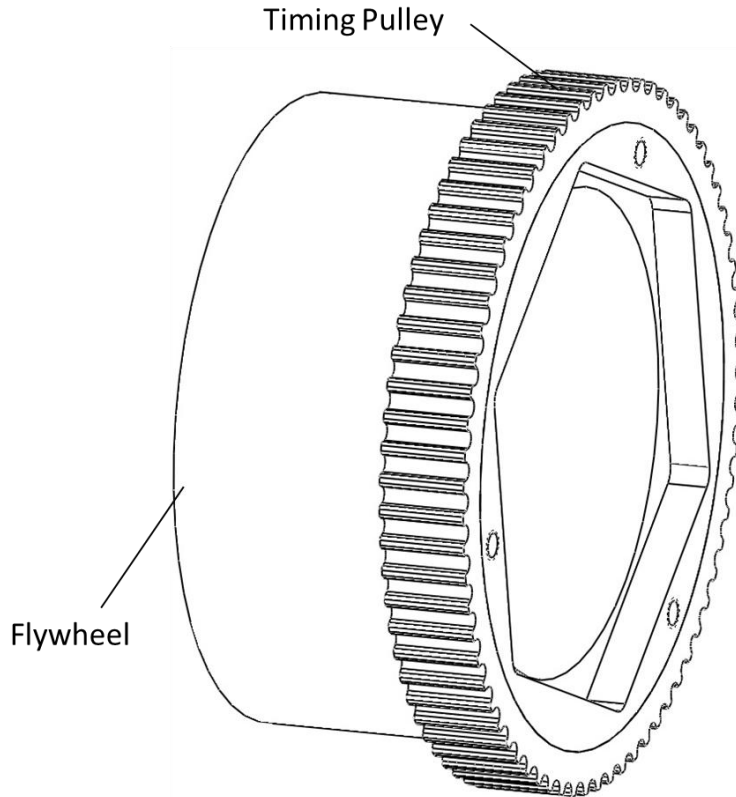


FIGURE 14: FLYWHEEL AND TIMING PULLEY CAD MODEL

This is a highly space and weight efficient design whose main strength is that it requires only two inputs, a source of power through the timing pulley, and a control input through the force-closed cam. To activate the mechanism the force-closed cam only needs to be rotated 120 degrees. The dwells are designed so that exact rotation of the force-closed cam is not critical, so long as error does not cumulatively add up over time. The mechanism is self-resetting via the power from the flywheel. The only drawback in this design is that every aspect must work as expected for the system to achieve its desired purpose. If the system is dry-fired then the four bar linkage is sped up and will run into a hard stop consisting of a rubber bumper. The dog clutch will still disengage and system damage will be avoided.

## 4.3 Feasibility Analysis

### 4.3.1 Overview

Before developing a full mathematical model of the dynamic system a feasibility analysis was performed in order to better define the project goals and verify that the embodiment of the design was practical. This was done using the software program MathCAD due to its capability to account for units. The methodology of the analysis focused on determining what was required of the mechanism to achieve the desired goal. This was done by making gross assumptions about the dynamics of the mechanism through basic kinematic and energy approaches. The initial assumption was made that a gear reduction would not be necessary and therefore an overload slip clutch was not needed. The analysis served to prove or disprove this assumption. The actual analysis discussed here can be found in Appendix A: Viability Analysis Calculations.

### 4.3.2 Required Energy Transfer and Dynamics

To determine the required energy transfer for the system, a number of prescribed parameters were necessary. These were determined when the design specifications were formulated. They were as follows: the opposing robot has a mass of thirty pounds, the desired vertical displacement over which the energy transfer can occur is six inches, and the desired throw height is ten feet. The kinetic energy required to raise a mass up to a given height is equal to its potential energy at that height. Therefore the desired energy to be transferred to the opposing robot was calculated with:  $Kinetic\ Energy = Mass * Gravity * Height$ . This resulted in a required total energy transfer of 3593 in\*lb (406 Joules). It was decided that the energy would be stored in a flywheel. A flywheel has two key design variables: its moment of inertia, and its rotational velocity. The relationship

between the energy stored in a flywheel and its moment of inertia is linear. However the energy stored in a flywheel is proportional to the square of the velocity. As such it is most efficient to maximize the velocity of the flywheel rather than its moment of inertia. For this feasibility analysis a flywheel moment of inertia of 5 in<sup>2</sup>\*lb and flywheel velocity of 8000 rpm were chosen. This resulted in a flywheel energy of 4540 in\*lb (513 Joules) which met the requirement that it be greater than the required energy.

The average force that must act on the opposing robot to achieve the energy level over a distance of six inches is 600 lbf. This was determined knowing that:  $Work = Force * Distance$ . Newton's second law indicates that the required average acceleration is then 643 ft/s<sup>2</sup>. The average acceleration was used simply because a better estimate was not available. In order to proceed with the analysis this assumption had to be made. Using basic kinematics equations it was then determined that the launch of the opposing robot must occur over .039 seconds. This in turn allowed for the maximum velocity required of the opposing robot to be calculated. This was done with the equation:  $Velocity = Average Acceleration * Time$ . This velocity is 25.1 ft/s

When the flywheel is suddenly coupled to the four-bar linkage its energy is transferred to the linkage causing the flywheel's velocity to decrease. The assumption was made that this velocity decrease occurs exponentially and is of the form:

$\omega(t) = \omega_o * e^{t*k}$  where  $\omega_o$  is the initial velocity and k is a constant that is calculated recursively until a value is found that results in the flywheel reaching  $\omega_2$ , the final velocity of the flywheel, in the desired amount of time. Once the speed was determined as a function of time, the derivative with respect to time was taken to determine acceleration as a function of time. The velocity and acceleration functions were then

plotted and are shown in Figure 15. To determine the position of the flywheel as a function of time the speed function was simply multiplied by time.

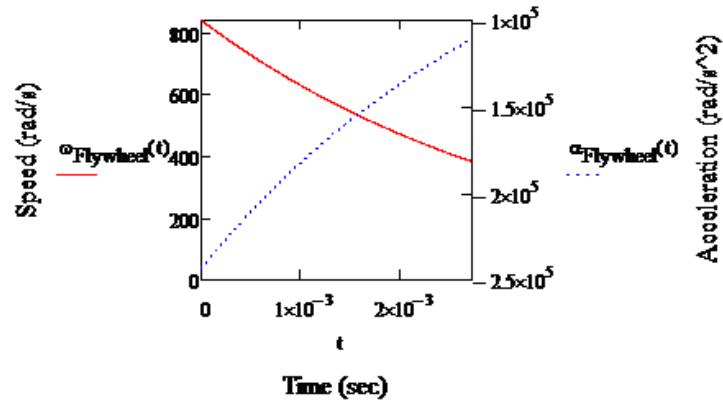


FIGURE 15: ASSUMED SPEED AND ACCELERATION OF THE FLYWHEEL AS A FUNCTION OF TIME

The torque was then calculated using the relationship  $Torque = Moment\ of\ Inertia * Angular\ Acceleration$ . The torque seen at the clutch after the gear reduction is plotted in Figure 16.

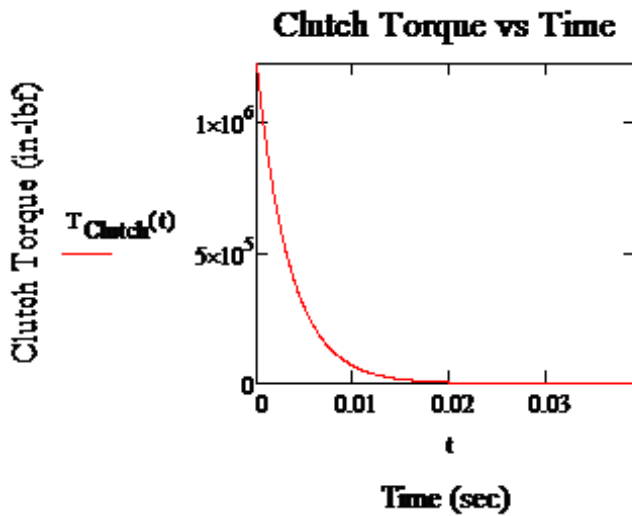


FIGURE 16: CLUTCH TORQUE VERSUS TIME

The maximum torque is at time zero and is equal to 3148 in-lbf. This quantity was used to determine the feasibility of different clutch types. A theoretical friction plate clutch with inner radius 0.625 inches, outer radius 2.5 inches and a coefficient of friction of 0.3 was calculated to require 6000 lbf of normal force between the friction clutch plates to transmit the required maximum torque. For a mechanism that must engage and disengage in a time span in the order of milliseconds, the required force in a device this size is not feasible due to packaging and weight constraints. This validated the previous decision that a dog-clutch would be the best solution.

Next the feasibility of a dog-clutch was validated. The values chosen for this part of the analysis were a result of working concurrently through multiple iterations on both the CAD model and the mathematical analysis. A dog clutch with the male side shown in Figure 17 having three evenly spaced protruding dog bosses 0.1875 inches tall and 0.7500 inches wide at an average radius of 1.4375 inches was designed. The female side had mating slots.

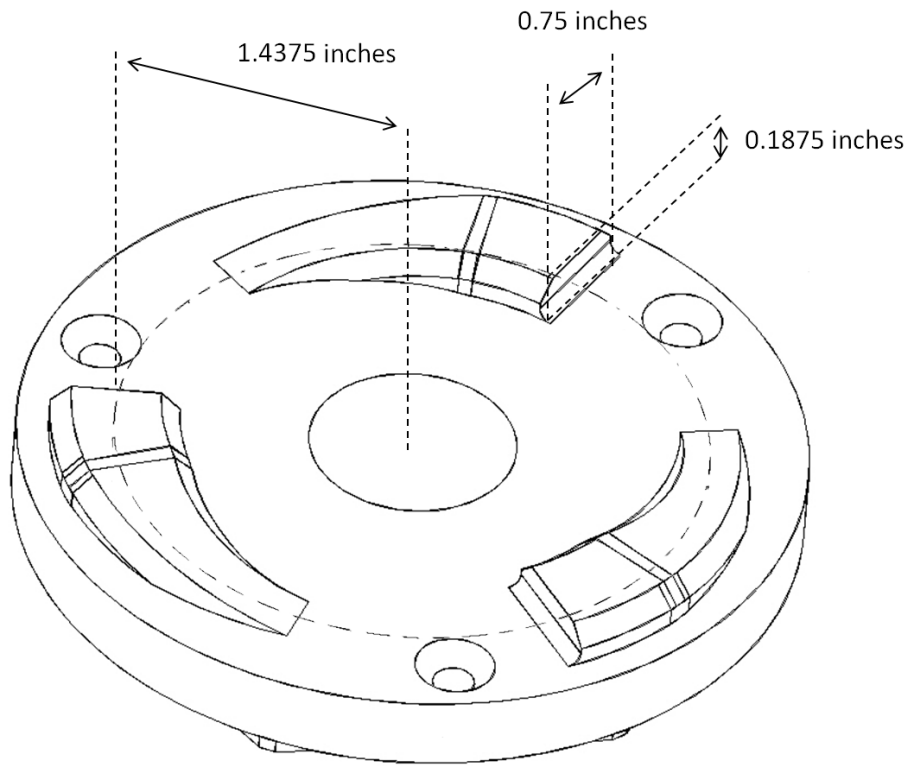


FIGURE 17: MALE SIDE DOG CLUTCH INITIAL DIMENSIONS

Three dogs divided the maximum force seen by each dog, at peak torque, to 750 lbf each. A rubber shock mount was designed into the impact face of the female side of the dog clutch to reduce the impact force. Rubber has no single value of modulus of elasticity. It varies depending on the temperature, compression, strain rate, and a variety of other factors. Therefore an estimated Young's Modulus of  $6.73 \times 10^4 \text{ psi}$  was chosen based on static load testing done in section 3.5.3 that acted as an extremely rudimentary representation of the actual material properties. The dog clutch design limited the size of the shock absorber to roughly  $0.75 \times 0.25 \times 0.25$  inches. This correlated to a spring constant value of  $3.785 \times 10^4 \frac{\text{lbf}}{\text{in}}$ . Energy methods allow for an estimation of the impact force of two colliding bodies. This was taken advantage of and an impact force of  $1.855 \times 10^4 \text{ lbf}$

was determined. This force allowed for stress analysis of the dog clutch. The impact force was roughly 25x the force seen from just the torque load. The ratio of the height of each dog boss to its footprint indicated that beam analysis was not appropriate. The direct shear force acting in the plane where the boss meets the clutch body resulted in a shear stress of  $5.152 \times 10^4 \text{ psi}$ . The compression force on the impact surface of the dog clutch resulted in a compressive stress of  $1.39 \times 10^5 \text{ psi}$ . Assuming a yield strength of  $1.65 \times 10^5 \text{ psi}$  for 4140 steel at Rockwell hardness C this resulted in respective safety factors of 3.2 and 1.3. A safety factor of 1.3 doesn't leave much margin for error, however the purpose of this analysis was only to determine if the approach was feasible and if further analysis was appropriate. These results indicated that further analysis was warranted before a final decision could be made.

## **4.4 Impact Mitigation**

### **4.4.1 Introduction**

The feasibility study indicated that for the approximated average value of Young's Modulus of rubber, the impact force was 25x the torque load. This was cause for concern and warranted a more in-depth study, given the low safety factor of 1.3 and potentially large margin of error. The feasibility analysis showed that the shock absorbers must be able to transfer 406 joules with an impact speed of approximately 70 MPH. This posed a significant engineering challenge that warranted an in-depth study.

### **4.4.2 Shock Absorption**

Until this point it had been assumed that rubber would be used as a shock absorber. This was valid for the feasibility analysis but in terms of the actual design the

method of shock absorption was of great importance. The goal was to reduce shock, or dampen the impact force. This problem statement enabled a variety of options. Possibilities included deformable metal, hydraulic pistons to act as dampers, springs, and a variety of rubber or plastic materials. Soft deformable metal would have worked very well to absorb a significant amount of energy in a small space. The disadvantage was that ductile metal would permanently deform when it absorbed the energy. This meant that for subsequent impacts the energy absorbing capacity would be diminished. Additionally the dog clutch is a close tolerance mechanism with a number of moving parts. The deformation of the metal shock absorber would have the possibility of jamming the mechanism. For these reasons it was decided that using a highly deformable metal would not be practical. A second option was a hydraulic piston built into the dog clutch to absorb the energy through the movement of the fluid through pin holes in the piston. The size of the holes would govern the damping coefficient. The problem with this solution was packaging. To build such a complicated mechanism into the dog clutch in a way that it would work reliably through its life was impractical. Springs offer the advantage of deforming when under load and then returning to their original shape when the load is released. This property makes them ideal in comparison to deformable metal; however they are limited in their energy absorption capabilities and introduce potential vibration issues. Additionally, packaging would have been quite a challenge. This leaves the final option of rubber or plastic materials. Attempting to model their behavior for this application was impractical given number of unknowns and complexities of material behavior at high strain-rates. Therefore testing was performed to validate this portion of the design. A variety of rubbers were selected for testing based on material properties and

availability. These included shore A 40 and 60 durometer cast urethane, Shore A 30, 60, and 80 durometer silicone rubber, natural gum rubber, foamed natural gum rubber, polyurethane foam, and EVA foam.

#### **4.4.3 Force versus Deflection at Low Strain Rate**

The first test performed was to determine the relationship between force and deflection at low strain rates. Rubber shock absorbers performance depends on shape and physical packaging constraints. An unrestrained rubber shock absorber will work much differently than one constrained in an enclosure. Therefore a mechanism was built to simulate the packaging of the rubber in the dog clutch. This can be seen in Figure 22. The mechanism consists of an aluminum block machined to accept the 0.75x0.25x0.25 inch rubber slug. Two shoulder bolts are screwed into this block. A second aluminum block with two bronze bushings was designed such that it could slide along the two shoulder bolts as shown in Figure 22. A protruding boss was milled into the sliding part such that it could slide into the slot that held the rubber in the stationary portion. This allowed for the rubber to be compressed in a way that closely approximated its packaging in the dog clutch. Loading the rubber through a range of forces and measuring the deflection enabled the relationship between force and deflection to be determined. To make these measurements a large arbor press was calibrated and used. An arbor press consists of a rack and pinion that converts torque on an input lever to linear movement and force. This capability was taken advantage of by applying a known torque on the lever arm, which resulted in a known force on the press. First, the press was calibrated by placing a scale in the press and hanging a bucket from the input lever. Bricks of a known weight were added to the bucket and the resultant force measured on the scale. This allowed for a

linear relationship to be determined between the weight of bricks and resultant force. Next, a dial indicator was placed on the top of the arbor press such that the movement of the rack portion of the press could be measured. The rubber holder was then placed in the press and the experiment performed for a variety of rubber materials. A diagram of the testing setup can be seen in Figure 18. This testing served two purposes: it acted as an initial test to determine the feasibility of the different materials, and gave an indication of the force versus deflection properties (at low strain rates) of viable materials.

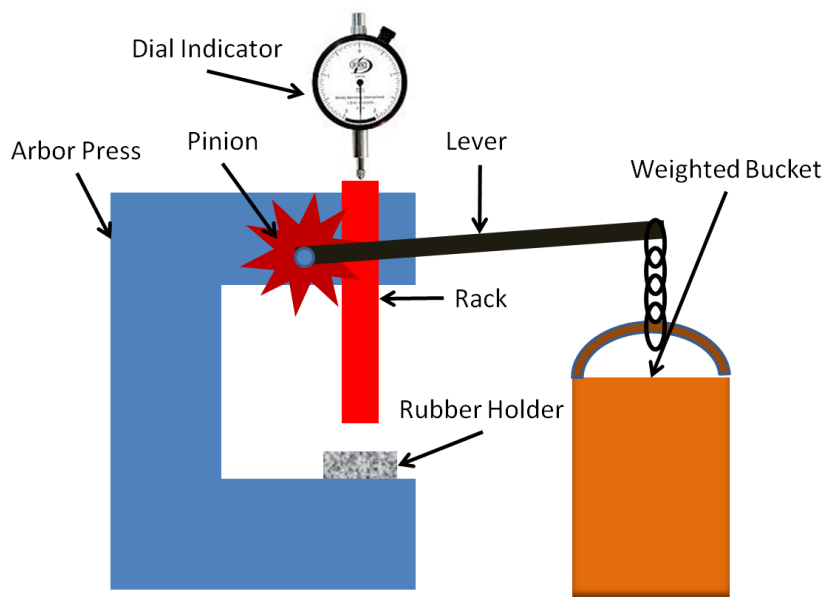


FIGURE 18: ARBOR PRESS BEING USED TO DETERMINE FORCE VS DEFLECTION

From this testing it was determined that the shore A 40 and 60 durometer cast urethanes were not a feasible material. The urethane tended to shear and break apart even at low strain rates. Additionally, after full compression it took hours to regain its original shape. Both of these characteristics were highly undesirable. The best material tested was the natural gum rubber. It regained its original shape almost instantly and had no visible damage. The force versus strain relationship determined for natural gum rubber can be seen in Figure 19.

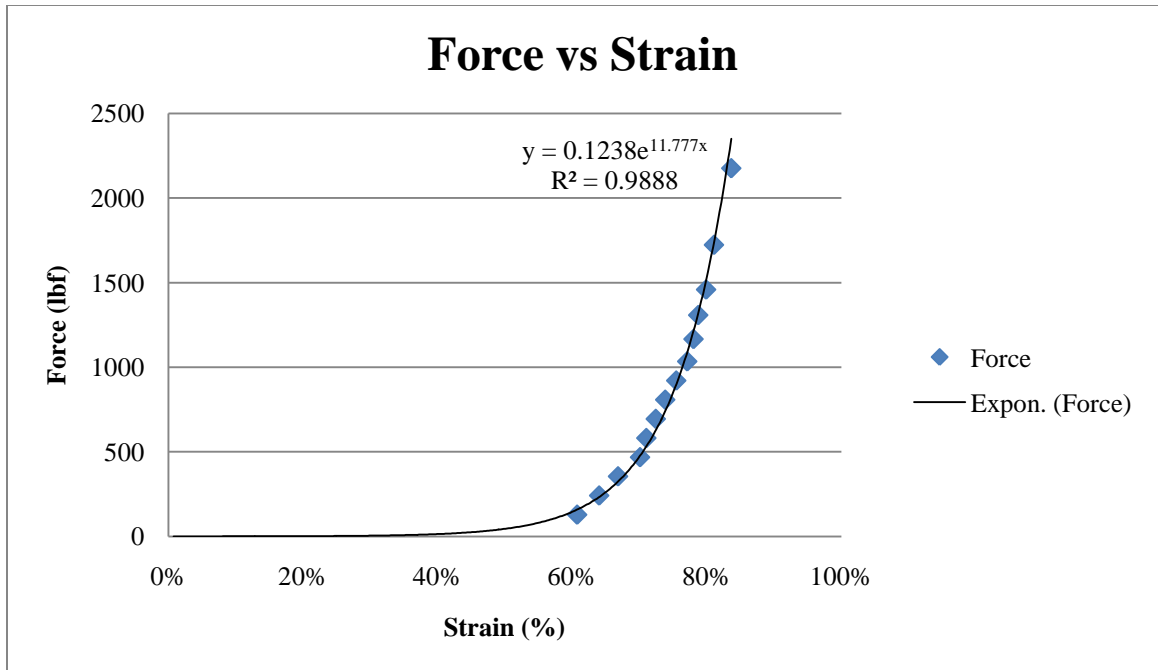


FIGURE 19: FORCE VS DEFLECTION, NATURAL GUM RUBBER

The key property of the relationship is that the force increases exponentially with the increase in deflection (% strain). This result was very useful for modeling purposes. The specific increase in force for a given high strain-rate compression could not be determined, but knowing the type of relationship allowed for a more accurate model. The natural gum rubber results were comparable to the behaviors of the other materials tested.

#### 4.4.4 Impact Testing

The relationship between force and compression for low strain rates had been determined. However that testing had provided no indication as to the viability of the different materials for the strain rates and energy transfer that was required of the shock absorber. Therefore testing was performed to determine if any of the materials could survive such extreme impacts. The required energy transfer was a total of 406 joules through three 0.25x0.25x0.75 inch rubber shock absorbers with an impact velocity of 70

MPH. A number of test requirements were formulated, along with the design and fabrication of the required test equipment. The first requirement of the test was a source of kinetic energy equal to at least 136 joules and moving at 70 mph. The 136 Joules was derived by dividing the total required energy of 406 joules by the number of teeth in the dog clutch that the energy is transmitted through. For testing simplicity it was decided that only options that had linear movement would be considered. These requirements concluded in the design and building of a large air-powered cannon. This consisted of an 8 foot by 3 inch diameter PVC pipe acting as an accumulator. This was attached to a 2.5 inch ball valve that connected to a 6 foot long by 3 inch diameter PVC barrel. A mass of 3.5 pounds was chosen which resulted in an energy value of 777 joules when moving at 70 mph. This was roughly 6x the required energy transfer to account for system losses throughout the entire test mechanism. A method for calibrating the air cannon was necessary to determine what pressure the accumulator should be charged to in order to achieve the desired projectile speed. A Canon 7D DSLR camera was used to take photographs of a 6.5 pound projectile as it exited the barrel at different pressures. During the photograph a flash strobe was set to go off at 120 Hz. This produced a freeze frame effect that allowed for the speed of the projectile to be calculated. The photograph for 80 PSI can be found in Figure 20.



FIGURE 20: PROJECTILE MOTION STROBE PHOTOGRAPH

Tests were run at 40, 60, 80 and 100 PSI. These four tests provided the relationship between pressure and projectile speed for this specific air cannon. Using this relationship the appropriate pressure to achieve the desired projectile velocity was calculated for a 3.5 pound projectile. This was determined to be 50 PSI. The associated calculations and test data can be found in **Appendix B: Impact Testing**.

The key condition in this testing was that the shock absorbers did not have to absorb all of the energy, only transfer it. Therefore the next requirement was that the test setup be such that the previously designed and built rubber holder be re-used so that the required energy was transferred through the rubber as the rubber was compressed. Additionally the rubber needed to see an impact speed on the order of 70 mph. First a large spring was chosen that was capable of absorbing the required energy. This spring was 12 inches in length, had an outer diameter of roughly 4 inches and a wire diameter of 0.5 inches, resulting in a spring rate of 207 lbs/inch. This spring was placed between a fixed plate of steel and a block of aluminum capable of sliding along two parallel shafts. This allowed the spring to be compressed between the plate and sliding aluminum block. The rubber holder was bolted onto the aluminum block. A 0.5 inch steel plate was bolted to the sliding part of the rubber holder to act as an impact surface. This assembly allowed for the steel impacting plate to be hit with the projectile from the air cannon. The sliding part would slide down the two shoulder bolts until the boss came into contact with the rubber sample being tested. This would begin to compress the rubber and it would absorb some of the impact energy. The energy not absorbed by the rubber would be transferred through the rubber into the aluminum block. This energy caused the aluminum block to slide down the two parallel shafts and compress the spring. The deflection of the spring

indicated how much energy was transferred through the rubber and into the spring. This rubber impact testing mechanism can be seen in Figure 21 and a close up of the rubber holder and steel projectile in Figure 22.

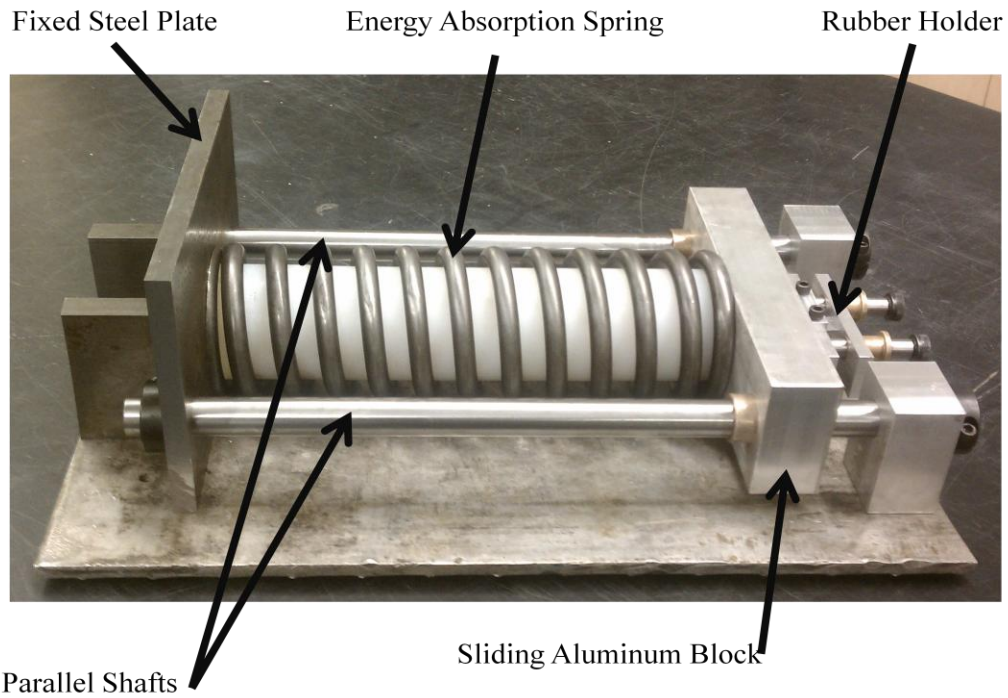


FIGURE 21: RUBBER IMPACT TESTING MECHANISM

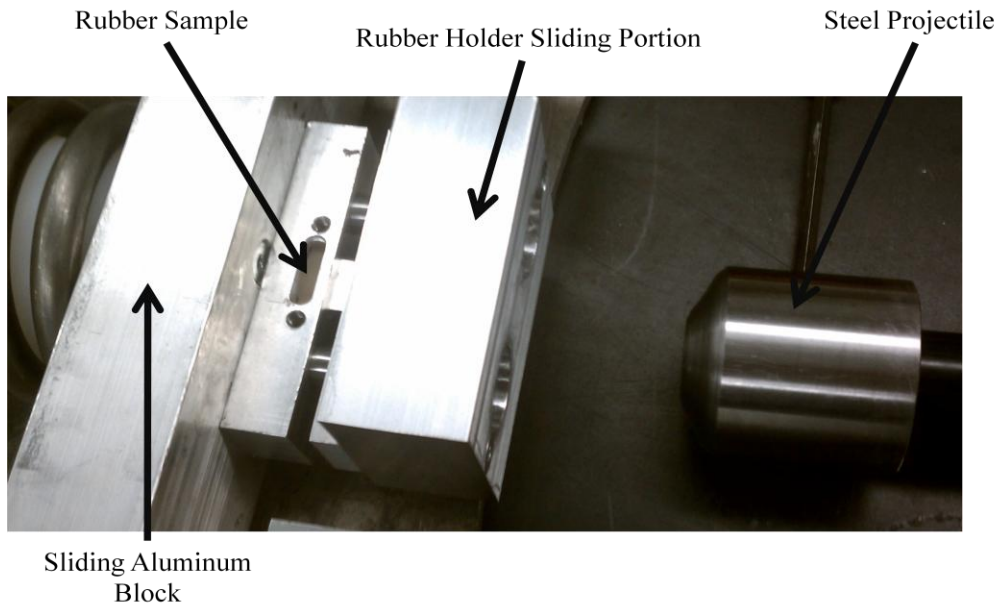


FIGURE 22: RUBBER HOLDER AND STEEL PROJECTILE

The rubber impact tester and air cannon were all mounted onto a 20 foot long wooden plank and set against a concrete wall. A wooden box was built around the rubber impact testing mechanism for safety purposes in order to contain any unexpected projectiles. This is shown in Figure 23.



FIGURE 23: RUBBER IMPACT TESTER

The completion of the rubber impact tester enabled the testing of the rubber sample candidates. The following rubbers were tested: Shore A 30, 60, and 80 durometer silicone, natural gum rubber, foamed natural gum rubber, polyurethane foam, and EVA foam. Figure 24 shows a new 60A silicon rubber sample before undergoing any testing. Figure 25 shows the same silicone rubber sample after undergoing one impact.



FIGURE 24: NEW 60A SILICON RUBBER SAMPLE



FIGURE 25: 60A SILICON RUBBER SAMPLE AFTER ONE IMPACT

Each of the materials were tested and all resulted in a spring deflection of roughly 2.5 inches. This corresponded to 73 Joules being transferred into the spring. Assuming that the energy transfer efficiency was between 40% and 80% due to friction between the bushings in the aluminum block and two parallel shafts, the rubber was required to transfer between 183 Joules and 71 Joules respectively. The actual efficiency was unknown so an assumption had to be made based on judgment, so 60% was used corresponding to 121 Joules of energy. This was close to the desired 136 joules given the large margin of error these calculations were subject to. After each type of rubber had been tested it was concluded that none of the rubber samples was capable of surviving a single impact. The material that best survived the impact was the natural gum rubber as

shown in Figure 26. Even this material was subject to catastrophic damage. The required amount of energy to be transferred through the small volume was too high. This meant that a more effective solution was required in order to properly mitigate the impact. Photographs of each failed rubber sample can be found in [Appendix B: Impact Testing](#).



FIGURE 26: NATURAL GUM RUBBER SAMPLE AFTER ONE IMPACT

#### **4.4.5 Reduced Impact Velocity and an Over-load Slip Clutch**

The goal of the feasibility analysis and rubber impact testing was to determine if the proposed design would be feasible with no gear reduction between the flywheel and the dog clutch. The results of the rubber impact testing showed that given the packaging constraints, rubber shock absorbers of the required size simply could not handle the impact velocity. Therefore a second method of reducing the impact force was necessary. To do this a gear reduction and overload slip clutch were added to the system. The added gear reduction reduced the relative velocities between the male and female side of the dog clutch. In order to ensure the gear train could withstand the high torque loads, an overload slip clutch was necessary. With respect to the impact force in the dog clutch, the slip clutch reduces the effective size of the flywheel, while allowing it to maintain the required energy level. In other words it limits the amount of energy that can be

transferred over a given deflection of the rubber shock absorber. An additional option to increase the life of the system is to increase the size of the rubber coupling so the energy is transferred through a greater volume. This design modification better defined the system and allowed for a mathematical model to be built.

## 4.5 Mathematical Model

### 4.5.1 Overview

A mathematical model of the system dynamics was created using MATLAB. The purpose of this model was to better understand the system in terms of what role each design parameter played in the system response. This served as a tool in the design process. The impact testing resulted in the decision that a torque limiting slip-clutch was required in order to minimize the impact force. This addition finalized the general design of the system which can be seen in Figure 27.

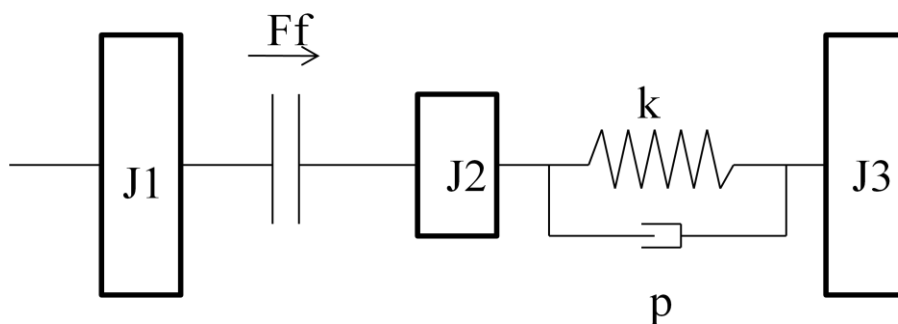


FIGURE 27: SYSTEM DIAGRAM OF FINAL DESIGN

This diagram illustrates items of interest in the system that were modeled. J1 is the flywheel which is connected through a gear train (not shown) to the overload slip clutch. The slip clutch is attached directly to the male side of the dog clutch and is able to transmit a maximum torque equal to  $F_f$  to J2. J2 represents the mass between the slip

clutch and rubber shock absorber. The rubber shock absorber is shown as a spring damper with a spring constant  $k$  and damping  $p$ . The female side of the dog clutch and four bar linkage are represented by J3.

Before the mathematical model was programmed, the approximate system behavior had to be predicted. This served to ensure that the model incorporated all of the necessary parameters and possible behaviors. The expected behavior was as follows. The dog clutch starts disengaged which means J3 is decoupled from the rest of the system. The flywheel (J1) is spun up to the desired speed so that is storing all of the required energy. J1 and J2 have the same velocity at this point because the torque is low enough that the slip clutch is not slipping. The dog clutch engages and couples the stationary J3 with the rest of the moving system. At this point the torque between J1 and J2 increases rapidly due to the difference in velocities but is limited to  $F_f$ . J2, which was previously moving is now decelerating while trying to accelerate J3 as it compresses the spring-damper. Eventually the spring-damper becomes fully compressed and the velocities of J2 and J3 are nearly identical except for vibrations due to the spring. At this point J2 continues to transfer its' energy to J2 and J3. This causes J1 to decelerate and J2 and J3 to accelerate. When the relative velocity between J1 and J2 becomes zero the overload clutch will stop slipping and the velocities of J1, J2, and J3 becomes approximately equal.

The expected behavior of the system behavior indicated that the overload slip clutch has two states: slip and stick. The slip state corresponds to when the torque trying to be transmitted through the clutch is higher than its rating. In this state it slips and transmits only its maximum rated value  $F_f$ . However when this torque becomes smaller

as the flywheel decelerates and four-bar accelerates, the overload clutch enters the stuck state, meaning that relative motion between J1 and J2 is zero. When this transition occurs the system switches from two degrees of freedom to one. Therefore, to properly model the system, the mathematical model had to be able to monitor what state the clutch was in (slip or stuck), and then act accordingly. First, the governing equations for each of these two states had to be defined.

## 4.5.2 Governing Equations

### Slip State

To model the slip state of the system it was decided that differential equations would be required. The property that the sum of the torques acting on mass in the system had to equal zero was used to create these equations. To do this, free body diagrams of each mass were created for the slip state. These can be seen in Figure 28.

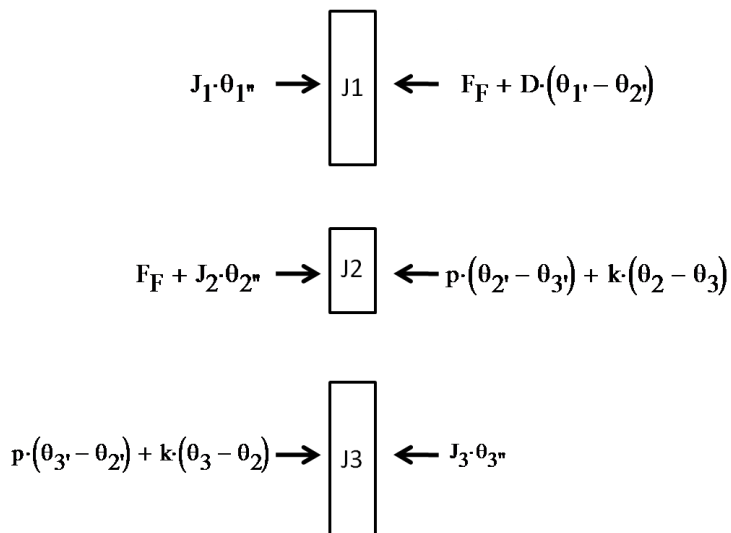


FIGURE 28: SLIP STATE FREE BODY DIAGRAMS

Using these free-body diagrams the governing differential equations were created.

$$J_1 \cdot \theta_1'' + D \cdot (\theta_1' - \theta_2') + F_F = 0 \quad (9a)$$

$$J_2 \cdot \theta_2'' + p \cdot (\theta_2' - \theta_3') + k \cdot (\theta_2 - \theta_3) - F_F = c \quad (9b)$$

$$J_3 \cdot \theta_3'' + p \cdot (\theta_3' - \theta_2') + k \cdot (\theta_3 - \theta_2) = 0 \quad (9c)$$

The use of these differential equations had a severe limitation. The mass J3 represents the four-bar linkage which has a variable effective moment of inertia. The solution of the differential equations was numerical and therefore discrete. Additionally the value of J3 is a function of theta, which is the angle of the input link of the four-bar linkage. This means for each discrete time interval that it solves the differential equations, it uses a different value for J3 but the last known velocity of J3. Therefore, for any given discrete step the velocity is independent of the effective moment of inertia for J3. This is inherently a problem because it means that the model of the system fails to conserve energy. As the effective moment of inertia of J3 increases, the model keeps the velocity constant and the system energy increases. The solution for this is explained in the implementation of the model.

### **Stick State**

There were two ways to model the stick state. Both methods had their own respective limitations. The first method was to use differential equations as used in the slip state. This was similarly accomplished by first creating a set of free-body diagrams to describe the forces acting on each mass in the system. These are comparable to the slip state except the overload slip clutch is removed. These can be seen in Figure 29.

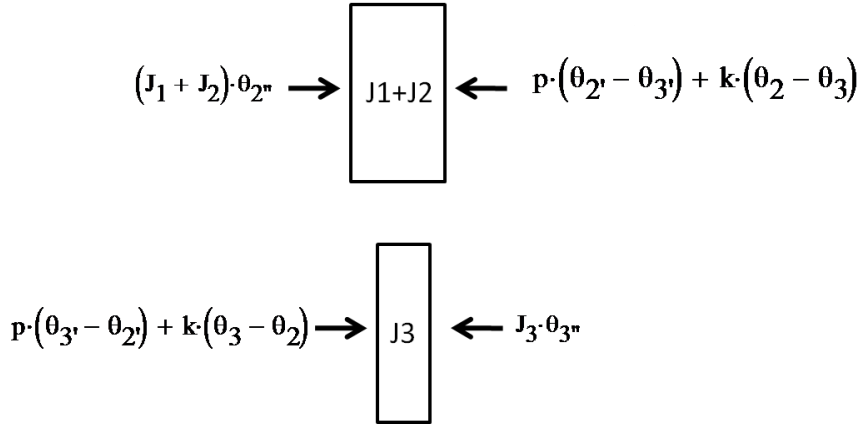


FIGURE 29: FREE BODY DIAGRAMS STUCK STATE

Using these free-body diagrams the governing differential equations were created.

$$(J_1 + J_2) \cdot \theta_2'' + p \cdot (\theta_2' - \theta_3') + k \cdot (\theta_2 - \theta_3) = C \quad (10a)$$

$$J_3 \cdot \theta_3'' + p \cdot (\theta_3' - \theta_2') + k \cdot (\theta_3 - \theta_2) = C \quad (10b)$$

These differential equations were subject to the same limitation as the slip differential equations. However in this case a second approach was available that better solved the problem.

The goal was to ensure that the model conserves energy in its calculations. The stick state occurs when the velocities of J1, J2, and J3 can all be considered to be equal. Therefore an energy based approach to the modeling of the system in the stick state was used. The energy balance equation for an object with an initial velocity that has its mass change is shown in Equation 11A.

$$\frac{1}{2} * J_{initial} * \omega_{initial}^2 = \frac{1}{2} * J_{final} * \omega_{final}^2 \quad (11a)$$

The goal was to find out  $\omega_{final}$ , so the equation was rearranged.

$$\omega_{final} = \sqrt{\frac{J_{initial} * \omega_{initial}^2}{J_{final}}} \quad (11b)$$

This introduces a new problem. The final effective moment of inertia,  $J_{final}$ , is a function of its position. However its position is a function of its speed, which is a function of its final effective moment of inertia, and so continues the infinite loop. Therefore an assumption had to be made so that a final angular velocity could be calculated. This assumption was that the discrete time step is small enough that the change in the velocity per step is very small. This allowed for an estimation of the final position to be determined based on the initial angular velocity and length of the time step. Using the position information, the final effective moment of inertia could be calculated, allowing the final speed to be calculated. The actual distance moved could then be calculated based on the average of the initial and final angular velocity and the time step size. The other limitation of this approach is that because it assumes for the remainder of the model that the velocities of J1, J2, and J3 all remain the same, then it cannot easily monitor whether it should switch back into the slip state.

To solve this problem a method of monitoring whether it should switch back was developed that focused on the energy in the system. The respective speeds for each of J1, J2, and J3 were calculated based on the assumption that energy is conserved and stays constant in the system with time. However the effective moment of inertia of J3 increases as the four-bar linkage goes through its range of motion. This means that the distribution of energy in the system changes. For simplicity J2 and J3 from this point on are considered to be rigidly connected because the spring is now in the fully compressed state. So by calculating the energy in the flywheel in the previous time step, and the energy in the flywheel for the current time step based on the old and current velocities, the change in energy can be determined. The only way for the energy to be transferred

out of the flywheel is through the overload slip clutch. The slip clutch has a maximum torque that it is capable of transferring before slipping. The energy transferred through the clutch is equal to this torque times the angular displacement. Therefore, the maximum torque rating of the clutch can be compared to the torque required to be transferred through the clutch to keep the velocity of each  $J_1$ ,  $J_2$ , and  $J_3$  the same. If the required torque is greater than the maximum torque then the slip clutch has switched back into the slip state. If this is the case the actual velocities of each part of the system must be calculated. As the model stands it is not equipped to do this yet. Instead it just indicates if the model should switch back to the slip state after it has entered the stick state. This limitation is acceptable if the implications are known. It means that more energy is transferred from the  $J_1$  to  $J_2+J_3$  than would actually happen, resulting in more energy transferred into the opposing robot. This can be considered to be a non-conservative case in terms of how much energy is transferred into the opposing robot.

### **4.5.3 Model Implementation**

#### **Main Program**

The expectations and requirements discussed in the previous section set up a framework for how the model would be implemented. The model was developed in MATLAB using a series of scripts and functions. The entirety of the model can be found in Appendix D: Mathematical Model of System Dynamics. A flowchart detailing the programs logical flow is shown in Figure 30.

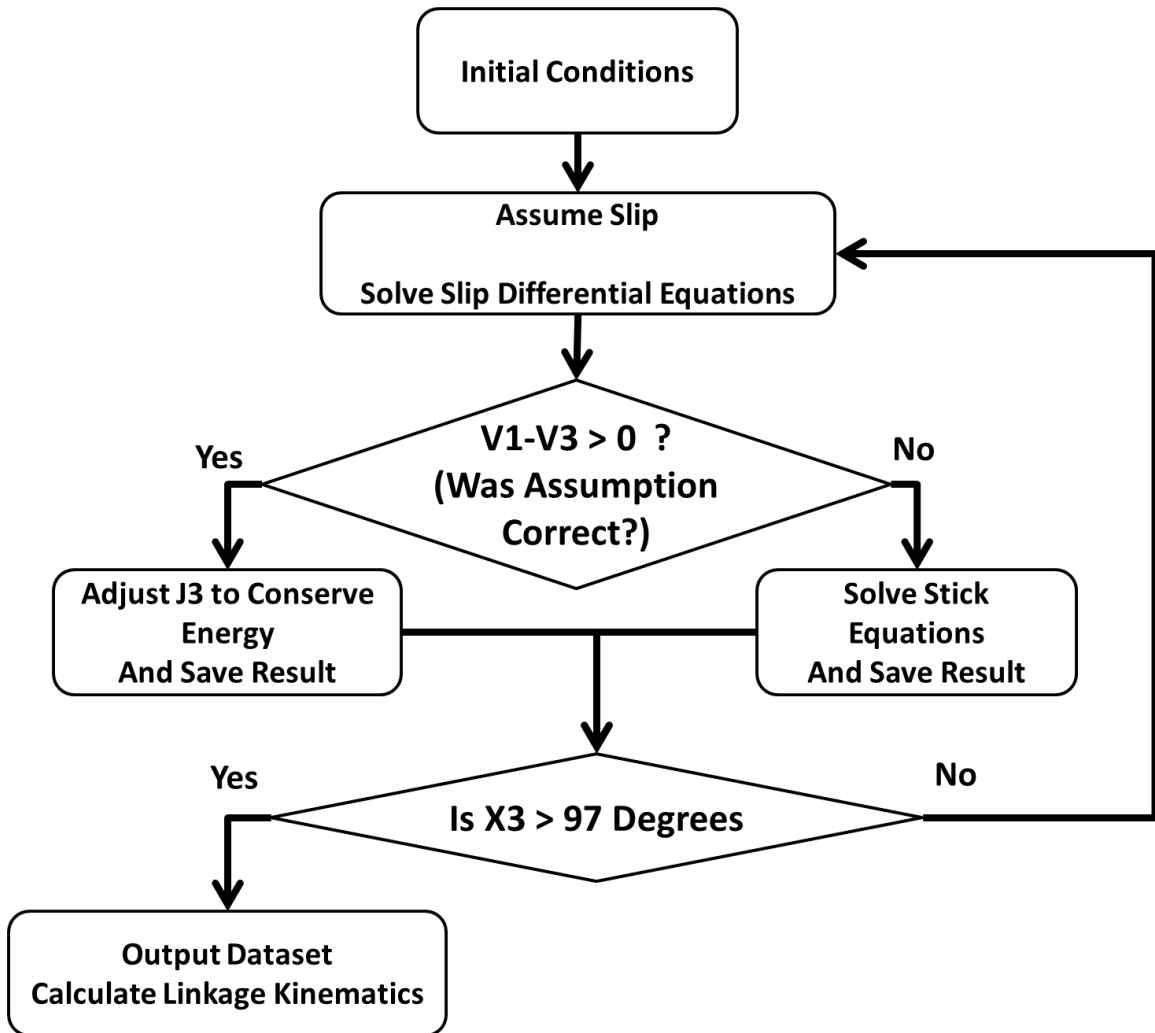


FIGURE 30: PROGRAM FLOWCHART

To solve the system of ordinary differential equations the MATLAB function ODE45 was used to provide a numerical solution. A script, Main.m was written that acts as the primary script from which all other functions are called. The model parameters and initial values are defined in this file. They include the initial position, velocity, and acceleration of J1, J2, and J3. The moment of inertia of J1 and J2, the maximum torque the slip clutch could provide, the rubber shock absorber parameters, the four-bar linkage parameters, and the time step. The simulation is all contained within a while loop that continues until the angle of the input link of the four-bar linkage has traveled to a defined angle. Two

checks are in place that break out of the loop if the flywheel reverses direction. This is unlikely but prevents the loop from running for infinite time if input parameters are set incorrectly. The simulation begins assuming that the clutch is in the slip state. Therefore the simulation calls the slip function with its input parameters being the current position and velocity of J1, J2, and J3 defined in the last time step or by initial values. The slip function returns a new set of positions and velocities which describe the state of the model for the newest time step. An If statement then determines if the relative velocity between J1 and J3 is greater than zero. This is checking if the clutch is actually in the slip state. J3 is used instead of J2 because at the beginning of the model at the instant the dog clutch is engaged the velocities of J1 and J2 are the same. J2 then slows down until it matches the speed of J3 because the rubber shock absorber has fully compressed. From this point on, J2 and J3 have very close to zero relative movement aside from spring vibrations. Therefore J3 can be used instead of J2 because it does not indicate the clutch is in the stick state when in fact the torque is greatest, and J2 and J3 are nearly the same by the time the clutch enters the stick state.

If the relative velocity between J1 and J3 is greater than zero then the assumption that it is in the slip state is correct. As discussed previously, the position and velocity results of the four-bar linkage, J3, are incorrect in that they do not reflect conservation of energy. To account for this, the energy in the four-bar linkage is calculated through an energy balance calculation based on the velocity of the four-bar linkage, and its change in effective moment of inertia. The average velocity over the previous time step, based on the original velocity and newly calculated velocity, is calculated and multiplied by the duration of the time step to determine the change in position. This change in position is

added to the previous position to determine the new position. The acceleration of J1, J2, and J3 is calculated based on their change in velocity from the previous iteration to current one over the time step. The model then saves the position, velocity, and acceleration of J1, J2 and J3 and the state of the clutch to a class structure.

If the relative velocity between J1 and J3 is equal to zero then the assumption that it is in the slip state is incorrect. The If statement then continues to the Else option which assumes that the clutch is in the stuck state. The stuck function is called with its input parameters being the position and velocity of J1, J2, and J3 determined in the previous time step or defined as initial values. The stuck function returns a new set of position and velocities which describe the state of the model for the newest time step. The acceleration is calculated for J1, J2, and J3 based on the change in velocity from the previous iteration to the current iteration over the time step. These results are checked to see if the energy lost from the flywheel over the last time step was capable of being lost given the maximum slip clutch torque. The model then saves the position, velocity, and acceleration of J1, J2 and J3 and the state of the clutch to the class structure. If the energy lost from the flywheel is possible given the slip clutch capacity, then the clutch state is recorded as stuck, otherwise it is recorded as being in the slip state. However, when recorded as in the slip state the simulation still considers the clutch to still be in the stick state. In other words, it records the values calculated based on the assumption that the clutch is in the stick state. Project time constraints prevented an appropriate fix to this limitation. However the model is able to indicate if this limitation is having an effect.

The If statement then concludes as the two states of the clutch have been covered and the While loop repeats itself. This continues until J3 reaches a defined angle. All of

the time, position, velocity, acceleration, and clutch state data is stored in the class structure in variable  $a$ . Next a kinematic approach was used to determine the position and velocity of the coupler point for the four-bar linkage through its entire range of motion based on the position and velocity of its input link J3. Relevant data produced by the simulation is then plotted.

### **Shock Absorber**

Modeling the shock absorber was done with two parameters:  $p$  and  $K$ , representing respectively the rubber's damping coefficient and the spring constant. As determined in experimental testing, the spring constant of rubber, specifically natural gum rubber, is dependent on its compressive deflection, or strain. As the strain increases the reaction force increases exponentially. However, as stated, rubber's behavior is heavily dependent on strain rate, which is prohibitively difficult to test in this impact case. Therefore a function titled SC.m was written that given an initial  $K_0$  value, and the positions of both sides of the spring, returns a  $K$  value. This is a piecewise function. For deflections in which the thickness of the rubber is greater than zero the spring constant is calculated as the ratio of  $K_0$  and the thickness. This means that as the thickness approaches zero the spring constant will rise asymptotically. However, the mathematical model is discrete, and if the time step is large enough the thickness can become less than zero in certain circumstances. If this happens the function saves the last known  $K$  value as  $K_{last}$ . It then calculates the  $K$  value based on equation 12a.

$$K = K_{last} * e^{abs(Thickness)} \quad (12a)$$

Values of  $K_0$  and  $p$  were chosen based on values that allowed the model behave as expected. For example it was known that the natural gum rubber was not going to vibrate

excessively, so a damping coefficient was chosen that produced expected vibrations without over-damping the system. The original spring constant was chosen so that J2 cannot pass through J3 because it was well known that this would not happen in the physical implementation of the mechanism.

## **4.5.4 Four-Bar Linkage Synthesis**

### **4.5.4.1 Approach**

The purpose of the four-bar linkage in this mechanism is to transfer the energy of the flywheel into the opposing robot, the goal being to launch the opposing robot through the air upwards and forwards. This meant that the synthesis approach focused on path generation. However, unlike most four-bar linkages the specific positions of the coupler point at various points throughout its motion were not critical. Therefore a graphical approach was not used; instead an analytical approach was chosen. Typical analytical approaches allow for linkage synthesis to have a set of prescribed values that are free choices and then a number of variables are calculated to achieve the desired motion. These values most often are a single or set of positions, velocities, or accelerations at points throughout the range of motion. However to accomplish the desired task, no specific values were required, and were therefore of low priority. Four linkage properties that were of a high priority were the effective moment of inertia of the linkage through its range of motion, the direction of the final coupler point velocity vector, the vertical displacement of the coupler point, and that the coupler point's vertical velocity component remain positive. The effective moment of inertia of a linkage through its range of motion is considerably difficult to prescribe when synthesizing a linkage. It is related primarily to the length of the input link, the transmission angles of the linkage, the

mass of each link, the location of its center of mass, and changes through its motion. The final velocity vector of the coupler point is a relatively easy parameter to prescribe. If desired, the vertical displacement of the coupler point can be prescribed through two-point position synthesis. Like the effective moment of inertia, the vertical component of velocity is a more difficult parameter to prescribe during synthesis for an entire range of motion. All of these linkage properties were critical to the functionality of the linkage. However no predetermined values existed and assigning them arbitrarily would have been unwise. Therefore, four synthesis criteria were created. First, the effective moment of inertia of the linkage throughout its range of motion had to be at a minimum. This was determined by taking the sum of the effective moment of inertia values for each whole number angle through the linkage's range of motion. Independently, this value was meaningless, however it allowed for the comparison of one linkage against others and indicated the amount of work that had to be done for a given range of motion. Second, it was desirable that the final velocity vector of the coupler point of the linkage be as vertical as possible. In other words the ratio of the vertical component of the velocity and horizontal component of the velocity had to be maximized. This will be henceforth referred to as the velocity component ratio ( $V_y/V_z$ ) which is just the tangent of the final velocity vector's direction.. It was also decided that the total vertical displacement of the coupler point should be maximized to increase the distance that the energy is imparted over. Finally, as stated, the vertical component of velocity had to remain positive for the given range of motion. It was known that these four linkage properties were not independent of one another. However, the relationship between them was unknown and trying to achieve the four goals would be nearly impossible using standard synthesis

techniques. Therefore it was decided that a computer based optimization would be necessary to achieve an optimum linkage.

#### **4.5.4.2 Optimization Implementation**

Initially MathCAD was used as the optimization tool. It has a function called minimize that allows it to calculate the minimum of a multivariable function, given a set of ranges for each variable. This allowed for a function to be written that took advantage of a penalty formulation to allow for optimization by evolutionary theory as done by Mundo, Danieli, and Yan(2006). This meant that the criteria defined could be formulated as a set of constraints that when violated would result in a large value being added to the objective function. This approach would in theory allow for the minimization algorithm to converge towards the desired optimum. However for efficiency the minimize function uses an algorithm that expects an input function with relative continuity. By introducing penalties the function result became quite random with many discontinuities. The MathCAD function has a predefined number of maximum iterations and as such was unable to find the true minimum in the solution space. Therefore MATLAB was chosen instead, along with a different optimization approach in order to maximize design flexibility.

Due to the problems encountered in finding the minimum value of a multivariable function through algorithms, a more straightforward approach was chosen. The optimization only had to be run a few times, and therefore speed and efficiency were not critical. Thus a brute force method was chosen. First input parameters for the optimization had to be selected. It was decided that these would be a set of ranges for the lengths of each link. A function was written that computed every combination of link

lengths for a given interval and stored it in matrix form. Next a set of functions were written based on the aforementioned design criteria that could be applied to each of the possible linkages.

First a method for calculating the effective moment of inertia of an arbitrary four-bar linkage at a given angle was necessary. The paper "Lagrangian Dynamic Formulation of a Four-Bar Mechanism with Minimal Coordinates" (Tang, 2006) formulated a single equation that describes the full dynamic motion of a four-bar linkage using the Lagrangian method (Tang, 2006). This equation is equation 13c.

$$M(\theta)\ddot{\theta} + V(\theta, \dot{\theta}) = \tau_{\theta} \quad (13b)$$

It is noted that the first term in the equation,  $M(\theta)\ddot{\theta}$ , has units of torque. The first value  $\ddot{\theta}$  is the second derivative of angular position, otherwise known as angular acceleration. A unit analysis then tells us that  $M(\theta)$  is the moment of inertia. Equation 13c is the compact form; refer to **Appendix C: Four-Bar Synthesis and Optimization** for the expanded form. Using this formulation, a closed form solution for the effective moment of inertia of a four-bar linkage was determined. To calculate the overall effective moment of inertia, the sum of the moments of inertia for each whole angle in the range of motion of the linkage was calculated. A kinematic approach was used in calculating the coupler point velocity through the desired range of motion and its total vertical displacement. As stated, the velocity component ratio was represented as a ratio of the vertical component of the final velocity and horizontal component of the final velocity. For more information refer to Norton's *Design of Machinery: An Introduction to the Synthesis and Analysis of Mechanisms and Machines*(Norton R. L., 2008).

These formulations were applied to each linkage and used as criteria for filtering.

A For loop was created that checked each linkage for the following criteria:

- The velocity of the coupler point remains greater than zero
- The linkage is geometrically possible (all answers are real)
- The ratio of the final vertical velocity component and final horizontal component is greater than a value set for that particular optimization.
- The total effective moment of inertia is between 0 and maximum value set for that particular optimization

If the linkage did not meet the criteria then it was deleted and only the satisfactory linkages saved. These saved linkages were stored in a new matrix along with the relevant parameters already calculated: the velocity component ratio, total moment of inertia, vertical displacement of the coupler point, and link lengths. These results were then sorted by total moment of inertia from least to greatest. The filtering processes acted as a set of bounds that created a solution space. The data set was then every solution that fit within that solution space, with consideration for the interval size. Using MATLAB's plotting tools two plots were created: the velocity component ratio versus total moment of inertia, and the coupler vertical displacement versus total moment of inertia. These plots graphically represented the relationship between the three criteria of interest. This relationship was then used as a powerful tool in finding the optimum linkage.

Engineering decisions are most often based on a balance between cost versus benefit. In such complicated systems improving one parameter can be detrimental to another.

Therefore the plot of the data set enabled a decision to be made that balanced the

minimization of the total moment of inertia and maximization of the velocity component ratio and coupler vertical displacement.

#### 4.5.4.3 Optimization Process and Results

The MATLAB code developed allowed for flexibility during the optimization process. This meant that a number of decisions had to be made prior to each optimization. The first of which was the link length ranges and optimization interval. The decision was made to approximate a coarse-fine field search. A coarse first pass optimization was performed that used a large set of ranges and interval size. This prevented the optimization from taking excessively long and would find a linkage that was close. A fine second optimization was then performed that used a much smaller range and interval to better define the linkage.

The values chosen for the link length ranges for the first pass optimization can be found in Table 2. These values were developed after finding a linkage that produced an approximation of the desired motion using Solidworks sketch tools. The full set of ranges was then developed based on practical minimum and maximum numbers. An interval of 0.1 inches was chosen so that the computing time was less than a day. These ranges and interval size resulted in 19,533,281 different linkages.

TABLE 2: OPTIMIZATION ONE: LINK LENGTH RANGES

<b>Link</b>	<b>Minimum (in)</b>	<b>Maximum (in)</b>
<b>1</b>	7	14
<b>2</b>	3	4
<b>3</b>	8	14
<b>4</b>	1	5

For this optimization the maximum value of the total moment of inertia was set at 10,000, which is higher than desirable. The minimum velocity component ratio was set to 1, which is also lower than desired but allowed for a better perspective on the relationship between the three criteria. After the filtering process, 33,762 viable linkages of the initial 20 million remained. The results are plotted in Figure 31 and Figure 32.

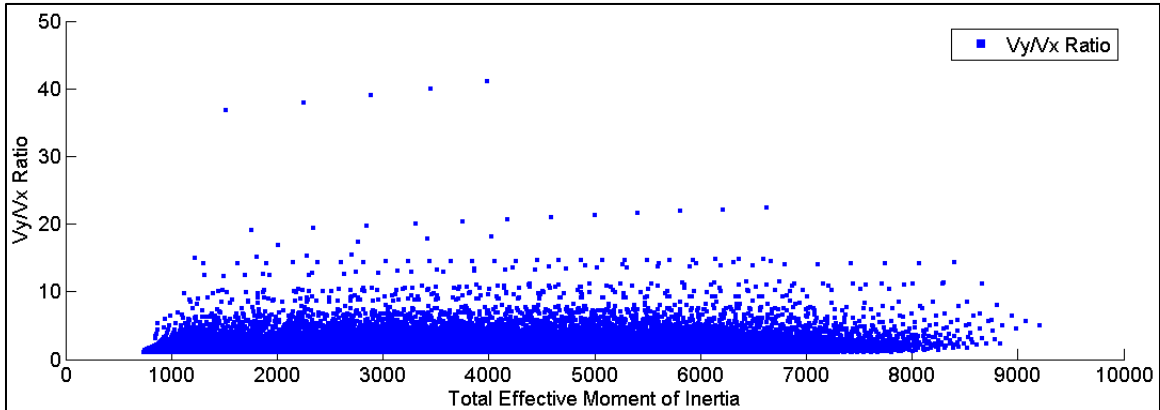


FIGURE 31: OPTIMIZATION ONE: TOTAL MOMENT OF INERTIA VERSUS THE VELOCITY COMPONENT RATIO

Figure 31 represents the relationship between the  $V_y/V_x$  ratio and the total effective moment of inertia over the desired range of motion. It includes every possible linkage that met the optimization criteria. The plot clearly shows that for the given ranges and filtering criteria there is a definite relationship between the velocity component ratio and solution density: the greater the velocity component ratio the fewer the number of viable linkages. This means that if a linkage was arbitrarily synthesized, the probability of creating one that is sub-optimal is quite high, which lends credibility to this approach. Additionally for total moment of inertia values above 1850 there are minimal gains in the velocity component ratio. For velocity component ratio values between 0 and 5 almost any effective total moment of inertia is possible. This means that in this range these two parameters are independent of one another. An ideal linkage would be in the top left

corner of the plot where the total moment of inertia is least and the velocity component ratio is highest. As a note, no units are given for the total moment of inertia to avoid confusion as to what the value represents.

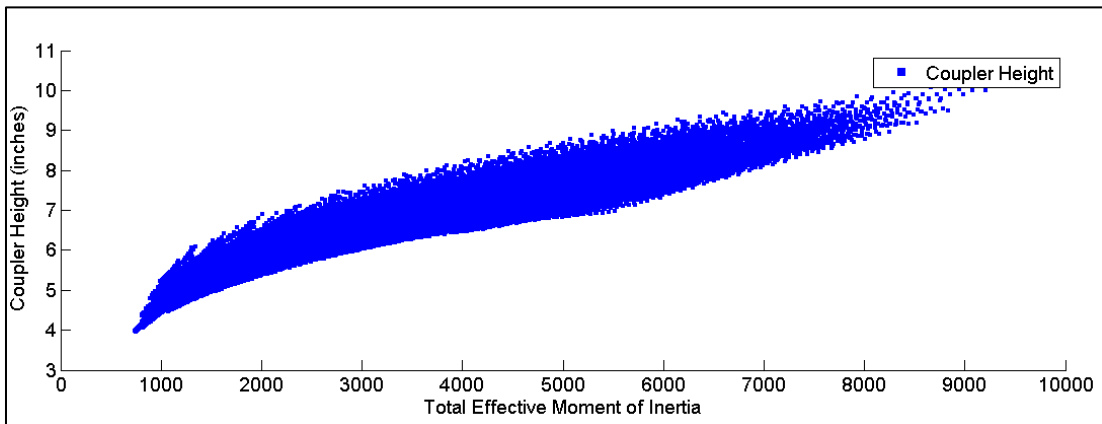


FIGURE 32: OPTIMIZATION ONE: TOTAL MOMENT OF INERTIA VERSUS COUPLER HEIGHT (VERTICAL DISPLACEMENT)

Figure 32 shows a very clear trend between total moment of inertia and coupler height. As the total moment of inertia increases, the maximum available coupler height, or total vertical displacement increases. Total moment of inertia values of 1850 allow for coupler heights between 4.5 inches and 6 inches. This range was deemed acceptable for the final design and therefore all linkages with a total moment of inertia value greater than 1850 were ignored. This decision prompted the plotting of the new solution space as shown in Figure 33.

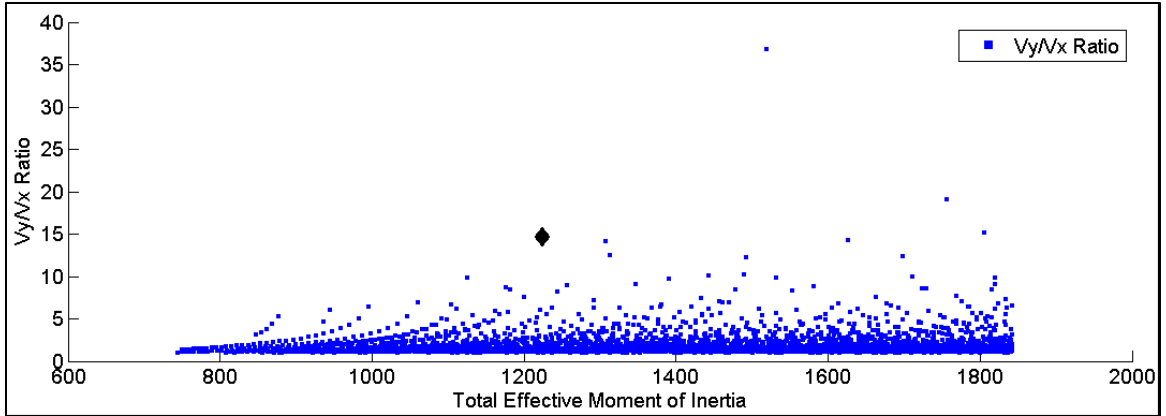


FIGURE 33: OPTIMIZATION ONE: TOTAL MOMENT OF INERTIA VERSUS THE VELOCITY COMPONENT RATIO

Figure 11 illustrates the same relationship shown in Figure 31 but in greater detail. For total moment of inertia values between 800 and 1100 the greatest velocity component ratio value is about 7 which is lower than desired. There are then three points that have the highest velocity component ratio at the expense of increased total moment of inertia. These points are listed in Table 3. The percent increase in total moment of inertia and the velocity component ratio is the percentage increase from option 1 to option 2 and option 2 to option 3. The "% Increase / % Increase" is the ratio of the increase in the velocity component ratio and total moment of inertia for that given option.

TABLE 3: OPTIMIZATION ONE: LINKAGE OPTIONS

Option	Total MOI	Vy/Vx Ratio	% Increase Total MOI	% Increase Vy/Vx Ratio	% Increase /%Increase
1	1126	9.8	N/A	N/A	N/A
2	1222	14.9	8.5%	52%	612%
3	1519	36.76	24%	246%	1025%

At this point a decision had to be made as to which linkage was "best". The increase in the velocity component ratio between option one and two is 52% and comes at minimal expense to the total moment of inertia (8.5%). The increase in the velocity component ratio from option 2 to 3 was significant (246%) and would make the final vertical

velocity much more vertical. However it came at the expense of an increase in total moment of inertia of 24%. The energy in the flywheel is limited, and the higher this number the less efficient the use of the energy. Therefore it was decided that the best compromise would be option two which is indicated in Figure 33 by the large diamond. Option two also has a vertical displacement of roughly 5.25 inches which is sufficient. The linkage lengths of option two can be found in Table 4.

TABLE 4: OPTIMIZATION ONE: LINKAGE DIMENSIONS

Link	Length (in)
1	11.6
2	3.3
3	10.4
4	2.3

Next the fine second pass optimization was performed. Using the optimized linkage values a smaller range was chosen that allowed for a smaller interval size. This new set of ranges is shown in Table 5.

TABLE 5: OPTIMIZATION TWO: LINK LENGTH RANGES

Link	Minimum (in)	Maximum(in)
1	11	12
2	3	4
3	10	11
4	2	3

The interval chosen for this optimization was 0.025 inches which resulted in 2,825,761 possible linkage combinations. The filter criteria was set such that any linkages with

velocity component ratios of less than 5 or total moment of inertia's greater than 2000 were ignored. This resulted in 3985 linkages that met the criteria. These results are plotted in Figure 34 and Figure 35 but with the maximum total moment of inertia shown less than 1300.

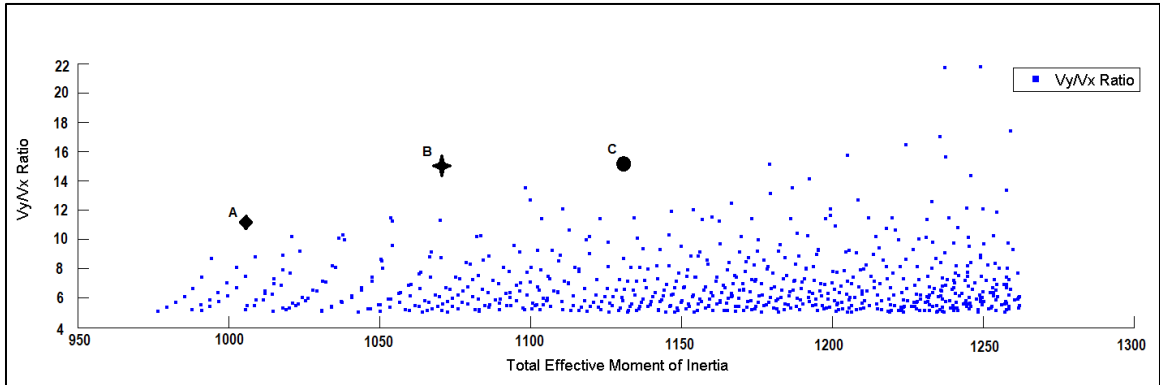


FIGURE 34: OPTIMIZATION TWO: TOTAL MOMENT OF INERTIA VERSUS THE VELOCITY COMPONENT RATIO

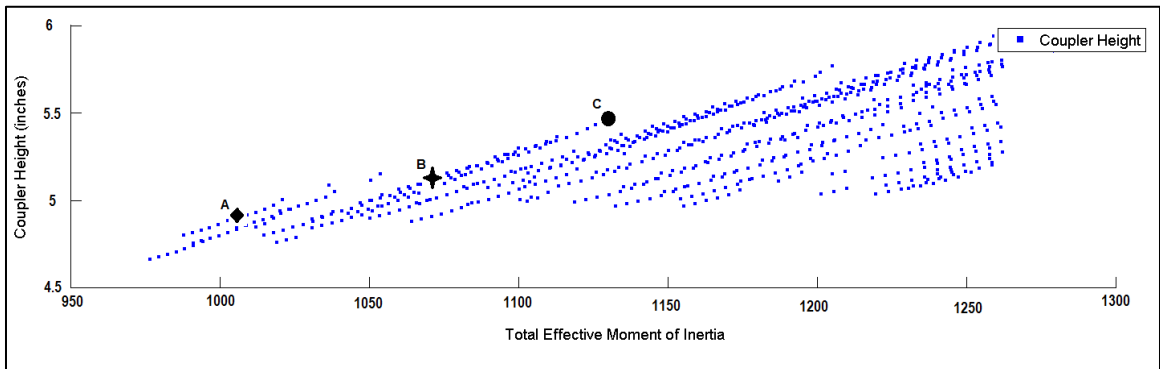


FIGURE 35: OPTIMIZATION TWO: TOTAL MOMENT OF INERTIA VERSUS COUPLER HEIGHT (VERTICAL DISPLACEMENT)

Similar to the first optimization, the second optimization resulted in three candidates, these being much more closely spaced due to the smaller solution space prescribed. These candidates are shown in Figure 34 as diamond A, star B, and circle C. Figure 35 illustrates the relationship of the total moment of inertia and coupler height (vertical displacement) for the second optimization. The three options (A, B, and C) are identified and indicate that the total vertical displacement can range between 5 inches and

5.5 inches for the best solutions. The values for these points are shown in Table 6. This table is of the same format as Table 3.

TABLE 6: OPTIMIZATION TWO: LINKAGE OPTIONS

<b>Option</b>	<b>Total MOI</b>	<b>Vy/Vx Ratio</b>	<b>% Increase Total MOI</b>	<b>% Increase Vy/Vx Ratio</b>	<b>% Increase /%Increase</b>
A	1006	11.63	N/A	N/A	N/A
B	1078	15.12	7%	30%	21%
C	1295	15.59	20%	3%	-15%

Like the first optimization, a decision had to be made as to which linkage was "best". The increase in the velocity component ratio between option A and B is 30% and comes at minimal expense to the total moment of inertia increase of 7%. The increase in the velocity component ratio from option B to C was minimal at 3% but was at the expense of an increase in total moment of inertia of 20%. Looking at the ratio of the percent increase in the velocity component ratio and the total moment of inertia the improvement from A to B is 21%, but for B to C there is a decrement of -15%. Therefore it was decided that the best linkage was option B which is indicated on Figure 34 by the star. The linkage lengths of option B can be found in Table 7. Figure 36 graphically illustrates the optimized linkage in the full extended position and coupler point motion through its full range of motion.

TABLE 7: OPTIMIZATION ONE: LINKAGE DIMENSIONS

<b>Link</b>	<b>Length (in)</b>
<b>1</b>	11.425
<b>2</b>	3.3
<b>3</b>	10.225
<b>4</b>	2.1

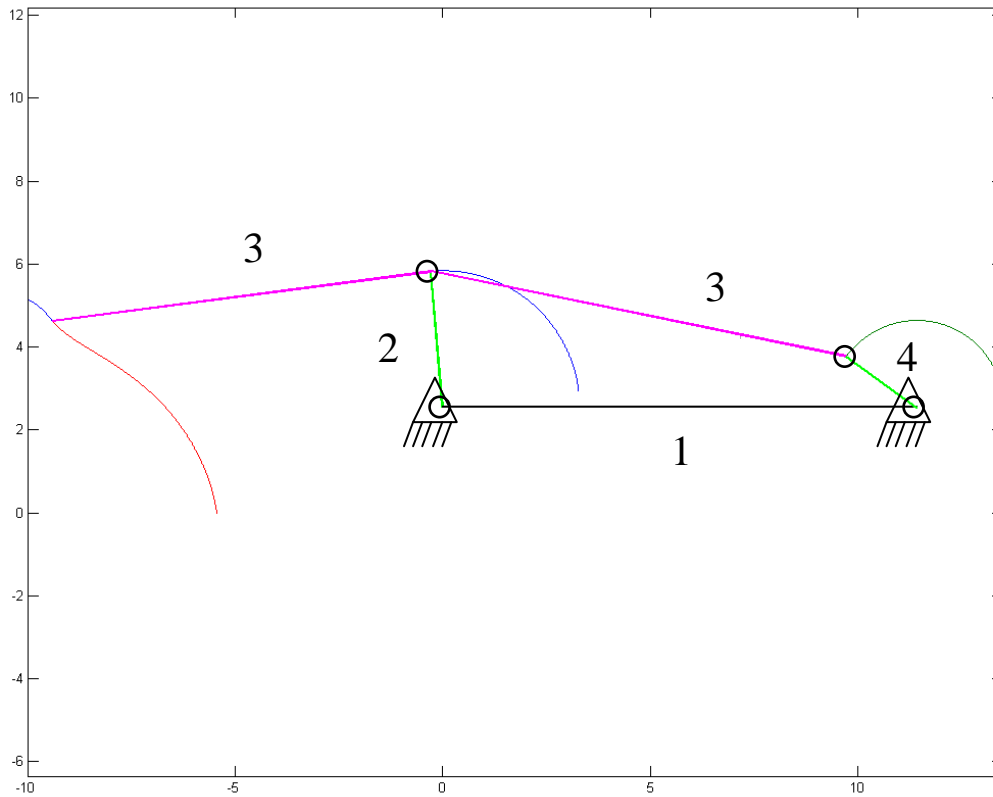


FIGURE 36: OPTIMIZED LINKAGE

#### 4.5.5 Model Results

The programming of the mathematical model and the synthesis of the four-bar linkage, including a method for determining its effective moment of inertia based on position, completed the mathematical model. The effective moment of inertia of the four-bar linkage can be seen in Figure 37, plotted as a function of crank angle. The varying effective moment of inertia of the four-bar linkage is caused by the change in transmission angles of the linkage, and moving location of its center of mass.

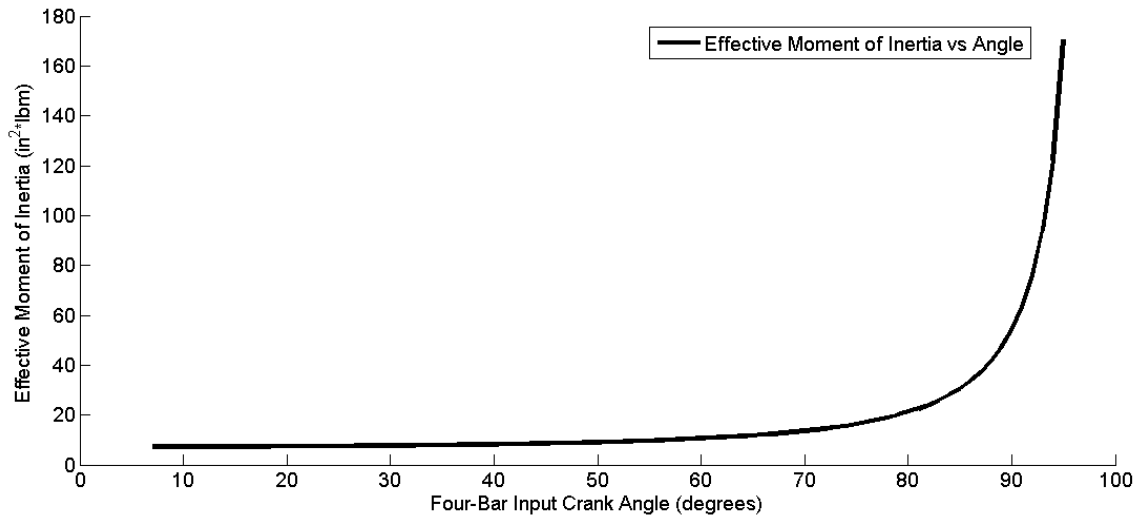


FIGURE 37: EFFECTIVE MOMENT OF INERTIA VERSUS ANGLE OF FOUR-BAR LINKAGE

The mathematical model underwent a number of tests to verify that its results were accurate. These primarily consisted of testing simplified scenarios that could be checked with calculations using basic kinematic or energy methods. The results of the model were then compared against those of the alternate method. When each segment of the model had been tested, the entire model was run. Figure 38 through Figure 40 show example results given arbitrary input parameters that show the full capability of the model. Figure 38 shows the angular positions X1, X2, and X3 of the rotating masses J1, J2, and J3 versus time for the duration for the simulation. J1, J2, and J3 represent the mass moments of inertia, respectively, of the flywheel, the male side of the dog clutch, and the effective moment of inertia seen by the four-bar linkage crank angle. The positions of these are designated by X1, X2, and X3 and the velocities are designated by V1, V2, and V3. Noteworthy are that the positions X1 and X2 are initially the same, and X3 is slightly ahead. This represents the spacing of the rubber shock absorber. The simulation starts at the engagement of the clutch so J1 works to accelerate J2 and J3. J2

compresses the spring damper between J2 and J3 causing the spacing to decrease. The plot and simulation stop when the angle of J3 reaches 95 degrees.

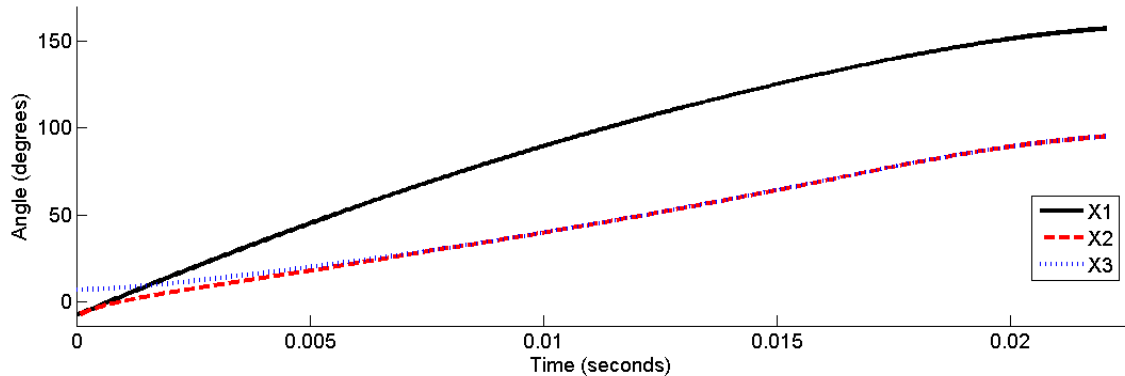


FIGURE 38: EXAMPLE RESULT, ANGULAR POSITION OF ROTATIONAL MASSES J1, J2 , AND J3 VERSUS TIME

Figure 39 shows the velocity of J1, J2, and J3 versus time for the duration of the simulation. J1 and J2 start at 2,000 rpm while J3 starts at 0 rpm. The clutch causes a constant deceleration of J1 as it applies a torque through the clutch into J2. J2 decelerates very quickly as it compresses the spring damper and accelerates J3. At roughly 0.001 seconds the velocities of J2 and J3 are roughly equal and they accelerate together as J1 imparts energy into them. At 0.017 seconds the velocities of J1, J2, and J3 are all equal. At this point the model detects that it is no longer in the slip state and switches to the stick state. This is indicated by the dashed-dotted line that switches from the initial speed of J1 (2000 rpm) to 0 rpm. The velocities of all three are then treated as equal. The effective moment of inertia of the four-bar linkage J3 continues to increase and the velocity of the system decreases until J3 reaches 95 degrees.

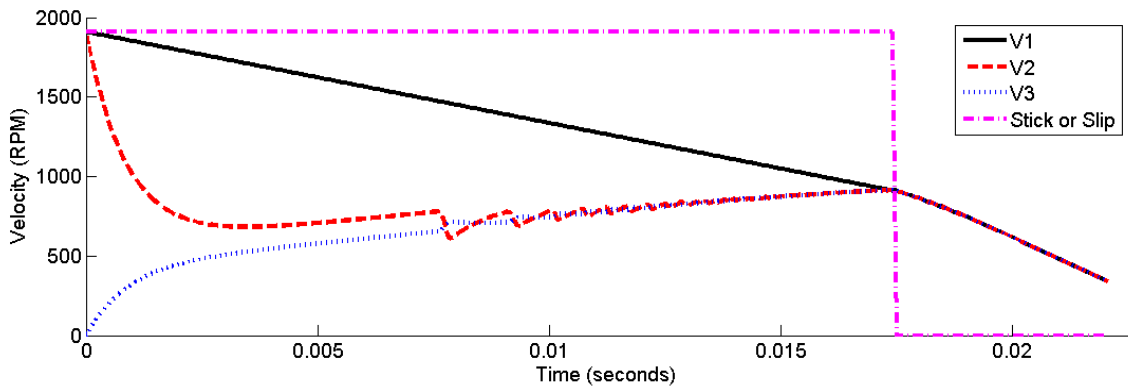


FIGURE 39: EXAMPLE RESULT, VELOCITY OF THE ROTATIONAL MASSES J1, J2, J3 VERSUS TIME

Figure 40 shows the movement of the four-bar linkage and the trajectory of the thirty pound robot after being launched by the linkage.

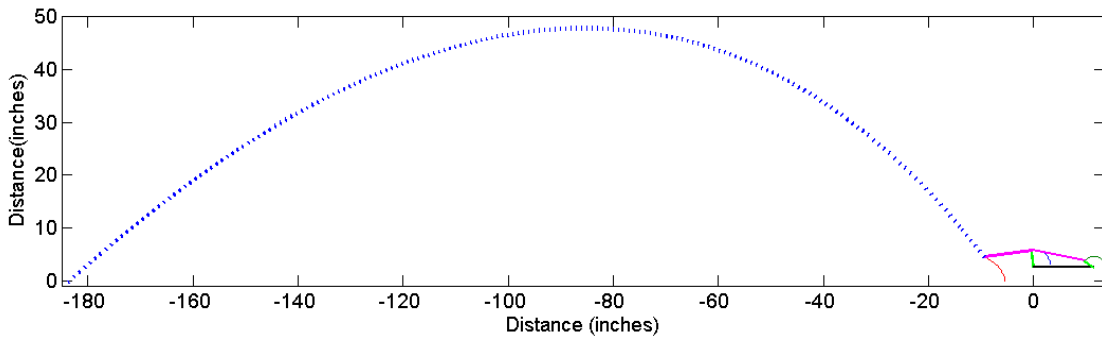


FIGURE 40: EXAMPLE RESULT, FOUR-BAR AND PROJECTILE TRAJECTORY

## 4.5.6 Clutch Verification

### 4.5.6.1 Simple Clutch-Flywheel Prototype

In order to verify the design of the dog-clutch and gather data to compare against the mathematical model, a simplified clutch-flywheel prototype was built. This can be seen in Figure 41.

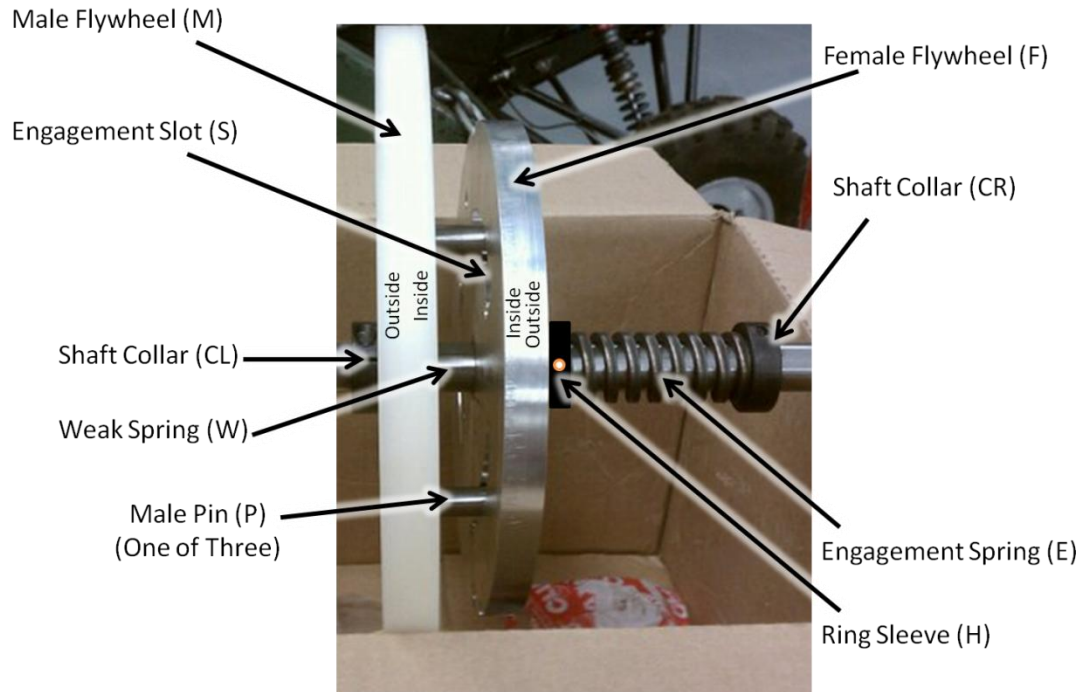


FIGURE 41: CLUTCH-FLYWHEEL PROTOTYPE

The prototype was comparable to the system modeled, but did not include the overload slip clutch. It consisted of two disks turning in bronze bushings on a steel shaft. One disk served as the male side of the dog clutch shown in Figure 42 and had three evenly spaced steel pins, labeled P, protruding from its face.

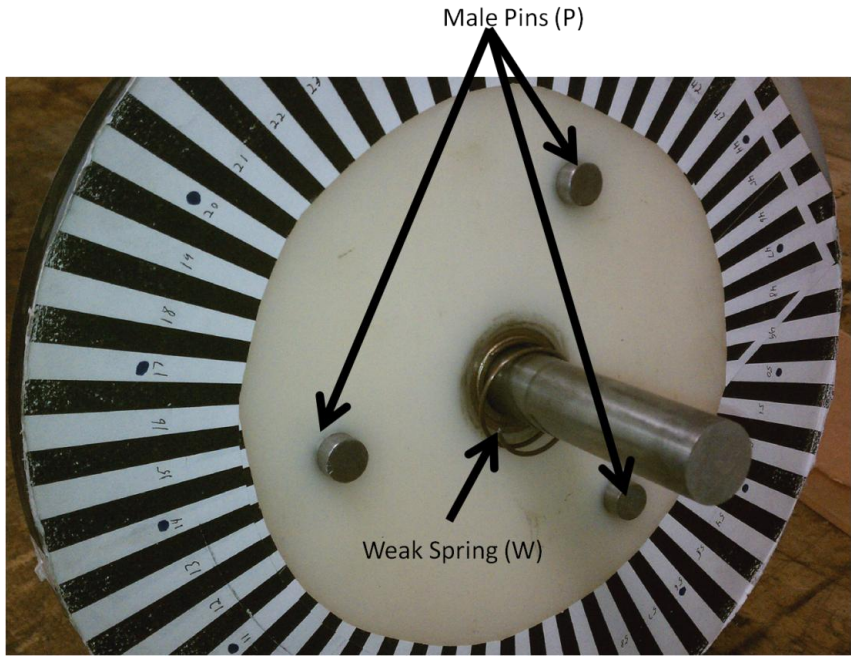


FIGURE 42: PROTOTYPE MALE SIDE DOG CLUTCH

The opposite disk contained three equally spaced slots (S) that the male side of the clutch (F) could engage into. One of these is shown in Figure 43. At the end of each slot (S) a 0.25x0.25x0.75 inch piece of natural gum rubber (R) was glued in to act as a shock absorber (R).

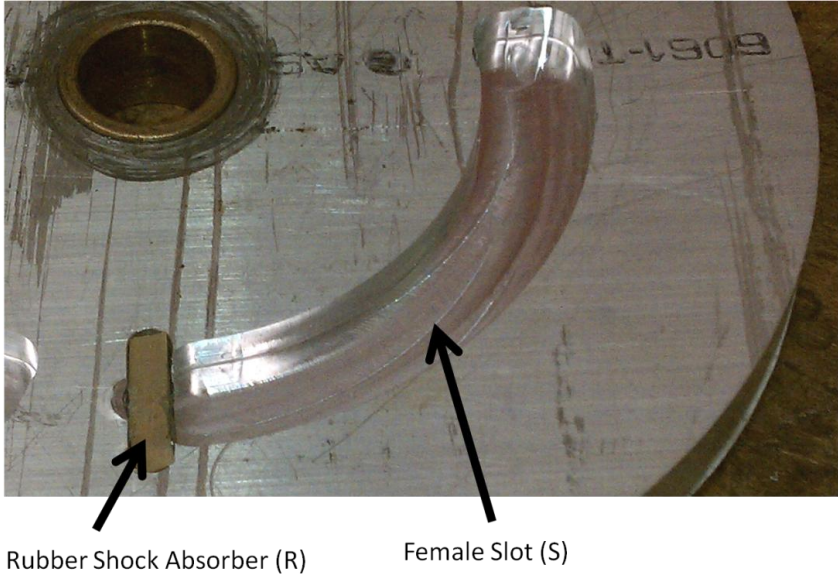


FIGURE 43: PROTOTYPE FEMALE SIDE DOG CLUTCH

A needle thrust washer and shaft collar (CL) on the outside of the male side (M) prevented it from moving axially in one direction. A weak coil spring (W) then separated the two inside surfaces of the clutch so that it did not engage unintentionally. Next, a large engagement spring (E) sat next to the outside of the female clutch flywheel and was backed up with a shaft collar (CR). The spacing was such that that when the male (M) and female side (F) were disengaged, the engagement spring (E) was compressed. A ring sleeve (H) with a small hole perpendicular to the axis of the shaft was placed between the engagement spring and female plate shown in Figure 41. A slot was cut into the shaft at the location where the ring sleeve (H) sat when the clutch was disengaged. The spring (E) could then be compressed and a pin placed through the hole in the ring sleeve (H) and into the slot. This kept the spring (E) compressed until the pin was removed. The male side of the dog clutch (M) was then spun up using a rubber coated wheel attached to a DC motor. With the male side at the desired speed, the pin was removed and the two plates engaged (M and F). This testing served to prove that the design concept was practical and could be implemented effectively. Each disk had a black and white pinwheel pattern similar to an encoder disk adhered to it. A high-speed video camera was then used to record the engagement of the two plates. This allowed for the change in velocity from before and after the engagement to be measured.

#### **4.5.6.2 Testing Results**

The high-speed video was able to capture the velocity of the two flywheels before and after the engagement but did not have the required frame rate to capture what happened during the impact. The initial speed of the male flywheel was 1300 rpm and the

final was 700 rpm. The initial speed of the female flywheel was 0 rpm and the final was 1500 rpm. This means that the energy in the storage (male) flywheel changed from 145 joules to 42 joules. The energy in the driven (female) flywheel changed from 0 joules to 90 joules. This data is shown in Table 8. This means that a total of 13 joules was absorbed by the rubber shock absorbers, and they were able to transmit 90 joules total, or 30 joules each. The test provided an example of how much the rubber shock absorbers could handle. One unexpected result was that the ratio of the flywheels was not big enough to properly represent what was expected in the final design. Upon impact the male flywheel transferred some energy into the female side. This caused the male side to slow down to a velocity lower than the new velocity of the female side. This was a critical behavior difference to what was expected in the final design due to the difference in flywheel moment of inertia ratios.

TABLE 8: PROTOTYPE TESTING RESULTS

	<b>Male Flywheel</b>	<b>Female Flywheel</b>
<b>Initial Speed</b>	1300 RPM	0 RPM
<b>Final Speed</b>	700 RPM	1500 RPM
<b>Initial Energy</b>	145 Joules	0 Joules
<b>Final Energy</b>	42 Joules	90 Joules

## 4.6 Final Design

### 4.6.1 Cost-Benefit Analysis of the Design

Deciding on the final design parameters consisted of a cost-benefit analysis of a number of factors. Overall goals were to maximize the height that the opposing robot was

thrown, maximize the calculated factor of safety of the dog clutch with respect to the impact force, and keep the physical implementation of the design practical in terms of size, weight, and cost. To balance these factors the mathematical model was used as a tool to determine how each parameter affected the final throw height. The moment of inertia of J2 was constrained to  $2.3 \text{ in}^2 * \text{lbm}$ . This was the minimum moment of inertia possible for the male side of the dog clutch that allowed it to have the required functionally. This value was minimized because the lower its value, the less energy to be absorbed on impact.

The moment of inertia of the flywheel was varied through a range of practical values while keeping all other parameters constant. It was determined that above a threshold value the moment of inertia of the flywheel played no role in the final throw height. The clutch was only able to transmit a limited amount of energy in the required time, and any flywheel energy above this remained in the flywheel. The role of the flywheel's moment of inertia was to change how quickly the system entered the stick state, if it did at all.

Next, the maximum torque capacity of the clutch was varied from  $1000 \text{ in} * \text{lb}$  to  $160,000 \text{ in} * \text{lb}$  while keeping all other parameters constant. This showed the result that for every increase in torque capacity of  $1000 \text{ in} * \text{lb}$  the final throw height increased by about 0.6 inches. This meant that to achieve any real benefit from the flywheel the clutch torque capacity would have to be extremely high.

The initial velocity of the flywheel and male side of the dog clutch was varied from  $100 \frac{\text{radians}}{\text{second}}$  to  $1000 \frac{\text{radians}}{\text{second}}$  while keeping all other parameters constant. This showed the expected result that as the velocity increased, the throw height increased an

amount proportional to the square of the change in velocity. This was dominated by the energy contained within the male side of the dog clutch. The results of this analysis can be seen in Figure 44.

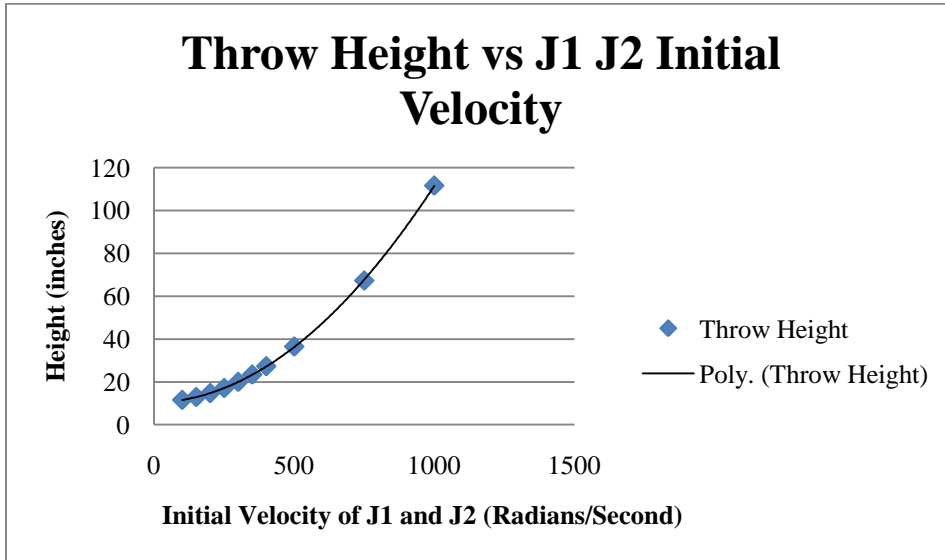


FIGURE 44: THROW HEIGHT VS J1 J2 INITIAL VELOCITY

Next, a MathCAD sheet was developed that calculated the factor of safety of the strength of the male dog teeth for different model parameters. This sheet can be found in Appendix E: Force and Stress Analysis. This was used in conjunction with the mathematical model to determine if there was any benefit to varying the ratio of the initial speed of the flywheel and slip clutch torque capacity to achieve the same throw height. A throw height of 67 inches was chosen based on the final throw height for an initial J1 and J2 velocity of  $800 \frac{\text{radians}}{\text{second}}$  and a torque capacity of  $0 \text{ in} * \text{ lbf}$ . The torque capacity was then increased incrementally and the initial velocity decreased appropriately to achieve a final throw height close to 67 inches. For each of these cases the safety factor was calculated. The safety factor was then divided by the final throw height to determine the safety factor per inch of throw height for each case. This analysis showed that for

cases of higher initial J1 and J2 velocities and lower torque capacities the safety factor was higher. The results of the analysis can be seen in Table 9.

TABLE 9: ROLE OF TORQUE CAPACITY ON SAFETY FACTOR PER INCH OF THROW HEIGHT

IV1	Ff	SF	Height	SF/Inch
800	0	3.038	68.45	.0440
800	500	3.004	67.95	.0442
800	1000	2.970	68.30	.0435
780	2000	2.974	67.06	.0443
775	3000	2.923	67.10	.0436
771	4000	2.869	67.87	.0423
768	5000	2.818	67.10	.0420
746	10000	2.559	67.25	.0381
720	20000	2.077	68.42	.0304

#### 4.6.2 Cost-Benefit Conclusion

The cost-benefit analysis indicated that in terms of factor of safety there was no benefit to placing a slip clutch between the flywheel and the dog clutch. Additionally the torque capacity of a slip clutch required to add any significant height to the final throw height was extremely high. These two results led to the conclusion that within practical limitations having a flywheel and over-load slip clutch added no real benefit to the system. This meant that final throw height is limited by the energy transfer capacity of the rubber shock absorbers and their ability to withstand high velocity impacts. Therefore the design was simplified to one having a much smaller flywheel fixed onto the male side of the dog clutch with no slip clutch.

#### 4.6.3 Final Design Parameters

The final design parameters were chosen based on results of the impact testing and calculated safety factor in order to ensure that the dog clutch would survive. The

elimination of the slip clutch from the design meant that the limiting factor in the design was the rubber shock absorber. Due to packaging constraints this severely limited the maximum throwing height of the mechanism. In order to provide a balance between performance and reliability a minimum safety factor of three was chosen for the dog clutch jaws. The primary uncertainty in this calculation was the effective average spring constant of the rubber shock absorber. A safety factor of three allowed for the estimated effective average spring constant to be incorrect by an order of magnitude and still maintain safety factor of one. To achieve a safety factor of three, it was decided that the flywheel would have an initial velocity of  $375 \frac{\text{radians}}{\text{second}}$  and a moment of inertia of  $6.5 \text{ in}^2 * \text{lbm}$ . This corresponds to a stored energy of 134 joules and 44 joules that have to be transferred by each rubber shock absorber. This is 150% of what was successfully tested in the prototype mechanism and should work well. To allow the model to behave appropriately an initial spring constant of  $6,000 \frac{\text{in} * \text{lb} * \text{f}}{\text{radian}}$  was required with a damping coefficient of  $5,000 \frac{\text{in} * \text{lb} * \text{f} * \text{second}}{\text{radian}}$ . This allowed for a maximum throw of 7.1 feet high by 28.4 feet forward and a total actuation time of 11.5 milliseconds.

## **Chapter 3: Results and Conclusions**

### **5. Results**

This project was very multi-segmented in that it involved strong elements of mechanism design, material behavior testing, and mathematical modeling and analysis. The mechanism design process utilized the design specifications to develop a set of core functional requirements for the mechanism. These were then used to develop a set of design parameters that described the physical embodiments of the solutions that fulfilled

those requirements. To accomplish this, the project goal, in addition to kinematic and energy analysis approaches were used to estimate the physical requirements of the system. This process resulted in uncertainty as to whether the rubber shock absorbers would be capable of transmitting the energy required to launch an opposing robot ten feet and still survive. To address this, an impact test mechanism was built to test various types of rubber materials. All test specimens failed and so a secondary solution was proposed. To validate this secondary solution a mathematical model of the dynamic system was created that incorporated the use of an overload slip-clutch between the flywheel and dog-clutch. The theory was that the transmission of the flywheel energy into the dog-clutch during impact could be limited. But after the impact event the slip clutch would then allow the flywheel energy to be transferred into the mechanism over time for the remainder of the motion. This more complex design increased the number of parameters in the system, and therefore gave more control and flexibility over the response of the mechanism. The mathematical model was then used as a tool to determine what role each parameter played in the maximum trajectory height. All data showed that the slip had minimal benefit. This resulted in the conclusion that if the impact force could only be mitigated through the rubber shock absorbers, then the ability of the rubber shock absorbers to survive the impact was the limiting factor in the mechanism. Therefore, the throw height of the mechanism was limited by the maximum transferrable energy. This energy quantity was calculated as 133 joules which gave a factor of safety of three, to account for uncertainties in the behavior of the rubber shock absorber. This allowed for a maximum throw of 7.1 feet high by 28.4 feet forward and a total actuation time of 11.5 milliseconds. A plot of the opposing robots trajectory can be seen in Figure 45.

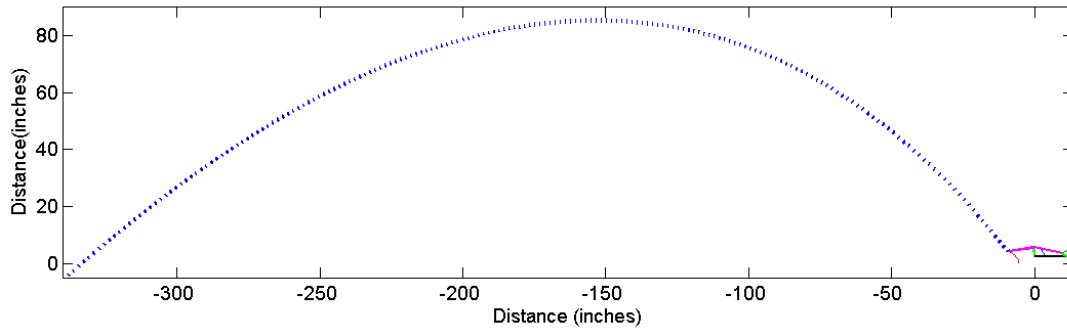


FIGURE 45: FINAL DESIGN, OPPOSING ROBOT TRAJECTORY

A plot of the angular position of the flywheel and crank of the four-bar linkage can be found in Figure 46. The slip clutch was removed in the final design, meaning that in order to simulate the system using the mathematical model,  $F_f$  is set to zero and  $J_2$  (the male side of the dog clutch) acts as the flywheel.  $J_1$  plays no role in the model as its mass is considered to be zero and the slip-clutch is non-existent.

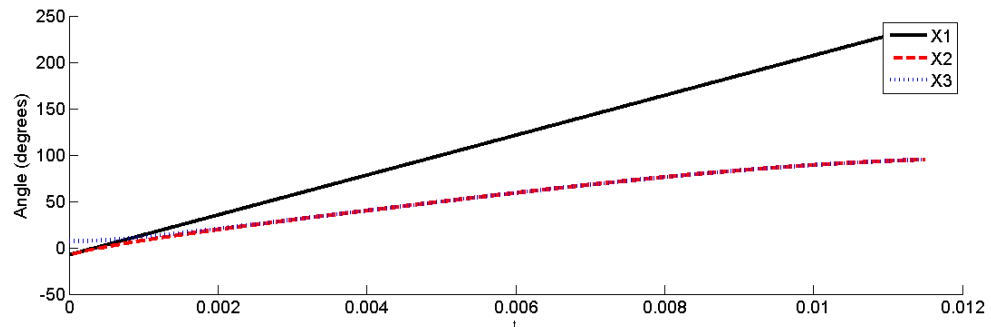


FIGURE 46: FINAL DESIGN, ANGULAR POSITION OF THE FLYWHEEL (X2) AND FOUR-BAR LINKAGE CRANK (X3) VERSUS TIME

A plot of the angular velocity of the flywheel and crank of the four-bar linkage can be found in Figure 47. As stated,  $V_2$  now represents the angular speed of the flywheel and  $V_3$ , the angular speed of the input crank on the four-bar linkage. While the slip state is shown it is meaningless as the slip-clutch is no longer part of the system.

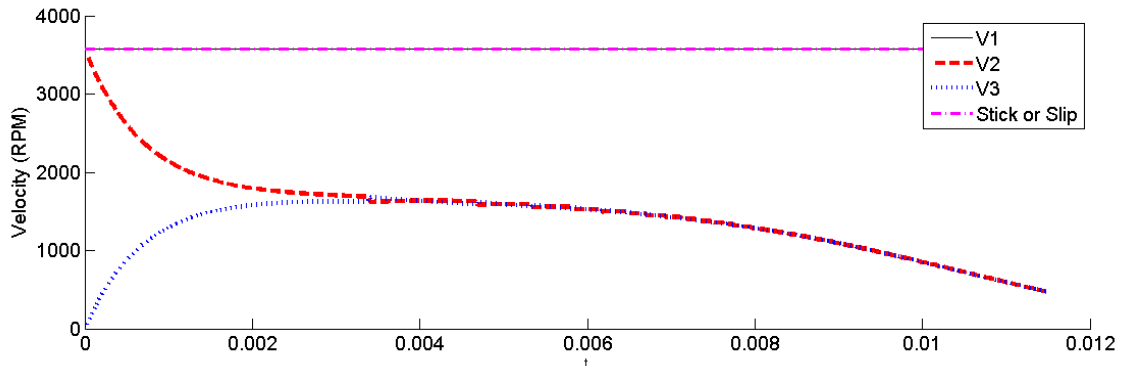


FIGURE 47: FINAL DESIGN, ANGULAR VELOCITY OF THE FLYWHEEL (V2) AND INPUT CRANK OF THE FOUR-BAR LINKAGE (V3) VERSUS TIME

The final mechanism design is shown in Figure 48.

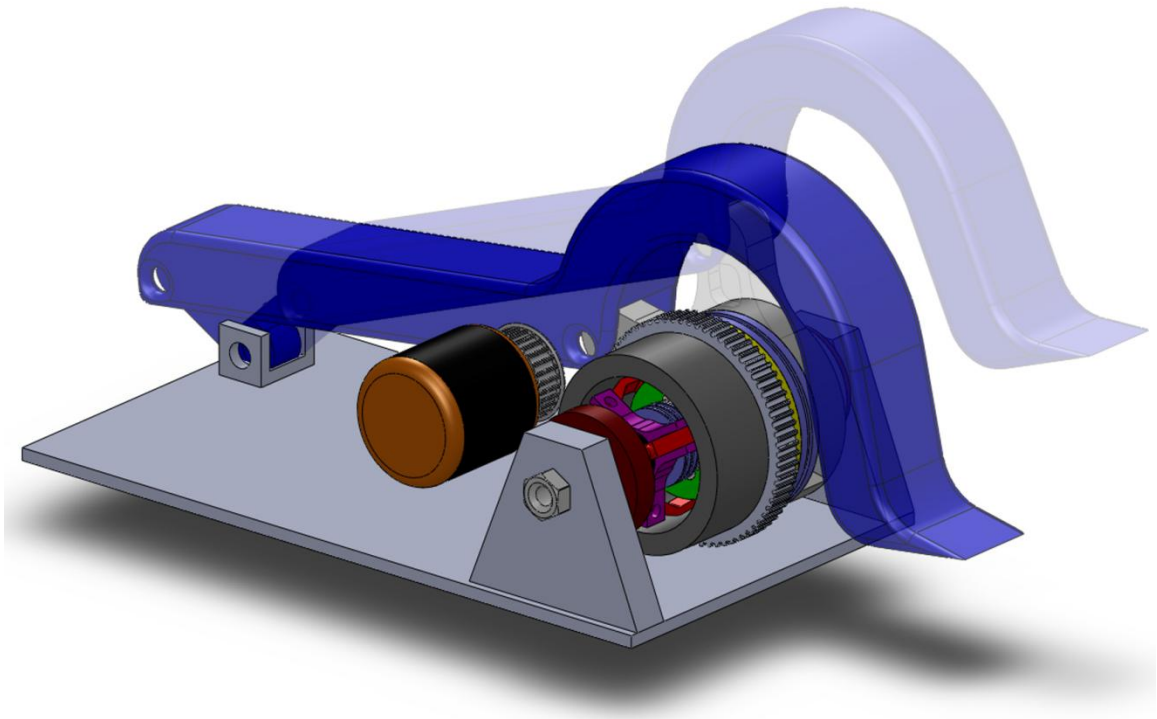


FIGURE 48, FINAL MECHANISM CAD DESIGN

## 6. Conclusion

The original goal of this research was to design and analyze a lightweight and compact energy transmission mechanism for the purpose of throwing an opposing thirty pound robot ten or more feet into the air in the sport of robotic combat. This goal was

pursued through a methodology that concurrently and iteratively included mechanism design, mathematical modeling and analyses, and experimental testing. The mechanism was designed utilizing Computer Aided Design (CAD) software and an iterative design process. The mathematical model served to analyze system performance in order to synthesize an acceptable solution for the prescribed set of constraints. Sub-system prototypes were built for experimental testing to verify portions of the design. This methodology enabled a complete understanding of the dynamic response of the proposed mechanism and its limitations. It was found that the maximum throw height is limited by the shock absorption capability of the dog-clutch during engagement. This, in turn, was limited by the ability of the rubber shock absorbers to survive impact and, then transfer the required energy without catastrophic failure. With this limitation in mind a lightweight and compact mechanism design is proposed that maintains a minimum safety factor of 3 for the jaws in the dog clutch. This design incorporates a flywheel, a self-resetting dog clutch with built in shock absorption capabilities, and an optimized four-bar linkage to deliver the energy. This finalized design is capable of launching an opposing robot 7.1 feet high by 28.4 feet forward. This final design does not meet the initial goal of 10 feet, but it will still serve the purpose of launching the opposing robot a considerable distance through the air and is highly likely to be effective in the combat arena.

## **7. Recommendations**

This research focused on the design of a functional mechanism and then the selection of key parameters within the mechanism through mathematical modeling and experimental testing of critical sub-systems. Therefore some elements of the design, while functional, have not yet been optimized in preparation for manufacturing. It is

recommended that these elements be examined and their designs adjusted accordingly to ensure that they function as expected. These cases include the sizing of the pins for the four-bar linkage joints, sizing of the links of the four-bar linkage, picking the cam profile types for the cams in the mechanism to achieve the required displacement, and choosing a DC motor to power the flywheel. The methodology to accomplish these requirements is well understood and can be found in Norton's textbook "Machine Design: An Integrated Approach" (Norton R. L., 2006).

It is recommended that after the finalization of the proposed design is complete that the mechanism be built and tested. If the mechanism works successfully, future work could include developing a more robust shock absorption approach to enable an increased throw height.

## Bibliography

All About Batteries. (2011). *Battery Energy -- What battery provides more?* Retrieved 2 25, 2011, from AllAboutBatteries: <http://www.allaboutbatteries.com/Battery-Energy.html>

Beacon Power Corporation. (2010). *About Flywheel Energy Storage*. Retrieved March 2, 2010, from Beacon Power: <http://www.beaconpower.com/products/about-flywheels.asp>

Belliveau, K. D. (2002). *An Investigation of Incipient Jump in Industrial Cam Follower Systems*. Thesis, Worcester Polytechnic Institute, Worcester, Ma.

Electromate Industrial Sales. (2010). *Servo Tek Products Company A Series- DC Tachometers*. Retrieved May 1, 2010, from Electromate: [http://www.electromate.com/products/series.php?&series\\_id=100055](http://www.electromate.com/products/series.php?&series_id=100055)

Electronic Manufacturers. (2007). *Angular Velocity Sensors*. Retrieved April 27, 2010, from Electronic Manufacturers: <http://www.electronics-manufacturers.com/products/sensors-transducers-detectors/angular-velocity-sensor/>

Haron, H. (n.d.). *Introduction to Lagrangian Mechanics*. Retrieved March 3, 2010, from Yaron Hadad: [http://www.yaronhadad.com/Site/Philosophi%C3%A6\\_Naturalis/Entries/2008/9/3\\_Introduction\\_to\\_Lagrangian\\_Mechanics\\_files/Lagrangian%20Mechanics.pdf](http://www.yaronhadad.com/Site/Philosophi%C3%A6_Naturalis/Entries/2008/9/3_Introduction_to_Lagrangian_Mechanics_files/Lagrangian%20Mechanics.pdf)

Heatherington, D. A. (2008, March 28th). *Flip-O-Matic*. Retrieved 2 1, 2011, from Dale's Homemade Robots: <http://www.wa4dsy.com/robot/flip-o-matic>

Johnson, W. (1972). *Impact Strength of Materials*. London, England: Edward Arnold Publishers Limited.

Kozesnik, A. J. (1962). *Dynamics of Machines*. (I. J. Radok, Ed., & H. Watney-Kaczerova, Trans.) Prague, Groningen: SNTL & Erven P. Noordhoff, LTD.

Li, H., Zhang, Y., & Zheng, H. (2008). Dynamic modeling and simulation of a new nine-bar press with hybrid-driven mechanism. *Journal of Mechanical Sicne and Technology* , 2436-2444.

Livermore Software Technology Group. (2007). *LS-DYNA*. Retrieved 4 25, 2011, from Livermore Software Technology Corp.: <http://www.lstc.com/lsdyna.htm>

Mabie, H. H., & Ocvirk, F. W. (1957). *Mechanisms and Dynamics of Machinery*. London: Chapman & Hall Limited.

MathWorks. (2011). *Building a Clutch Lock-Up Model*. Retrieved 12 11, 2010, from [www.Mathworks.com](http://www.Mathworks.com): [http://www.mathworks.com/products/simulink/demos.html?file=/products/demos/shipping/simulink/sldemo\\_clutch.html](http://www.mathworks.com/products/simulink/demos.html?file=/products/demos/shipping/simulink/sldemo_clutch.html)

Mitchel & Gauthier Associates. (1990, June 1). *Simulation of Frictional Surfaces and Clutch Mechanisms*. Retrieved 2 15, 2010, from acslxtreme: <http://www.acslxtreme.com/support/TechPapers/Automotive/Automotive/127.pdf>

Mundo, D., Danieli, G. A., & Yan, H. S. (2006). Kinematic Optimization of Mechanical Presses by Optimal Synthesis of Cam-Integrated Linkages. *Transactions of the CSME/de la SCGM* , 30 (4), 519-532.

Norton, R. L. (2008). *Design of Machinery: An Introduction to the Synthesis and Analysis of Mechanisms and Machines*. New York, New York: McGraw-Hill.

Norton, R. L. (2006). *Machine Design - An Integrated Approach. 3rd Edition*. Upper Saddle River, NJ: Pearson Prentice Hall.

Ofria, C. (2007). *A Short Course on Automobile Engines*. Retrieved March 2, 2010, from Family Car Parts: <http://www.familycar.com/Engine.htm>

Ogura Industrial Corp. (n.d.). *Ogura Clutch*. Retrieved April 5, 2010, from Electro Magnetic Clutches & Brakes: <http://www.ogura-clutch.com/downloads/ogura-industrial-products.pdf>

Serrarens, A., Dassen, M., & Steinbuch, M. (2004). Simulation and Control of an Automotive Dry Clutch. *FrA05,6* (pp. 4078-4083). Boston, Ma: AACC.

Shen, W., & Weileun, F. (2007). Design of a Friction Clutch Using Dual Belleville Structures. *Transactions of the ASME* , 986-990.

Slocum, A. H. (1992). *Precision Machine Design*. Dearborn, Michigan: Society of Manufacturing Engineers.

Tang, C. P. (2006, March). *Lagrangian Dynamic Formulation of a Four-Bar Mechanism with Minimal Coordinates*. Retrieved December 28, 2010, from University of Texas at Dallas: <http://www.utdallas.edu/~chinpei/pdf/FourbarMinimalCoordinates.pdf>

Tso, P.-L., & Li, C.-H. (1998). Study of Servo Press with a Flywheel. *Journal of Advanced Mechanical Design, Systems, and Manufacturing* , 2 (1), 1-11.

## Appendix A: Viability Analysis Calculations

The following calculations are to determine the maximum velocities and accelerations that are required to achieve the desired results. It was created to be used as a starting point so that design decisions could be made about the design in general. It is not expected that it will accurately or very closely model exactly what the system will do.

### Givens:

Mass of opposing robot to be thrown

$$\text{Mass}_R := 30\text{lb}$$

Vertical Displacement of 4-bar coupler point

$$\text{Throw} := 6\text{in}$$

Desired Height to throw

$$\text{Height}_D := 10\text{ft}$$

Moment of Inertia of flywheel

$$I_{\text{Flywheel}} := 5\text{in}^2 \cdot \text{lb}$$

Speed of Flywheel

$$\omega_1 := 8000 \frac{\text{rev}}{\text{min}}$$

Gear ratio between flywheel and clutch

$$\eta := 1$$

Equations:

Energy required to achieve desired height

$$PE := \text{Mass}_R \cdot \text{Height}_D \cdot g = 406.745\text{J}$$

Energy of the flywheel at given speed. Should be greater than PE

$$E_{\text{Flywheel}} := \frac{1}{2} \cdot I_{\text{Flywheel}} \cdot \omega_1^2 = 513.464\text{J}$$

Average force required given the energy required and distance to impart it

$$\text{Force}_{\text{avg}} := \frac{PE}{\text{Throw}} = 600\text{lbf}$$

Average acceleration required given the average force and mass of the opposing robot

$$\text{Accel}_{\text{avg}} := \frac{\text{Force}_{\text{avg}}}{\text{Mass}_R} = 643.481 \frac{\text{ft}}{\text{s}^2} \quad \text{Minimum Required}$$

Speed of the flywheel after transferring energy to opposing robot

$$\omega_2 := \frac{\sqrt{I_{\text{Flywheel}}^2 \cdot \omega_1^2 - 2 \cdot I_{\text{Flywheel}} \cdot PE}}{I_{\text{Flywheel}}} = 3.647 \times 10^3 \frac{\text{rev}}{\text{min}}$$

Throw time required to achieve the average acceleration over the given throw distance

$$\text{Time}_{\text{Throw}} := \frac{\sqrt{0^2 - 4 \cdot .5 \text{Accel}_{\text{avg}} \cdot \text{Throw}}}{2 \cdot .5 \text{Accel}_{\text{avg}}} = 0.039\text{s}$$

Maximum velocity reached during throw given the average acceleration

$$\text{Velocity}_{\text{Peak}} := \text{Accel}_{\text{avg}} \cdot \text{Time}_{\text{Throw}}$$

At this point it is assumed that the speed of the flywheel begins at  $w_1$  and finishes at  $w_2$ . It does this over time period "max". A second assumption is made that the change in speed from  $w_1$  to  $w_2$  occurs exponentially, as shown in the function  $w.\text{init}$

This function defines the transition type

$$\omega_{\text{init}}(t, \text{max}) := \omega_1 \cdot e^{\left( \frac{\ln\left(\frac{\omega_1}{\omega_2}\right)}{-\text{max}} \right) t}$$

This allows for MathCAD to iterate to approximate a solution for the launch time given that it must decrease in speed over 90 degrees. An estimated time is input and it outputs a more accurate time.

$$\omega_{\text{Clutch.Iterate}}(t) := \frac{(90\text{deg})}{\eta} \left( \frac{\int_0^t \omega_{\text{init}}(T, t) dT}{t} \right)$$

This iterates the Time.Launch until the result of w.Clutch.Iterate is close enough to Time.Throw that it meets the error criteria, I.E. it is very close to zero.

$$\text{Time}_{\text{Launch}} := \begin{cases} T \leftarrow \text{Time}_{\text{Throw}} \\ \text{while } \left| \omega_{\text{Clutch.Iterate}}(T) - T \right| > .000001 \\ T \leftarrow \omega_{\text{Clutch.Iterate}}(T) \end{cases} \quad \begin{array}{l} \text{This iterates until it reaches} \\ \text{a solution for time within} \\ \text{desired error value} \end{array}$$

The final solution for the launch time

$$\text{Time}_{\text{Launch}} = 2.707 \times 10^{-3} \text{ s}$$

The assumed speed of the flywheel after being coupled to the four-bar linkage as a function of time

$$\omega_{\text{Flywheel}}(t) := \omega_1 \cdot e^{\left( \frac{\ln\left(\frac{\omega_1}{\omega_2}\right)}{-\text{Time}_{\text{Launch}}} \right) t}$$

The average speed of the flywheel during deceleration

$$\omega_{\text{avg}} := \frac{\int_0^{\text{Time}_{\text{Launch}}} \omega_{\text{Flywheel}}(t) dt}{\text{Time}_{\text{Launch}}}$$

The acceleration of the flywheel by taking the derivative of the speed function

$$\alpha_{\text{Flywheel}}(t) := \left( \frac{\ln\left(\frac{\omega_1}{\omega_2}\right)}{-\text{Time}_{\text{Launch}}}\right) \cdot \omega_1 \cdot e^{\left( \frac{\ln\left(\frac{\omega_1}{\omega_2}\right)}{-\text{Time}_{\text{Launch}}}\right) \cdot t}$$

Speed of the clutch as a function of time

$$\omega_{\text{Clutch}}(t) := \frac{\omega_{\text{Flywheel}}(t)}{\eta}$$

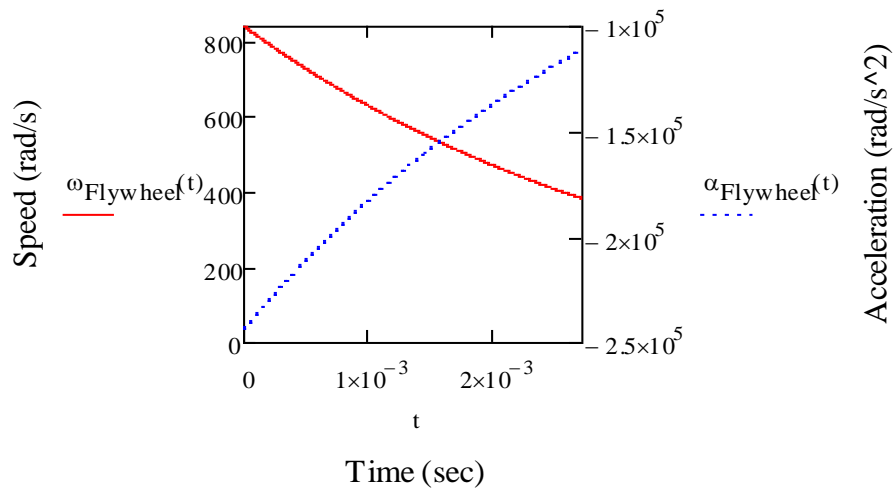
Position of the flywheel as a function of time

$$\theta_{\text{Flywheel}}(t) := \omega_{\text{Flywheel}}(t) \cdot t$$

Position of the clutch as a function of time

$$\theta_{\text{Clutch}}(t) := \frac{\theta_{\text{Flywheel}}(t)}{\eta}$$

Plot of the speed and acceleration of the flywheel as a function of time



Torque output of the flywheel

$$T_{\text{Flywheel}}(t) := -\alpha_{\text{Flywheel}}(t) \cdot I_{\text{Flywheel}}$$

Torque seen at the clutch after gear reduction

$$T_{\text{Clutch}}(t) := T_{\text{Flywheel}}(t) \cdot \eta$$

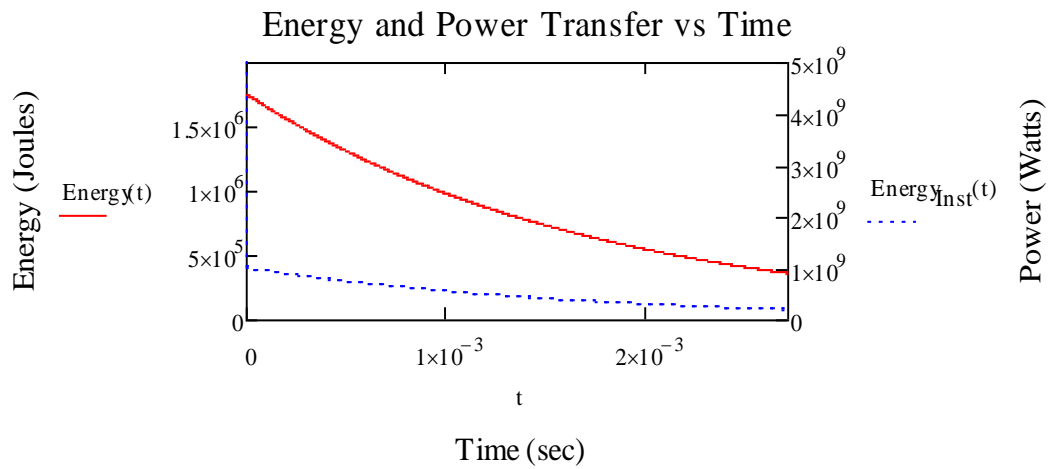
Energy function in terms of time

$$\text{Energy}(t) := \frac{1}{2} \cdot I_{\text{Flywheel}} \cdot \omega_{\text{Flywheel}}(t)^2$$

Rate of change of energy transfer, Instantaneous power transfer

$$\text{Energy}_{\text{Inst}}(t) := \frac{d}{dt} \text{Energy}(t) \cdot -1$$

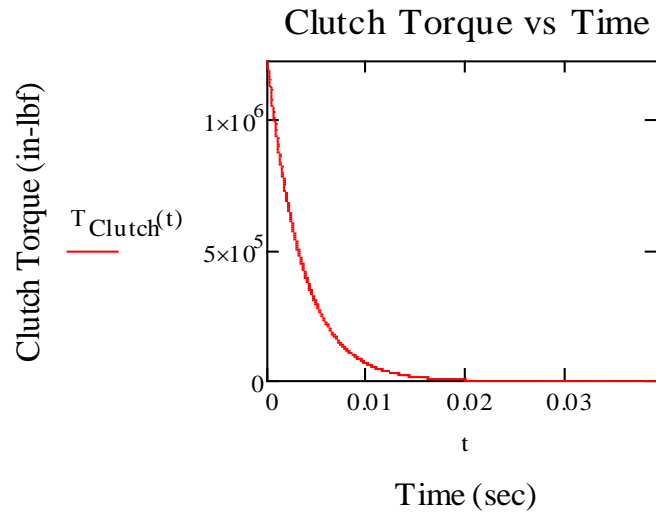
Plot showing Energy and Energy.Inst over time



## Friction Clutch Feasibility Analysis

The previous analysis allows for a friction clutch feasibility analysis

The torque seen at the clutch varies as a function of time. The following plot illustrates that.



The maximum torque is at time zero

$$\text{Torque}_{\text{Max}} := T_{\text{Clutch}}(0\text{sec}) = 3.148 \times 10^3 \cdot \text{in} \cdot \text{lbf}$$

A theoretical friction disk clutch is then formulated with an inner radius of  $r_1$  and outer radius of  $r_2$

$$r_1 := .625\text{n}$$

$$r_2 := 2.5\text{n}$$

The effective radius of the clutch is then calculated

$$R := \frac{2}{3} \cdot \frac{r_2^3 - r_1^3}{r_2^2 - r_1^2} = 1.75 \text{ in}$$

The force required on the friction plates to transfer the required torque is then calculated

$$F_n := \frac{\text{Torque}_{\text{Max}}}{R \cdot \mu} = 5.997 \times 10^3 \cdot \text{lbf}$$

The force required to transfer the desired torque is far too high. It would be impractical to engage and disengage that much force quickly enough with the size and weight restrictions.

## Dog-Clutch Feasibility Analysis

The feasibility of a dog clutch is determined

Average radius of dogs

$$R_{\text{Dog}} := 1.4375n$$

Number of Dogs

$$\text{Number}_{\text{Dogs}} := 3$$

Height of dogs

$$\text{Height} := .1875n$$

Width of dogs

$$\text{Width} := .75n$$

Dog Contact Patch Area

$$\text{Area} := \text{Height} \cdot \text{Width} = 0.141n^2$$

Max force seen by all dogs combined

$$\text{Force}_{\text{NetDogs}} := \frac{\text{Torque}_{\text{Max}}}{R_{\text{Dog}}} = 2.19 \times 10^3 \cdot \text{lbf}$$

Max force seen by an individual dog

$$\text{Force}_{\text{Dog}} := \frac{\text{Force}_{\text{NetDogs}}}{\text{Number}_{\text{Dogs}}} = 730.051 \text{lbf}$$

Young's Modulus of Material

$$E_{\text{Steel}} := 210 \text{GPa} = 3.046 \times 10^7 \text{psi}$$

There is no single valid modulus of elasticity for rubber. It changes as it compresses and is highly dependent on strain rate. This value is simple a rough estimation

$$E_{\text{Rubber}} := .464 \text{GPa} = 6.73 \times 10^4 \text{psi}$$

Spring Constant of Rubber

$$k := \frac{E_{\text{Rubber}} \cdot (\text{Area})}{.25 \text{in}} = 3.785 \times 10^4 \cdot \frac{\text{lbf}}{\text{in}}$$

Kinetic energy dissipation factor. Minimal so equal to 1

$$\eta_i := 1$$

Impact force using energy estimation methods

$$F_i := \frac{\omega_1}{\eta} \cdot \sqrt{\eta_i \cdot I_{\text{Flywheel}} \cdot \eta^2 \cdot k} = 1.855 \times 10^4 \cdot \text{lbf}$$

Ratio of impact force to loading due to torque transfer

$$\frac{F_i}{\text{Force}_{\text{Dog}}} = 25.405$$

The ratio of the foot print of a dog boss versus the height indicates that beam calculations will not be valid. Therefore only shear and compressive stresses are evaluated.

Area of the footprint of a dog

$$\text{Footprint} := .36 \text{in}^2$$

Shear Stress on single dog

$$\tau_{\text{Direct}} := \frac{F_i}{\text{Footprint}} = 5.152 \times 10^4 \text{ psi}$$

Compressive Stress on impact surface

$$\sigma_{\text{Compressive}} := \frac{F_i}{\text{Height} \cdot \text{Width}} = 1.319 \times 10^5 \cdot \text{psi}$$

Yield Stress of 4140 Steel at 40 Rockwell C

$$\text{Stress}_{\text{Yield}} := 165000 \text{ psi} = 1.138 \text{ GPa}$$

Safety Factor in Compression

$$\text{SF}_{\text{Compressive}} := \frac{\text{Stress}_{\text{Yield}}}{\sigma_{\text{Compressive}}} = 1.251$$

Safety Factor in Shear

$$\text{SafetyFactor1} := \frac{\text{Stress}_{\text{Yield}}}{\tau_{\text{Direct}}} = 3.203$$

Conclusion: It is feasible to use a dog clutch

## Clutch Engagement Mechanism Design

### Spring Engagement

Mass of the male side of the dog clutch that must move axially via the spring force

$$\text{Mass}_{\text{Male}} := 3\text{lb}$$

Desired Deflection

$$\Delta L := .2\text{in}$$

Spring Specifications as gotten from manufacturer

Inner Diameter

$$D_i := .755\text{in}$$

Outer Diameter

$$D_o := 1.5\text{in}$$

Overall Height

$$\text{OH} := .093\text{in}$$

Thickness

$$\text{Thck} := .045\text{in}$$

Force when flat

$$F_{\text{flat}} := 400\text{bf}$$

Poisson's Ratio for Steel

$$\nu := .3$$

Maximum Deflection

$$h := \text{OH} - \text{Thck} = 0.048\text{in}$$

Diameter Ratio

$$R_d := \frac{D_o}{D_i} = 1.987$$

Usable deflection to maximize spring life

$$\delta_{\text{max}} := .85h - .15h = 0.034\text{in}$$

Number of springs required to achieve desired deflection

$$N_s := \text{Round}\left(\text{round}\left(\frac{\Delta L}{\delta} + .5, 0\right) + .5, 2\right) = 6$$

Spring Constant

$$K_1 := \frac{6}{\pi \cdot \ln(R_d)} \cdot \left[ \frac{(R_d - 1)^2}{R_d^2} \right]$$

Modulus of Elasticity of Spring

$$E_{\text{spring}} := \frac{F_{\text{flat}} \cdot K_1 \cdot D_o^2 (1 - \nu^2)}{4h \cdot \text{Thck}^3}$$

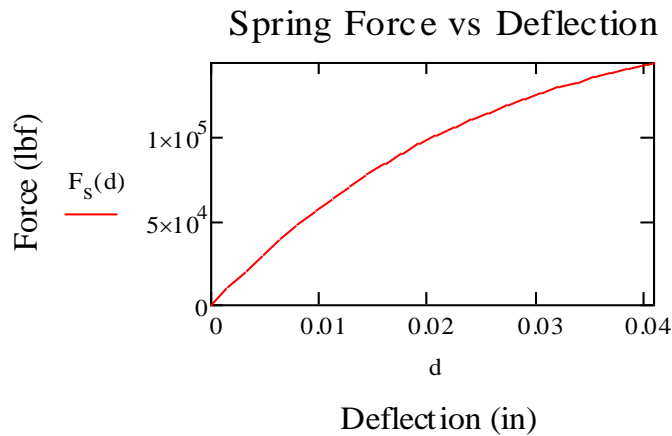
Spring Constant Function

$$F_s(y) := \frac{4 \cdot E_{\text{spring}} \cdot y}{K_1 \cdot D_o^2 \cdot (1 - \nu^2)} \cdot \left[ (h - y) \left( h - \frac{y}{2} \right) \text{Thck} + \text{Thck}^3 \right]$$

Time necessary to engage given the desired angle it should engage in

$$\text{Time}_{\text{Eng}}(\theta) := \frac{\theta}{\left( \frac{\omega_{\text{Flywheel}}(0)}{\eta} \right)}$$

Plot of spring force vs deflection



Acceleration of the male side of the dog clutch due to spring force as a function of deflection

$$\alpha_s(d) := \left[ \frac{F_s(d)}{\text{Mass Male}} \right]$$

Velocity of the male side of the dog clutch due to spring force as a function of deflection

$$\text{Vel}(d) := \sqrt{\frac{\int_{.15 \cdot h}^{.15 \cdot h + d} F_s(y) dy \cdot 2}{\text{Mass Male}}}$$

Time for spring expand a given deflection

$$\text{Time}_{\text{Trans}}(d) := \frac{\text{Vel}(d)}{\alpha_s(d)}$$

Force of spring given a deflection with proper indexing

$$\text{Force}_S(d) := F_s(.15h + d)$$

Force at zero deflection

$$\text{Force}_S(0) = 113.675 \text{ lbf}$$

Force at maximum deflection

$$\text{Force}_S(\delta) = 373.365 \text{ lbf}$$

Total deflection

$$\Delta D := \delta \cdot N_s = 0.202 \text{ in}$$

Number of springs required

$$N_s = 6$$

Total spring length uncompressed

$$L_i := (OH - .15h) \cdot N_s = 0.515 \text{ in}$$

Total spring length compressed

$$L_f := L_i - \Delta D = 0.313 \text{ in}$$

Total time to decompress

$$\text{Time}_{\text{Trans}}(\delta) = 1.1 \times 10^{-3} \text{ s}$$

Time necessary to engage given the desired angle it should engage in. Used to manually iteratively verify feasibility of specified springs

$$\text{Time}_{\text{Eng}}(50\text{deg}) = 1.042 \times 10^{-3} \text{ s}$$

Face Cam Analysis

Degrees through which one of the three cam faces travel through

$$\text{degrees} := 35\text{deg}$$

Radius at which the cams are located

$$\text{radius} := .75 \text{ in}$$

Length of the arc the cam passes through

$$\text{Length}_{\text{Arc}} := \text{degrees} \cdot \sqrt{\text{radius}^2 + \left(\frac{\text{Height}}{\text{degrees}}\right)^2} = 0.495 \text{ in}$$

Steepness angle of the face cam

$$\text{Angle}_{\text{Arc}} := \text{atan}\left(\frac{\text{Height}}{\text{Length}_{\text{Arc}}}\right) = 20.745\text{deg}$$

Torque required to compress spring

$$\text{Torque}_{\text{FaceCam}}(d) := \frac{\text{Force}_S(d)}{\tan(\text{Angle}_{\text{Arc}})} \cdot \text{radius}$$

Function to determine energy used to compress spring

$$\text{Energy}_{\text{FaceCam}}(d) := \text{Torque}_{\text{FaceCam}}(d) \cdot \text{degrees}$$

Energy used to compress the spring

$$\text{Energy}_{\text{FaceCam}}(\delta) = 51.026\text{J}$$

Percent of remaining energy in flywheel after launch used to compress spring

$$\frac{\text{Energy}_{\text{FaceCam}}(\delta)}{E_{\text{Flywheel}} - \text{PE}} = 47.814\%$$

## Appendix B: Impact Testing

An air cannon was built and tested in order to accelerate a projectile to a desired speed of 70 mph. In order to determine the appropriate pressure to operate the cannon and achieve the desired velocity, a series of tests were performed. The speed of the projectile out of the barrel of the cannon was measured using strobe flash photography. A single photograph was taken as the projectile left the barrel with a flash strobe operating at 120 Hz. This produced the photographs shown in Figure 49 through Figure 52. Cloth wadding was used in all testing to create a tighter air seal between the projectile and the air cannon barrel.

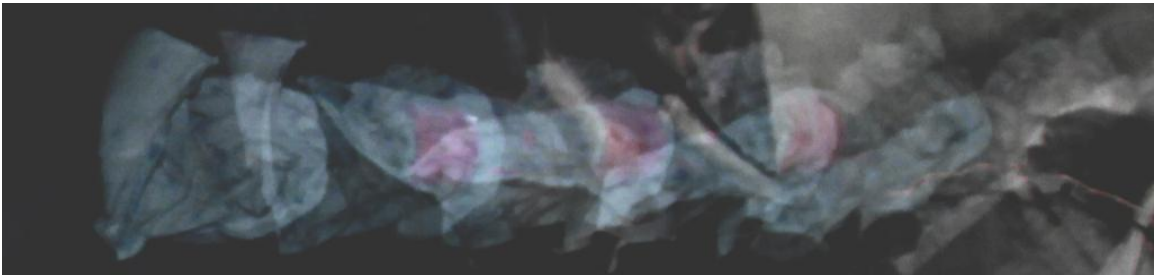


FIGURE 49: PROJECTILE MOTION 40 PSI



FIGURE 50: PROJECTILE MOTION 60 PSI



FIGURE 51: PROJECTILE MOTION 80 PSI



FIGURE 52: PROJECTILE MOTION 100 PSI

Using Windows Paint, the number of pixels between each strobe flash was measured and this converted to inches using the length of the projectile as a reference measurement.

The speed of the strobe was 120 Hz which allowed the speed of the projectile to be calculated. The data collected can be found in Table 10.

TABLE 10: PROJECTILE MOTION DATA COLLECTED

Length (px)	Length (in)	Scale (in/px)	X Traveled (px)	X Traveled (in)	Time (Sec)	Speed (in/sec)	PSI	Speed MPH
28.2843	2	0.0707	116	8.2024	0.0083	984	60	56
61.5224	2	0.0325	203	6.5992	0.0083	792	40	45
37.4833	2	0.0534	190	10.1378	0.0083	1217	80	69
49.3660	2	0.0405	295	11.9516	0.0083	1434	100	81

This data allowed for the relationship between the pressure and speed to be calculated.

This relationship is shown in Figure 53.

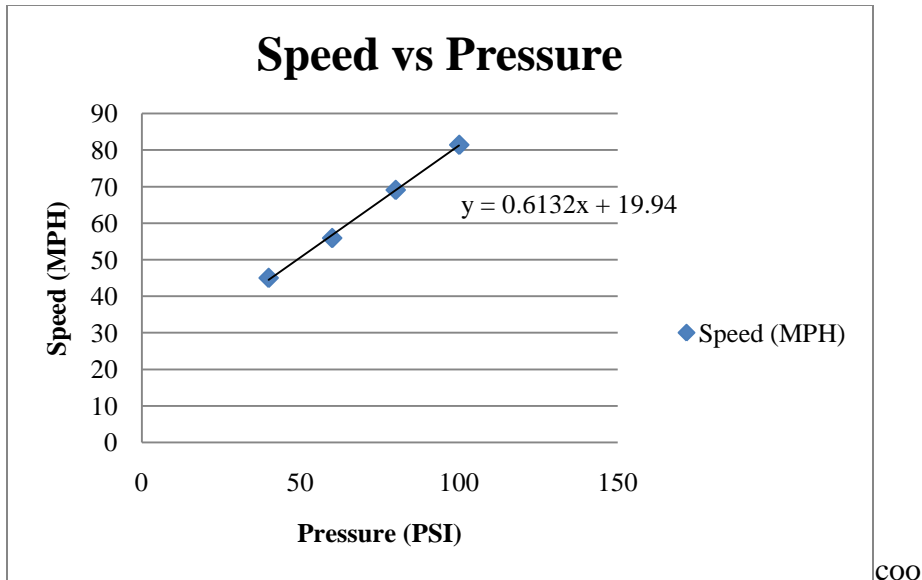


FIGURE 53: SPEED VS PRESSURE

MathCAD was then used to determine what pressure to operate the air cannon at for a given projectile weight.

Velocity as a function of pressure relationship

$$\text{Vel}(p) := \left[ \left( 0.6132 \frac{p}{\text{psi}} \right) + 19.94 \right] \cdot \frac{\text{mi}}{\text{hr}}$$

Average Acceleration of Projectile in Barrel

$$\text{acc}(p) := \frac{(\text{Vel}(p))^2}{2 \cdot 6\text{ft}}$$

Average Force (F=M\*A) with a 6.5lb projectile

$$\text{Force\_act}(p) := \text{acc}(p) \cdot 6.5\text{lb}$$

Effective Radius of Barrel

Represents the effective radius based on the average force based on the relationship

Force=Pressure\*Area. Takes into account all system losses

$$\text{Rad}(p) := \sqrt{\frac{\text{Force\_act}(p)}{p \cdot 3.14}}$$

Force as a Function of Pressure  
Uses the effective radius of the barrel

$$\text{Force}(p) := 3.14 \text{Rad}(p)^2 \cdot p$$

Energy as a Function of Pressure (Work=Force\*Distance)

$$\text{Energy}(p) := \text{Force}(p) \cdot 6\text{ft}$$

Final Projectile Velocity as a Function of Pressure

Based on the energy function calculation and assuming a 3.5lb projectile weight

$$\text{Velocity}(p) := \sqrt{\frac{\text{Energy}(p) \cdot 2}{3.5\text{b}}}$$

These functions allow for the determination of what pressure to run the air cannon at to achieve a desired velocity and energy

Pressure:

$$n := 50\text{psi}$$

Energy:

$$\text{Energy}(n) = 754.29\text{J}$$

Velocity:

$$\text{Velocity}(n) = 68.956 \frac{\text{mi}}{\text{hr}}$$

The following are the test results of each type of rubber tested after one impact each. They are shown in Figure 54, Figure 55, Figure 56, Figure 57, Figure 58, Figure 59, and Figure 60.



FIGURE 54: 30A SILICON RUBBER SAMPLE AFTER ONE IMPACT

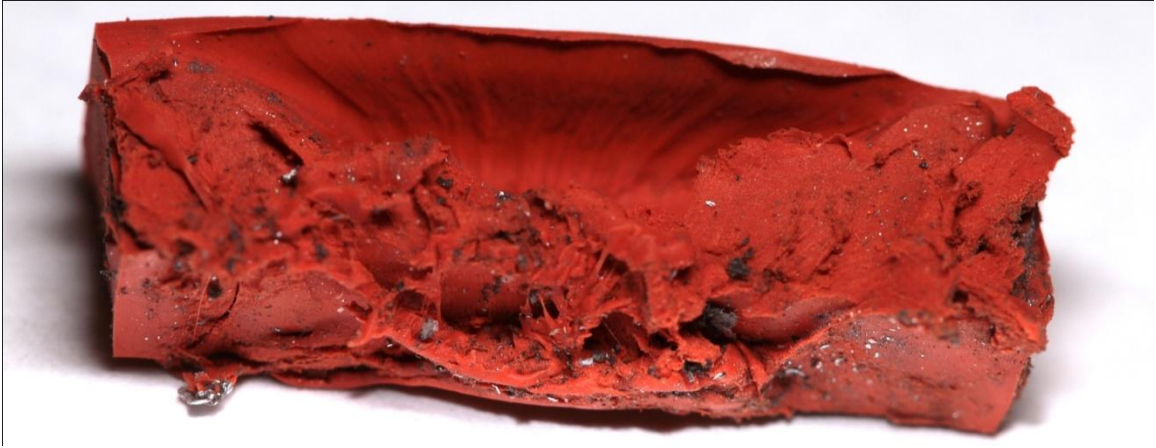


FIGURE 55: 40A SILICON RUBBER SAMPLE AFTER ONE IMPACT



FIGURE 56: 60A SILICON RUBBER SAMPLE AFTER ONE IMPACT



FIGURE 57: NATURAL RUBBER SAMPLE AFTER ONE IMPACT



FIGURE 58: EVA FOAM RUBBER SAMPLE AFTER ONE IMPACT



FIGURE 59: NATURAL FOAM GUM RUBBER SAMPLE AFTER ONE IMPACT



FIGURE 60: POLYURETHANE FOAM RUBBER SAMPLE AFTER ONE IMPACT

## Appendix C: Four-Bar Synthesis and Optimization Programs

### FourBarOptimizer.m

```
%FourBarOptimizer.m
% Written by: Brian Benson 2010/2011

% Given a minimum and maximum length for each link in a four-bar
linkage
% and a desired interval, this script filters through every linkage and
% returns those that meet the defined criteria
% To use simply run this script.

%Clear all variables and the command window
clc
clear
clear all;
clear global;

warning off all %Turn off warnings

MinA=11; %Minimum Length of Link A (Lo)
MaxA=12; %Maximum Length of Link A (Lo)
MinB=3;%Minimum Length of Link B (L1)
MaxB=4; %Maximum Length of Link B (L1)
MinC=10;%Minimum Length of Link C (L2)
MaxC=11; %Maximum Length of Link C (L2)
MinD=2;%Minimum Length of Link D (L3)
MaxD=3; %Maximum Length of Link D (L3)
Interval=.025; %Interval to increment each link by for iteration

RANGE=BruteForce (MinA,MaxA,MinB,MaxB,MinC,MaxC,MinD,MaxD,Interval);
%Creates a matrix of every possible linkage with defined ranges.

[HRange WRANGE]=size(RANGE); %Calculates the Height and Width of the
range

holder=[]; %Initializes the holder matrix
for n=1:HRange %Run for entire length of RANGE

    %Calculate the Velocity Ratio, Total Moment of Inertia, Coupler
Vertical
    %Displacement, and a true or false of if the coupler vertical
    %acceleration stayed positive. Sets each of these to their
    respective
    %variables
    [VelRat MOITotal Height PosAccel]=VELMOI(RANGE(n,1), RANGE(n,2),
RANGE(n,3), RANGE(n,4));

    %IF acceleration remains positive and the velocity ratio is a real
    %number, and the total moment of inertia is a real number (both of
    %these relate to if the linkage is geometrically possible for the given
    %range, and the Velocity Ratio (VCY/VCX) is greater than a given value,
```

```

%and the total moment of inertia is greater than zero (should never be
%negative) and the total moment of inertia is less than a given value

    if PosAccel==0 && isreal(VelRat) && isreal(MOITotal) && VelRat>5 &&
MOITotal >0 && MOITotal<2000

        %Then store the calculated values in the "holder" matrix along with
the length of each link
        holder=[holder; VelRat MOITotal Height RANGE(n,1) RANGE(n,2)
RANGE(n,3) RANGE(n,4)];
        else
            %Otherwise do nothing
        end
    end
end

result=sortrows(holder,2); %Sort the result of the above for loop from
least to greatest by the total moment of inertia

[Hresult Wresult]=size(result); %Calculate the Height and Width of the
result

Result=[]; %Initialize the Result Matrix
for n=1:round(Hresult*1) %Cut the end off the Result matrix, keeping a
percentage defined by the number multiplied by Hresult. Allows for less
results to be plotted then were calculated
    Result=[Result;result(n,:)];
end

figure
subplot(2,1,1)
hold on
scatter(Result(:,2),Result(:,1),10,'s','filled') %Plot each total
moment of inertia versus the velocity ratio
legend('Velocity Ratio');ylabel('Velocity Ratio');xlabel('Total
MOI');%Legend
subplot(2,1,2)
hold on
scatter(Result(:,2),Result(:,3),10,'s','filled') %Plot each total
moment of inertia versus the vertical displacement of the coupler
point.
legend('Coupler Height');ylabel('Coupler Height
(inches)');xlabel('Total MOI');%Legend

```

## BruteForce.m

```
function [Final] = BruteForce(MinA, MaxA, MinB, MaxB, MinC, MaxC, MinD,
MaxD, Interval)
%BruteForce.m
% Written by: Brian Benson 2010/2011
% BruteForce.m accepts four ranges, each defined by a minimum and
%maximum, and an interval. These are ranges A, B, C, and D. Each %range
%is used to define a vector with starting value Min and %incremented by
%the interval to the Max value for that given range. These vectors are
%then used to determine every unique combination of values that create
%a vector with 4 columns. Values from range A can only be used in
%column 1 (or A) and the same is true for ranges B,C, and D. The total
%number of possibilities is the size of Range A * size of Range B *
%size of Range C * Size of Range D.

A=MinA:Interval:MaxA; %Vector Range A
B=MinB:Interval:MaxB; %Vector Range B
C=MinC:Interval:MaxC; %Vector Range C
D=MinD:Interval:MaxD; %Vector Range D

A=A'; %Transpose of A
B=B'; %Transpose of B
C=C'; %Transpose of C
D=D'; %Transpose of D

[HA WA]=size(A); %Height and Width of A
[HB WB]=size(B); %Height and Width of B
[HC WC]=size(C); %Height and Width of C
[HD WD]=size(D); %Height and Width of D

FirstColumn=[]; %Initializes the first column
FirstColumnOnes=ones(HB*HC*HD,1); %Create a vector of length HB*HC*HD
with values 1
for n=1:HA %Run for entire length of Range A
    FirstColumn=[FirstColumn; FirstColumnOnes.*A(n,1)]; %Set the first
column to Range A where each number in Range A is repeated HB*HC*HD
times
end

SecondColumn=[]; %Initializes the second column
SecondColumnOnes=ones(HC*HD,1); %Create a vector of length HC*HD with
values 1
for n=1:HB %Run for entire length of Range B
    SecondColumn=[SecondColumn; SecondColumnOnes.*B(n,1)]; %Set the
second column to Range B where each number in Range B is repeated HC*HD
times
end
SecondColumn=repmat(SecondColumn,HA,1); %Set the second column defined
above to repeat itself HA times

ThirdColumn=[]; %Initializes the second column
ThirdColumnOnes=ones(HD,1); %Create a vector of length HD with values 1
for n=1:HC %Run for entire length of Range C
```

```
    ThirdColumn=[ThirdColumn; ThirdColumnOnes.*C(n,1)]; %Set the second
column to Range C where each number in Range C is repeated HD times
end
ThirdColumn= repmat(ThirdColumn,HA*HB,1); %Set the third column defined
above to repeat itself HA*HB times

FourthColumn=repmat(D,HA*HB*HC,1); %Set the fourth column to repeat
range D HA*HB*HC times

Final=[FirstColumn SecondColumn ThirdColumn FourthColumn]; %Combine
vectors A,B,C, and D to the Final Matrix

end
```

## MOIOPT.m

```
function [ Inertia ] = MOIOPT(Theta, Lo,L1,L2,L3)
%MOIOPT.m
% Written by: Brian Benson 2010/2011
% MOIOPT.m calculates the moment of inertia for use in the
% FourBarOptimizer.m program. It accepts an angle in degrees and
% lengths of the different links in inches. It outputs the moment of
%inertia in in^2*lb

%INPUTS%
theta=Theta/57.3; %Converts the angle from degrees to radians

%These inputs are defined in the Main.m file.

%%Set Global Variables
global I1 I2U I2L I3 ML1 ML2 ML3

Lc1=(.5*L1)/3.5;
Lc2=(9.1*L2)/9.5;
Lc3=L3/2;
I1=4.32;

if theta<.12+(5/57.3) %For first 5 degrees of movement
    I2=I2U; % Effective Moment of Inertia of Link 2 Unloaded (No robot
on it)
else
    I2=I2L;%Otherwise consider the four-bar to be loaded (Robot on it)
end

k1=-2.*L1.*L3.*sin(theta);
k2=2.*L3.*(Lo-L1.*cos(theta));
k3=Lo.^2+L1.^2-L2.^2+L3.^2-2.*Lo.*L1.*cos(theta);

phi=2*atan2(-k1-sqrt(k1.^2+k2.^2-k3.^2),k3-k2);
alpha=atan2(-L1.*sin(theta)+L3.*sin(phi),Lo-
L1.*cos(theta)+L3.*cos(phi));

J1=.5.*(ML1.*Lc1.^2+I1+ML2.*L1.^2);
J2=.5.*(ML2.*Lc2.^2+I2);
J3=.5.*(ML3.*Lc3.^2+I3);

S1=(L1.*sin(phi-theta))./(L2.*sin(alpha-phi));
S2=(L1.*sin(alpha-theta))./(L3.*sin(alpha-phi));

P1=ML2.*L1.*Lc2;
C1=cos(theta-alpha);

Inertia=2.*(J1+J2.*S1.^2+J3.*S2.^2+P1.*C1.*S1); %Final Effective Moment
of Inertia
end
```

## VelMOI.m

```
function [VelocityRatio, TotalMOI, Height, PosVelocity] =
VELMOI(Lo,L1,L2,L3)
%VELMOI.m
% Written by: Brian Benson 2010/2011
% VELMOI.m calculates the Velocity Ratio, TotalMOI, Height, and
% whether acceleration remains positive throughout the range of motion
%(true or false). It accepts the lengths of the different links in
%inches.

start=8; %Degrees to start range of motion of input link of the four-
bar
final=90; %Degrees to start range of motion of input link of the four-
bar
angle=start:final; %Creates a vector of numbers from start to final in
intervals of 1

%%PosVelocity
Cposition=[]; %Initializes the Coupler point vertical position vector
for n=start:final %For every angle between start and final
    [placeholder,Cy]=VelRatio(n,Lo,L1,L2,L3); %Calculate the vertical
position of the coupler point for every angle
    Cposition=[Cposition;Cy]; %Store the coupler point vertical
position in the Cposition vector
end

velocity=diff(Cposition); %Calculates the vertical velocity of the
coupler point through the range of motion
check=[]; %Initializes the check vector

for n=1:(final-start-1) %For each whole angle in the range of motion
    if velocity(n,1)>0 %If the velocity is greater than zero
        check=[check;0]; %Store 0 in the check vector
    else
        check=[check;1]; %Otherwise store a 1 indicating that velocity is
negative and the four-bar fails
    end
end

%%TotalMOI
MOI=MOIOPT(angle,Lo,L1,L2,L3); %Calculate the moment of inertia for the
entire range of motion
TotalMOI=sum(MOI); %Sum the moments of inertia for every angle in the
range

%%PosVelocity
PosVelocity=sum(check); %False (0) if velocity is always above zero,
True (>0) if velocity is below zero

%%HEIGHT
[VelocityRatio Cy]=VelRatio(final,Lo,L1,L2,L3); %Calculate and store
the final vertical coupler position
[placeholder Cy1]=VelRatio(start,Lo,L1,L2,L3); %Calculate and store
initial vertical coupler position
```

```

Height=abs(Cy1-Cy); %Calculate the total vertical displacement of the
coupler point
end

```

## VelRatio.m

```

function [ VelocityRatio, Cy] = VelRatio(theta,Lo,L1,L2,L3)
%VELRatio.m
% Written by: Brian Benson 2010/2011
% VELMOI.m calculates the Velocity Ratio, and vertical position %of
the coupler point. It accepts the lengths of the different links in
%inches and the angle of the input link in degrees.

theta2=theta/57.3; %Converts angle to radians
V3=10; %Arbitrary Input link angular velocity
zeta3=198/57; %Angle of vector p from point 2,3 to coupler point
P=9.21; % Distance of point A from coupler point

%KINEMATICS CALCULATION: Refer to Norton's Design of Machinery for
explanations of terms.
K1=Lo./L1;
K2=Lo./L3;
K3=(L1.^2-L2.^2+L3.^2+Lo.^2)./(2.*L1.*L3);
K4=Lo./L2;
K5=(L3.^2-Lo.^2-L1.^2-L2.^2)./(2.*L1.*L2);

A=cos(theta2)-K1-K2.*cos(theta2)+K3;
B=-2.*sin(theta2);
C=K1-(K2+1).*cos(theta2)+K3;
D=cos(theta2)-K1+K4.*cos(theta2)+K5;
E=-2.*sin(theta2);
F=K1+(K4-1).*cos(theta2)+K5;

theta4=2.*atan((-B-sqrt(B.^2-4.*A.*C))./(2.*A)); %Angle of link 4 to
ground from the right
theta3=2.*atan((-E-sqrt(E.^2-4.*D.*F))./(2.*D)); %Angle of link 3 to
ground from the right

Cx=P.*cos(theta3+zeta3)+L1.*cos(theta2); %X Position of coupler point
Cy=P.*sin(theta3+zeta3)+L1.*sin(theta2); %Y Position of coupler point

w3=((L1.*V3)./L2).*(sin(theta4-theta2)./sin(theta3-theta4));
%%Verified

VAX=L1.*V3.*-sin(theta2); %Velocity of point A X direction %%Verified
VAY=L1.*V3.*cos(theta2); %Velocity of point A Y Direction %%Verified

VPAX=P.*w3.*-sin(theta3+zeta3);% X Velocity of point P relative to
point A
VPAY=P.*w3.*cos(theta3+zeta3); % Y Velocity of point P relative to
point A

VPX=-VAX-VPAX; %X velocity of point P relative to ground %%Verified

```

```
VPy=VAy+VPay; %Y velocity of point P relative to ground %%Verified  
VelocityRatio=VPy/VPx; %Final Velocity Ratio  
end
```

## Appendix D: Mathematical Model of System Dynamics

### Main.m

```
%Main.m
% MATHEMATICAL MODEL OF THESIS SYSTEM DYNAMICS
% Written by: Brian Benson 2010/2011
% Calculates the dynamics of a flywheel, overload slip-clutch,
% spring/damper, four-bar mechanism for the inputted parameters
%To use simply run this script.

%Clear all variables and the command window
clc;
clear;
clear all;
clear global;

%%Set Global Variables
global m1 m2 Ff K p D ts L1 L2 L3 Lo Lc1 Lc2 Lc3 I1 I2U I2L I3 ML1 ML2
ML3

%%MODEL PARAMTERS

%Initial Values
IV1=375; %Initial speed of flywheel in rad/s
IV2=IV1; %Initial speed of mass 2 in rad/s
IV3=0; %Initial speed of Fourbar input link in rad/s

IX3=.12; %Initial angle to start FourBar at in rad
IX2=IX3-(15/57.3); %Initial angle to start mass 2 in rad
IX1=IX2; %Initial angle to start flywheel in rad

IA1=0; %Initial Acceleration to start flywheel at in rad/s^2
IA2=0; %Initial Acceleration to start mass 2 at in rad/s^2
IA3=0; %Initial Acceleration to start input link to fourbar at in
rad/s^2

%%MECHANISM PARAMTERS
m1=1; %Effective Moment of Inertia of Flywheel seen by Four-Bar
(in^2*lb)
m2=6.5; %Effective Moment of Inertia of transmission between slip
clutch and four-bar seen by four-bar (in^2*lb)
Ff=0; %Maximum Frictional Force of Slip Clutch (in*lb)
K=6000; %Spring Constant of rubber coupling. Input parameter to
K(deflection) function
p=5000; %Damping Coefficient of rubber coupling
D=0; %Damping Coefficient of Slip Clutch

%LINKAGE VALUES
Lo=11.425;%Ground Length (in)
L1=3.3; %Crank Length (in)
L2=10.225; %Coupler Length (in)
```

```

L3=2.1; %Follower Length (in)

%%Point A is the joint between L0 and L1
Lc1=.429; %Distance of center of mass of link L1 from ground pivot
Lc2= 9.1; %Distance of center of mass of link L2 from point A
Lc3=L3./2; %Distance of center of mass of link L3 from ground pivot
zetaML2= 198/57; %Angle of vector going from point A to center of mass
zeta3=198/57; %Angle of vector p from point 2,3 to coupler point
P=9.21; % Distance of point A from coupler point

I1=4.32; %Moment of Inertia of Link 1 in^2*lbf
I2U=20; %Moment of Inertia of Link 2 Unloaded in^2*lbf
I2L=471; %Moment of Inertia of Link 2 Loaded in^2*lbf
I3=.2; %Moment of Inertia of Link 3 in^2*lbf

ML1=0.004715; %mass of link 2 (blob)
ML2= 0.0892; %mass of link 2 (blob)
ML3=0.0057; %mass of link 4 (blob)

YOffset=0; %Vertical position of pivot 1,4 referenced from pivot 1,2

%Model Parameters
ts=.000005; %Time Step in Seconds

%%INITIAL CONDITIONS

counter=0; %Records the stuck or slip condition of the clutch.

%%%%%%%% X1 V1 A1 X2 V2 A2 X3 V3 A3 Count T X
V A X V A X V A C
a=Clutch( IX1, IV1, IA1, IX2, IV2, IA2, IX3, IV3, IA3, counter, [0,
IX1, IV1, IA1, IX2, IV2, IA2, IX3, IV3, IA3, IV1]);

%%SIMULATION

%The simulation consists of a while loop that continues until a given
%maximum angle is reached. For each loop it calculates for one time
%step "ts". It assumes that the model starts off in the slipping state.
%It then monitors the model behavior for a switch to the stuck state at
%which point it switches.

while a.X3*57.3<95 %When the position of X3 is greater than 95 degrees
stop the simulation

%Checks

```

```

    if a.V1<.001, break, end %Stop Simulation if V1 becomes less than
zero
    if a.X1<IX1 ,break,end %Stop simulation if X1 becomes less then
the initial position I.E. if it goes backwards
    if a.mat(end,1)>.5, break, end %Stop simulation after 0.5 seconds

%Actual Simulation
n=Slip(a.X1, a.V1, a.X2, a.V2, a.X3, a.V3); %%Run the simulation
for one instance assuming that the clutch is slipping

    if (n(1,3)-n(1,7)>.01);%If difference between V1 and V3 is greater
than .01 then save slip data

        set_X2(a,slip(end,4)); %Sets X2 to Clutch Class Struct
        set_V2(a,slip(end,5)); %Sets V2 to Clutch Class Struct
        set_A2(a, Accel(ts,a.mat(end,6),a.V2)); %Calculate A2 based on
Velocity and Time Difference Ratio. Sets A2 to Clutch Class Struct

        AdjV3=MOICONS(a.mat(end,8), slip(end,6),slip(end,7));
%Calculates an adjusted new velocity of the fourbar linkage based on
the increase in effective moment of inertia
        AdjX3=(a.mat(end,9)+AdjV3)/2*ts+a.mat(end,8); %Calculates the
average speed over the last time step and multiplies by time to get the
newest position

        set_V3(a,AdjV3); %Sets V3 to Clutch Class Struct
        set_X3(a,AdjX3); %Sets X3 to Clutch Class Struct
        set_A3(a, Accel(ts,a.mat(end,9),a.V3)); %Calculate A3 based on
Velocity and Time Difference Ratio. Sets A3 to Clutch Class Struct

        set_V1(a,slip(end,3)); %Sets V1 to Clutch Class Struct
        set_X1(a,slip(end,2)); %Sets X1 to Clutch Class Struct
        set_A1(a, Accel(ts,a.mat(end,3),a.V1)); %Calculate A1 based on
Velocity and Time Difference Ratio. Sets A1 to Clutch Class Struct

        set_count(a,IV1); %Sets Counter to initialspped to signify
clutch is in the slip state
        set_mat(a,a.mat,[a.mat(end,1)+slip(end,1),a.X1, a.V1, a.A1,
a.X2, a.V2, a.A2, a.X3, a.V3, a.A3, a.count]); %Adds the new values to
the matrix

    else %Otherwise calculate the stuck values and save those

        stuck=Stuck2(a.X2, a.V2, a.X3, a.V3); %Calculate the next set of
values assuming that clutch is stuck

        X2o=a.X2; %Store the old X2 Value to X3o
        E1o=.5*m1*a.V1^2; %Energy stored in Mass 1 (Flywheel) in
previous iteration
        X2f=stuck(end,2); %Store the new X2 value
        DiffX1=X2f-X2o; %Calculate the difference between the old and
new X2 location, which is the amount X1 moved through

```

```

        Elf=.5*m1*stuck(end,3)^2; %Energy stored in Mass 1 (Flywheel)
in current iteration
        Torque=(Elo-Elf)/DiffX1 %Calculates the torque required in
in*lbft to transfer the amount of energy that is transferred in the
Stuck() function

        if Ff<Torque
            set_count(a,0); %Sets counter to indicate that it is in the
stuck state
        else
            set_count(a,IV1*.5); %Sets counter to indicate that it is
in the slip state
        end
        set_X2(a,stuck(end,2)); %Sets X2 to Clutch Class Struct
        set_V2(a,stuck(end,3)); %Sets V2 to Clutch Class Struct
        set_A2(a, Accel(ts,a.mat(end,6),stuck(end,3))); %Calculate A2
based on Velocity and Time Difference Ratio. Sets to Clutch Class
Struct

        set_X3(a,stuck(end,4)); %Sets X3 to the previous distance
between X3 and X2 plus the distance of X2 to Clutch Class Struct
        set_V3(a,stuck(end,5)); %Sets V3 to Clutch Class Struct
        set_A3(a, Accel(ts,a.mat(end,9),a.V3)); %Calculate A3 based on
Velocity and Time Difference Ratio. Sets to Clutch Class Struct

        %In the stuck position V1 and V2 are identical but there
position
        %is offset an initial amount. This must be accounted for:
        displacement=a.X2-a.mat(end,5); %Displacement of X2 in last
loop
        newx1=a.mat(end,2)+displacement; %New Location of X1 based on
the diff

        set_X1(a,newx1); %Sets X1 to Clutch Class Struct
        set_V1(a,stuck(end,3)); %Sets V1 to Clutch Class Struct
        set_A1(a, a.A2); %Calculate A1 based on Velocity and Time
Difference Ratio. Sets to Clutch Class Struct

        set_mat(a,a.mat,[a.mat(end,1)+stuck(end,1), a.X1, a.V1, a.A1,
a.X2, a.V2, a.A2, a.X3, a.V3, a.A3, a.count]); %Adds the new values to
the matrix in the struct
    end
end

Result=a.mat; %Sets the resulting matrix to the variable 'Result'

%%Sets the results to individual vectors for ease of use
T=Result(:,1);
X1=Result(:,2);
V1=Result(:,3);
A1=Result(:,4);
X2=Result(:,5);
V2=Result(:,6);
A2=Result(:,7);

```

```

X3=Result(:,8);
V3=Result(:,9);
A3=Result(:,10);
StickSlip=Result(:,11);

%KINEMATICS CALCULATIONS: Refer to Norton's Design of Machinery for
%explanations of terms.

K1=Lo./L1;
K2=Lo./L3;
K3=(L1.^2-L2.^2+L3.^2+Lo.^2)./(2.*L1.*L3);
K4=Lo./L2;
K5=(L3.^2-Lo.^2-L1.^2-L2.^2)./(2.*L1.*L2);

A=cos(X3)-K1-K2.*cos(X3)+K3;
B=-2.*sin(X3);
C=K1-(K2+1).*cos(X3)+K3;
D=cos(X3)-K1+K4.*cos(X3)+K5;
E=-2.*sin(X3);
F=K1+(K4-1).*cos(X3)+K5;

theta4=2.*atan((-B-sqrt(B.^2-4.*A.*C))./(2.*A)); %Angle of link 4 to
ground from the right
theta3=2.*atan((-E-sqrt(E.^2-4.*D.*F))./(2.*D)); %Angle of link 3 to
ground from the right

PosMax=Lc1.*cos(X3); % X position of center of mass of link 2 relative
to ground
PosMay=Lc1.*sin(X3); % Y position of center of mass of link 2 relative
to ground

PosAx=L1.*cos(X3); % X position of point A relative to ground
PosAy=L1.*sin(X3); % Y position of point A relative to ground

PosBx=L3.*cos(theta4)+Lo; % X position of point B relative to ground
PosBy=L3.*sin(theta4)+YOffset; % Y position of point B relative to
ground

Cx=P.*cos(theta3+zeta3)+L1.*cos(X3); % X Position of coupler point
Cy=P.*sin(theta3+zeta3)+L1.*sin(X3); % Y Position of coupler point

%PosM3x=Lc2.*cos(theta3+zetaML2)+L1.*cos(X3); %X Position of center of
mass of link 3
%PosM3y=Lc2.*sin(theta3+zetaML2)+L1.*sin(X3); %Y Position of center of
mass of link 3

w3=((L1.*V3)./L2).*(sin(theta4-X3)./sin(theta3-theta4)); %%Angular
Velocity of Link 3
w4=((L1.*V3)./L3).*(sin(X3-theta3)./sin(theta4-theta3)); %%Angular
Velocity of Link 4

VAx=L1.*V3.*-sin(X3); %Velocity of point A X direction
VAy=L1.*V3.*cos(X3); %Velocity of point A Y Direction

```

```

%VMax=Lc1.*V3.*-sin(X3); %Velocity of point A X direction %%Verified
%VMay=Lc1.*V3.*cos(X3); %Velocity of point A Y Direction %%Verified

VPax=P.*w3.*-sin(theta3+zeta3);% X Velocity of point P relative to
point A
VPay=P.*w3.*cos(theta3+zeta3); % Y Velocity of point P relative to
point A

VPx=VAx+VPax; %X velocity of point P relative to ground
VPy=VAy+VPay; %Y velocity of point P relative to ground
VP=sqrt (VPx.^2+VPy.^2); %Velocity Vector Magnitude point P

EBotx=.5*VPx.^2.*30/386; %Energy of the opposing robot based on X
velocity
EBoty=.5*VPy.^2.*30/386; %Energy of the opposing robot based on Y
velocity
EBot=.5*VP.^2.*30/386; %Total energy in opposing robot

%Calculates the energy of each part of the system throughout the
movement
Energy1=(.5*m1.*V1.^2)/3417; %Energy in Mass 1
Energy2=(.5.*m2.*V2.^2)/3417; %Energy in Mass 2
Energy4bar=(.5.*MOI(X3).*V3.^2)/3417; %Energy in robot (ignoring weight
of four-bar)
Energy3=(EBot)/3417; %Energy in robot (ignoring weight of four-bar)
EnergySpring=.5*K*(X3-X2).^2; %Energy stored in spring

VFx=VPx(end,1); %Final X Velocity of Coupler Point
VFy=VPy(end,1); %Final Y Velocity of Coupler Point

t=(0:ts:2.1*VFy/386); %Vector of time steps in model
DistanceY=VFy*t-.5*cosd(11)*386*t.^2+Cy(end,1); %Y Trajectory of
Opposing Robot
DistanceX=VFx*t-.5*sind(11)*386*t.^2+Cx(end,1); %X Trajectory of
Opposing Robot

%PLOTS THE RESULTS
%%%POSITION
figure
subplot(2,1,1)
hold on
plot(T, X1*57.3, 'Color', 'k') %Plot X1 vs Time
plot(T, X2*57.3,'Color', 'r','LineStyle','--') %Plot X2 vs Time
plot(T, X3*57.3,'Color', 'b','LineStyle',':') %Plot X3 vs Time
legend('X1','X2','X3');ylabel('Angle (degrees)');xlabel('t')

%VELOCITY
subplot(2,1,2)
hold on
plot(T, V1*9.549,'Color', 'k') %Plot V1 vs Time
plot(T, V2*9.549,'Color', 'r','LineStyle','--') %Plot V2 vs Time
plot(T, V3*9.549,'Color', 'b','LineStyle',':') %Plot V3 vs Time
plot(T, StickSlip*9.549,'Color', 'm','LineStyle','-.') %Plot Stick or
Slip

```

```

legend('V1','V2','V3','Stick or Slip');ylabel('Velocity
(RPM)');xlabel('t')

%Torque
[HT2 WT2]=size(A2*m2); %HT2 is the height, WT2 is the width
[HT3 WT3]=size(A3.*MOI(X3)); %HT3 is the height, WT3 is the width

%%{
%ACCELERATION%
figure
subplot(4,1,1)
hold on
plot(T, A1, 'Color', 'k') %Plot A1 vs Time
plot(T, A2, 'Color', 'r','LineStyle','--') %Plot A2 vs Time
plot(T, A3, 'Color', 'b','LineStyle',':') %Plot A3 vs Time
legend('A1','A2','A3');ylabel('Acceleration (rad/s^2)');xlabel('t');
%Legend

%Torque PLOT
subplot(4,1,2)
hold on
plot(T, A1*m1, 'Color', 'k') %Plot T1 vs Time
plot(T, A2*m2, 'Color', 'r','LineStyle','--') %Plot T2 vs Time
plot(T, sum(A2*m2)/HT2, 'Color', 'r','LineStyle','--') %Plot T2 Average
vs Time
plot(T, A3.*MOI(X3), 'Color', 'b','LineStyle',':') %Plot T3 Average vs
Time
plot(T, sum(A3.*MOI(X3))/HT3, 'Color', 'b','LineStyle',':') %Plot T3
Average vs Time
legend('T1', 'T2', 'T2 AVG', 'T3', 'T3
AVG');ylabel('Torque(in/lb)');xlabel('t');%Legend

subplot(4,1,3)
hold on
plot(T,sum(A3.*MOI(X3))/HT3- A1*m1, 'Color', 'k') %Plot T1 vs Time
legend('T3-T1');ylabel('Torque(in/lb)');xlabel('t');%Legend

subplot(4,1,4)
hold on
plot(T,sum(A2.*m2)/HT3- A1*m1, 'Color', 'k') %Plot T1 vs Time
legend('T2-T1');ylabel('Torque(in/lb)');xlabel('t');%Legend

%Energy Plot
figure
subplot(2,1,1)
hold on
plot(T,Energy3, 'Color', 'b');% Plot Energy Other Robot
legend('Energy Opposing Robot');ylabel('Energy(J)');xlabel('t');%Legend

subplot(2,1,2)
hold on
plot(T,Energy1, 'Color', 'k');%Plot Energy Flywheel
plot(T,Energy4bar, 'Color', 'r');%Plot Energy Flywheel

```

```

legend('Energy Flywheel', 'Energy Four
Bar');ylabel('Energy (J) ');xlabel('t');%Legend

figure
hold on
plot(T,-VPx,'Color','k');%Plot X Velocity of Coupler Point
plot(T,VPy,'Color','r','LineStyle','--');% Plot Y Velocity of Coupler
Point
plot(T,VP,'Color','b','LineStyle',':');% Plot Velocity Magnitude of
Coupler Point
legend('Velocity X','Velocity Y', 'Velocity Magnitude');ylabel(' X and
Y Velocity of Coupler Point (in/s) ');xlabel('t');%Legend
%%}

figure
%PLOT FINAL SYSTEM RESPONSE AND ANIMATE THROUGH MOTION
for n = HT2:HT2
plot(PosAx,PosAy+abs(Cy(1,1)), PosBx, PosBy+abs(Cy(1,1)), Cx,
Cy+abs(Cy(1,1)),0,0+abs(Cy(1,1)), Lo, YOffset+abs(Cy(1,1))%, ICX, ICY)
ylabel('Distance (inches) ');xlabel('Distance (inches) ');%Legend
hold on

%line([PosM3x(1,n) ICX(1,n)], [PosM3y(1,n) ICY(1,n)], 'Color','k',
'LineWidth', 1) % IC Vector
%quiver(PosMax,PosMay,F02x,F02y, 'LineWidth', 1, 'Color', 'k') %Force
Vector Crank
%quiver(PosM3x,PosM3y,F03x,F03y, 'LineWidth', 1, 'Color', 'k') %Force
Vector Coupler
%quiver(PosMax,PosMay,VMax,VMay, 'LineWidth', 1, 'Color', 'c')
%Velocity Vector Crank
%quiver(PosM3x,PosM3y,VPMx,VPMY, 'LineWidth', 1, 'Color', 'c')
%Velocity Vector Coupler

hold off

line([0 PosAx(n,1)], [0+abs(Cy(1,1)) PosAy(n,1)+abs(Cy(1,1))],
'Color','g', 'LineWidth', 2) %Crank
line([0 Lo], [0+abs(Cy(1,1)) YOffset+abs(Cy(1,1))], 'Color','k',
'LineWidth', 2) %Ground
line([PosAx(n,1) PosBx(n,1) ], [PosAy(n,1)+abs(Cy(1,1))
PosBy(n,1)+abs(Cy(1,1)) ], 'Color','m', 'LineWidth', 2) %Coupler
line([Lo PosBx(n,1)], [YOffset+abs(Cy(1,1)) PosBy(n,1)+abs(Cy(1,1))],
'Color','g', 'LineWidth', 2) %Follower
line([PosAx(n,1) Cx(n,1)], [PosAy(n,1)+abs(Cy(1,1))
Cy(n,1)+abs(Cy(1,1))], 'Color','m', 'LineWidth', 2) % Coupler Point

hold on
plot(DistanceX,DistanceY+abs(Cy(1,1)), 'LineStyle',':')

hold off

axis equal
M(n)=getframe;
end

```

## Clutch.m

```
%Clutch.m
% Written by Brian Benson 2010/2011
%Defines the clutch class and the functions that can be used to modify
%the clutch class

classdef Clutch < handle
    properties
        X1 %Position of M1
        V1 %Velocity of M1
        A1 %Acceleration of M1
        X2
        V2
        A2
        X3
        V3
        A3
        count %Stores the state of the system
        mat %matrix that stores all of the simulation data
    end
    methods
        function obj=set_X1(obj,X1)
            obj.X1=X1;
        end
        function obj=set_V1(obj,V1)
            obj.V1=V1;
        end
        function obj=set_A1(obj,A1)
            obj.A1=A1;
        end
        function obj=set_X2(obj,X2)
            obj.X2=X2;
        end
        function obj=set_V2(obj,V2)
            obj.V2=V2;
        end
        function obj=set_A2(obj,A2)
            obj.A2=A2;
        end
        function obj=set_X3(obj,X3)
            obj.X3=X3;
        end
        function obj=set_V3(obj,V3)
            obj.V3=V3;
        end
        function obj=set_A3(obj,A3)
            obj.A3=A3;
        end
        function obj=set_count(obj,count)
    end
end
```

```

        obj.count=count;
    end
    function obj=set_mat(obj, mat1, mat2)
        obj.mat=[mat1; mat2];
    end

    function obj=Clutch(X1,V1,A1, X2, V2, A2, X3, V3, A3 ,count,
mat)
        obj.X1=X1;
        obj.V1=V1;
        obj.A1=A1;
        obj.X2=X2;
        obj.V2=V2;
        obj.A2=A2;
        obj.X3=X3;
        obj.V3=V3;
        obj.A3=A3;
        obj.count=count;
        obj.mat=mat;
    end
end
end
end

```

## Slip.m

```
function [N] = Slip(X1, V1, X2, V2, X3, V3)
%Slip.m
% Written by: Brian Benson 2010/2011
% Slip.m takes 6 initial value conditions for the position and
%velocity of M1, M2, and M3 and returns a matrix of the solution of the
%ode45 for the time step ts. Used for when the clutch is in the slip
%state (2 DOF)

options=odeset('RelTol',1e-6); %Sets the RelTol to 10^-6

Xo = [X1 V1 X2 V2 X3 V3]; %Sets the initial conditions to a vector Xo

global ts %Initialize global variables

tspan = [0 ts]; %timespan for each iteration

[t,X] = ode45(@MassSpringMass,tspan,Xo,options); %call the solver

N=[t,X]; %Store Solution in N
end

function [dx_dt]= MassSpringMass(t,y)

%Variable Key for Reference:
%Y1=X1
%Y2=V1
%Y3=X2
%Y4=V2
%Y5=X3
%Y6=V3

global m1 m2 Ff K p D %Initialize global variables

m3=MOI(y(5)); %Defines the effective moment of inertia for M3 with the
input value in radians
k=SC(K,y(5),y(3)); %Defines the k value with the function SC(K, posM3,
posM2)

%Differential Equations in State Space Form that describe the system
dx_dt(1) = y(2);
dx_dt(2) = (D*y(4)/m1) - (D*y(2)/m1) - (Ff/m1);
dx_dt(3) = y(4);
dx_dt(4) = (Ff/m2) - (k*y(3)/m2) + (k*y(5)/m2) - (p*y(4)/m2) + (p*y(6)/m2);
dx_dt(5) = y(6);
dx_dt(6) = (k*y(3)/m3) - (k*y(5)/m3) + (p*y(4)/m3) - (p*y(6)/m3);

dx_dt = dx_dt'; %transpose dx_dt so it is a column vector
end
```

## Stuck.m

```
function [N] = Stuck2(X1, V1, X2, V2)
%Stuck.m
% Written by: Brian Benson 2010/2011
% Stuck.m takes 4 initial value conditions for the position and
%velocity of M2, and M3 and returns a vector of the solution based on
%previous velocity and increased MOI of system using
%an energy balance. It is assumed that relative torque between M2 and
%M3 will remain small that it can be assumed the velocities stay equal.

x2=X2+((V1+v2)/2)*ts; %Calculates the new position based on the average
of the initial and final velocity

global ts m1 m2%Initialize global variables

v2=sqrt(((MOI(X2)+m1+m2)*V1^2)/(m1+m2+MOI(X2+V1*ts))); %Calculates the
new velocity

v1=v2; %Sets the velocity of M2 equal to M3
x1=X1+((V1+v2)/2)*ts; %Calculates the new position based on the average
of the initial and final velocity

N=[ts x1 v1 x2 v2]; %Stores the results in N

end
```

## Accel.m

```
function [ accel] = Accel(TS, V1, V2)
%Accel.m
% Written by: Brian Benson 2010/2011
%Calculates the acceleration of a mass given the time step and two
speeds

Dt=TS; %Delta Time (Time Step)
Dv=V2-V1; %Delta Velocity

accel=Dv/Dt; %Acceleration

end
```

## SC.m

```
function [K] = SC(k,X3, X2)
%SC.m
% Written by Brian Benson 2010/2011
% Calculates the spring constant of the rubber coupling given two
%positions and an initial spring constant starting point. Assumes that
%the spring constant goes up as compression increases. A very basic
%estimate.

global lastK %Initializes global variable last K. Stores the last used
K value

Diff=X3-X2; %Position difference between mass 2 and 3

if Diff>0 %If the difference is greater than zero
    K=k./Diff; %Set the K to the initial k over the difference
    lastK=K; %Save lastK as the current K
else %If the difference is less than or equal to zero
    K=lastK*exp(abs(Diff)); %Increase the K value exponentially with
the starting value being the lastK

end
```

## MOI.m

```
function [ Inertia ] = MOI(theta)
%MOI.m
% Written by Brian Benson 2010/2011
%Calculates the Moment of Inertia based on Theta
%Input is an angle is radians
%Output is a Moment of Inertia is in^2*lb

%INPUTS%
%These inputs are defined in the Main.m file.
global L1 L2 L3 Lo Lc1 Lc2 Lc3 I1 I2U I2L I3 ML1 ML2 ML3

if theta<.12+(5/57.3) %For first 5 degrees of movement
    I2=I2U; % Effective Moment of Inertia of Link 2 Unloaded (No robot
on it)

else
    I2=I2L; %Otherwise consider the four-bar to be loaded (Robot on it)
end

%INPUTS%

k1=-2.*L1.*L3.*sin(theta);
k2=2.*L3.*(Lo-L1.*cos(theta));
k3=Lo.^2+L1.^2-L2.^2+L3.^2-2.*Lo.*L1.*cos(theta);

phi=2*atan2(-k1-sqrt(k1.^2+k2.^2-k3.^2),k3-k2);
alpha=atan2(-L1.*sin(theta)+L3.*sin(phi),Lo-
L1.*cos(theta)+L3.*cos(phi));

J1=.5.*(ML1.*Lc1.^2+I1+ML2.*L1.^2);
J2=.5.*(ML2.*Lc2.^2+I2);
J3=.5.*(ML3.*Lc3.^2+I3);

S1=(L1.*sin(phi-theta))./(L2.*sin(alpha-phi));
S2=(L1.*sin(alpha-theta))./(L3.*sin(alpha-phi));

P1=ML2.*L1.*Lc2;
C1=cos(theta-alpha);

Inertia=2.*(J1+J2.*S1.^2+J3.*S2.^2+P1.*C1.*S1); %Final Effective Moment
of Inertia
end
```

## Appendix E: Force and Stress Analysis of Dog Clutch Jaws

### Givens

Mass of opposing robot to be thrown

$$\text{Mass}_R := 30\text{lb}$$

Gear ratio between flywheel and clutch

$$\eta := 1$$

Moment of Inertia of flywheel

$$I_{\text{Flywheel}} := 0\text{lb}\cdot(2\text{in})^2 = 0$$

Moment of Inertia of male side of the clutch

$$I_{\text{Clutch}} := 6.5\text{in}^2\cdot\text{lb}$$

Speed of Flywheel

$$\omega_1 := 375 \frac{\text{rad}}{\text{sec}} = 3.581 \times 10^3 \cdot \frac{\text{rev}}{\text{min}}$$

Maximum Torque Overload Slip Clutch

$$F_f := 0\text{in}\cdot\text{lbf}$$

### Dog-Clutch Feasibility Analysis

The safety factor for the dog-clutch teeth is determined

Average radius of dogs

$$R_{\text{Dog}} := 1.4375\text{in}$$

Number of Dogs

$$\text{Number}_{\text{Dogs}} := 3$$

Height of dogs

$$\text{Height} := .25\text{in}$$

Width of dogs

$$\text{Width} := .75\text{in}$$

Dog Contact Patch Area

$$\text{Area} := \text{Height} \cdot \text{Width} = 0.187\text{in}^2$$

Young's Modulus of Material

$$E_{\text{Steel}} := 210\text{GPa} = 3.046 \times 10^7 \text{ psi}$$

There is no single valid modulus of elasticity for rubber. It changes as it compresses and is highly dependent on strain rate. This value is simple a rough estimation

$$E_{\text{Rubber}} := 1\text{GPa} = 1.45 \times 10^5 \text{ psi}$$

Spring Constant of Rubber

$$k := \frac{E_{\text{Rubber}} \cdot (\text{Area} \cdot .75)}{.25\text{in}} = 8.158 \times 10^4 \frac{\text{lbf}}{\text{in}}$$

Kinetic energy dissipation factor. Minimal so equal to 1

$$\eta_i := 1$$

Energy Transferred through the overload slip clutch for compression of rubber coupling

$$\theta_{\text{RubberCompression}} := 5\text{deg}$$

Angular Deflection is dependent on  $F_i$  so this term is found iteratively

$$E_{\text{Slip}} := F_i \cdot \theta_{\text{RubberCompression}} = 0 \cdot \text{J}$$

Energy in Male Side of the Clutch at Impact

$$E_{\text{Clutch}} := \frac{I_{\text{Clutch}} \cdot \eta^2 \cdot \left(\frac{\omega_1}{\eta}\right)^2}{2} = 133.745 \cdot \text{J}$$

Impact force using energy estimation methods with an overload slip clutch

$$F_i := 1.3 \cdot \sqrt{\frac{(E_{\text{Clutch}} + E_{\text{Slip}})}{\text{Number}_{\text{Dogs}}}} \cdot 2 \cdot k = 1.043 \times 10^4 \cdot \text{lbf}$$

Check to determine how much the rubber compresses (in degrees). This number is entered above iteratively.

$$\frac{\frac{F_i}{k}}{2 \cdot \pi \cdot R_{\text{Dog}}} \cdot 360\text{deg} = 5.096 \cdot \text{deg}$$

The ratio of the foot print of a dog boss versus the height indicates that beam calculations will not be valid. Therefore only shear and compressive stresses are evaluated.

Area of the footprint of a dog

$$\text{Footprint} := .36\text{in}^2$$

Shear Stress on single dog

$$\tau_{\text{Direct}} := \frac{F_i}{\text{Footprint}} = 2.898 \times 10^4 \text{ psi}$$

Compressive Stress on impact surface

$$\sigma_{\text{Compressive}} := \frac{F_i}{\text{Height} \cdot \text{Width}} = 5.563 \times 10^4 \text{ psi}$$

Yield Stress of 4140 Steel at 40 Rockwell C

$$\text{Stress}_{\text{Yield}} := 165000 \text{ psi} = 1.138 \text{ GPa}$$

Safety Factor in Compression

$$\text{SF}_{\text{Compressive}} := \frac{\text{Stress}_{\text{Yield}}}{\sigma_{\text{Compressive}}} = 2.966$$

Safety Factor in Shear

$$\text{SF}_{\text{Shear}} := \frac{\text{Stress}_{\text{Yield}} \cdot .58}{\tau_{\text{Direct}}} = 3.303$$

[http://www.roymech.co.uk/Useful\\_Tables/Matter/shear\\_tensile.htm](http://www.roymech.co.uk/Useful_Tables/Matter/shear_tensile.htm)